



May 2, 2002

L-2002-082
10 CFR 50.4
10 CFR 50.60(a)

U. S. Nuclear Regulatory Commission
Attn: Document Control Desk
Washington, DC 20555

RE: St. Lucie Unit 1
Docket No. 50-335
Reactor Vessel Surveillance Capsule
Report of Test Results - Revision 1 (TAC MB0554)

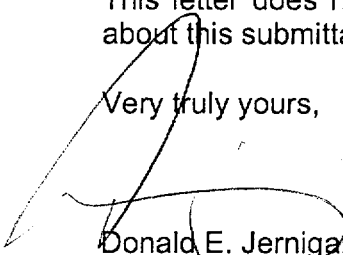
Florida Power & Light Company (FPL) is submitting revision 1 of Westinghouse report titled *Analysis of Capsule 284° From the Florida Power and Light Company St. Lucie Unit 1 Reactor Vessel Radiation Surveillance Program*, WCAP-15446, dated January 2002. The enclosed is a revised summary technical report for the capsule removed during the Fall 1999 St. Lucie Unit 1 refueling outage (SL1-16). Revision 1 of the Westinghouse report (WCAP-15446) was issued to correct a non-conservative error in the fluence analysis. Reevaluation with the new fluence data verified the conclusions reported in revision 0 as correct. No changes in any conclusions resulted from this revision.

The original report was submitted pursuant to the requirements of 10 CFR 50.60(a) and 10 CFR 50 Appendix H, *Reactor Vessel Material Surveillance Program Requirements*, paragraph I.A, by FPL letter L-2000-193 on September 27, 2000.

The report includes the data required by ASTM E-185, as specified in paragraph III.B.1 of 10 CFR 50 Appendix H, and the results of all applicable fracture toughness tests conducted on the beltline materials in the irradiated and unirradiated conditions. FPL has confirmed no technical specification or operating procedure changes are required due to the revision.

This letter does not contain any regulatory commitments. If there are any questions about this submittal, please contact George Madden at 772-467-7155.

Very truly yours,


Donald E. Jernigan
Vice President
St. Lucie Plant

Enclosure

DEJ/GRM

A008



WCAP-15446

Revision 1

ANALYSIS OF
CAPSULE 284° FROM THE
FLORIDA POWER AND
LIGHT COMPANY ST.
LUCIE UNIT 1 REACTOR
VESSEL RADIATION
SURVEILLANCE
PROGRAM

Westinghouse Energy Systems LLC



WCAP-15446, Revision 1

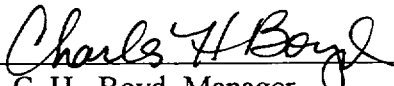
**Analysis of Capsule 284° from the Florida Power & Light
Company St. Lucie Unit 1
Reactor Vessel Radiation Surveillance Program**

**T. J. Laubham
D.M. Chapman
J. Conermann**

January 2002

Prepared by the Westinghouse Electric Company
for the Florida Power & Light Company

Approved:


C. H. Boyd, Manager
Equipment & Materials Technology

WESTINGHOUSE ELECTRIC COMPANY LLC
Nuclear Services Division
P.O. Box 355
Pittsburgh, Pennsylvania 15230-0355
© 2002 Westinghouse Electric Company
All Rights Reserved

TABLE OF CONTENTS

LIST OF TABLES	ii
LIST OF FIGURES	iv
PREFACE & RECORD OF REVISION.....	vi
EXECUTIVE SUMMARY (OR) ABSTRACT	vii
1 SUMMARY OF RESULTS	1-1
2 INTRODUCTION.....	2-1
3 BACKGROUND	3-1
4 DESCRIPTION OF PROGRAM.....	4-1
5 TESTING OF SPECIMENS FROM CAPSULE 284°	5-1
5.1 OVERVIEW.....	5-1
5.2 CHARPY V-NOTCH IMPACT TEST RESULTS.....	5-3
5.3 TENSILE TEST RESULTS.....	5-4
6 RADIATION ANALYSIS AND NEUTRON DOSIMETRY.....	6-1
6.1 INTRODUCTION	6-1
6.2 DISCRETE ORDINATES ANALYSIS.....	6-2
6.3 NEUTRON DOSIMETRY.....	6-4
6.4 PROJECTIONS OF REACTOR VESSEL EXPOSURE.....	6-13
7 SURVEILLANCE CAPSULE REMOVAL SCHEDULE.....	7-1
8 REFERENCES.....	8-1
APPENDIX A LOAD-TIME RECORDS FOR CHARPY SPECIMEN TESTS	
APPENDIX B CHARPY V-NOTCH PLOTS FOR EACH CAPSULE USING HYPERBOLIC TAGENT CURVE-FITTING METHOD	
APPENDIX C CHARPY V-NOTCH SHIFT RESULTS FOR EACH CAPSULE HAND-FIT VS. HYPERBOLIC TANGENT CURVE-FITTING METHOD (CVGRAPH, VERSION 4.1)	
APPENDIX D ST. LUCIE UNIT 1 SURVEILLANCE PROGRAM CREDIBILITY ANALYSIS	

LIST OF TABLES

Table 5-1	Charpy V-Notch Data for the St. Lucie Unit 1 Lower Shell Plate C-8-2 Irradiated to a Fluence of 1.45×10^{19} n/cm ² (E > 1.0 MeV) (Longitudinal Orientation).....	5-6
Table 5-2	Charpy V-notch Data for the St. Lucie Unit 1 Lower Shell Plate C-8-2 Irradiated to a Fluence of 1.45×10^{19} n/cm ² (E > 1.0 MeV) (Transverse Orientation).....	5-7
Table 5-3	Charpy V-notch Data for the St. Lucie Unit 1 Surveillance Weld Metal Irradiated to a Fluence of 1.45×10^{19} n/cm ² (E > 1.0 MeV).....	5-8
Table 5-4	Charpy V-notch Data for the St. Lucie Unit 1 Heat Affected Zone (HAZ) Metal Irradiated to a Fluence of 1.45×10^{19} n/cm ² (E > 1.0 MeV).....	5-9
Table 5-5	Instrumented Charpy Impact Test Results for the St. Lucie Unit 1 Lower Shell Plate C-8-2 Irradiated to a Fluence of 1.45×10^{19} n/cm ² (E > 1.0 MeV) (Longitudinal Orientation).....	5-10
Table 5-6	Instrumented Charpy Impact Test Results for the St. Lucie Unit 1 Lower Shell Plate C-8-2 Irradiated to a Fluence of 1.45×10^{19} n/cm ² (E > 1.0 MeV) (Transverse Orientation).....	5-11
Table 5-7	Instrumented Charpy Impact Test Results for the St. Lucie Unit 1 Surveillance Weld Metal Irradiated to a Fluence of 1.45×10^{19} n/cm ² (E > 1.0 MeV).....	5-12
Table 5-8	Instrumented Charpy Impact Test Results for the St. Lucie Unit 1 Representative Heat Affected Zone (HAZ) Material Irradiated to a Fluence of 1.45×10^{19} n/cm ² (E > 1.0 MeV)	5-13
Table 5-9	Effect of Irradiation to 1.45×10^{19} n/cm ² (E > 1.0 MeV) on the Notch Toughness Properties of the St. Lucie Unit 1 Reactor Vessel Surveillance Materials.....	5-14
Table 5-10	Comparison of the St. Lucie Unit 1 Surveillance Material 30 ft-lb Transition Temperature Shifts and Upper Shelf Energy Decreases with Regulatory Guide 1.99, Revision 2, Predictions	5-15
Table 5-11	Tensile Specimens From Lower Shell Course Plate C-8-2, Weld, and Heat Affected Zone Material.....	5-16
Table 6-1	Calculated Fast Neutron Exposure Rates and Iron Atom Displacement Rates at the Surveillance Capsule Center	6-16
Table 6-2	Calculated Azimuthal Variation of Fast Neutron Exposure Rates and Iron Atom Placement Rates at the Reactor Vessel Clad/Base Metal Interface.....	6-17
Table 6-3	Relative Radial Distribution of ϕ (E > 1.0 MeV) Within the Reactor Vessel Wall.....	6-18
Table 6-4	Relative Radial Distribution of ϕ (E > 0.1 MeV) Within the Reactor Vessel Wall.....	6-19

LIST OF TABLES (CONTINUED)

Table 6-5	Relative Radial Distribution of dpa/sec Within the Reactor Vessel Wall.....	6-20
Table 6-6	Nuclear Parameters Used in the Evaluation of Neutron Sensors	6-21
Table 6-7	Monthly Thermal Generation During The First Fifteen Fuel Cycles of the St. Lucie Unit 1 Reactor (Reactor Power of 2700 MWt).....	6-22
Table 6-8	Measured Sensor Activities and Reaction Rates - Surveillance Capsule 284°	6-25
	- Surveillance Capsule 104°	6-26
	- Surveillance Capsule 97°	6-27
Table 6-9	Summary of Neutron Dosimetry Results Surveillance Capsules 97°, 104°, and 284°	6-28
Table 6-10	Comparison of Measured, Calculated, and Best Estimate Reaction Rates at the Surveillance Capsule Center	6-29
Table 6-11	Best Estimate Neutron Energy Spectrum at the Center of Surveillance Capsule - Capsule 284°	6-30
	- Capsule 104°	6-31
	- Capsule 97°	6-32
	-	
Table 6-12	Comparison of Calculated and Best Estimate Integrated Neutron Exposure of the 97°, 104°, and 284° Surveillance Capsules	6-33
Table 6-13	Azimuthal Variations of the Neutron Exposure Projections on the Reactor Vessel Clad/Base Metal Interface at Core Midplane	6-34
Table 6-14	Neutron Exposure Values Within The St. Lucie Unit 1 Reactor Vessel.....	6-36
Table 6-15	Updated Lead Factors for St. Lucie Unit 1 Surveillance Capsules	6-40
Table 6-16	C _j Values for the St. Lucie Unit 1 Sensor Reaction Rate Evaluation.....	6-41
Table 7-1	St. Lucie Unit 1 Reactor Vessel Surveillance Capsule Withdrawal Schedule	7-1

LIST OF FIGURES

Figure 4-1	Arrangement of Surveillance Capsules in the St. Lucie Unit 1 Reactor Vessel.....	4-3
Figure 4-2	Typical St. Lucie Unit 1 Surveillance Capsule Assembly.....	4-4
Figure 4-3	Typical St. Lucie Unit 1 Surveillance Capsule Charpy Impact Compartment Assembly.....	4-5
Figure 4-4	Typical St. Lucie Unit 1 Surveillance Capsule Tensile and Flux Monitor Compartment Assembly	4-6
Figure 5-1	Charpy V-Notch Impact Energy vs. Temperature for St. Lucie Unit 1 Reactor Vessel Lower Shell Plate C-8-2 (Longitudinal Orientation).....	5-17
Figure 5-2	Charpy V-Notch Lateral Expansion vs. Temperature for St. Lucie Unit 1 Reactor Vessel Lower Shell Plate C-8-2 (Longitudinal Orientation).....	5-18
Figure 5-3	Charpy V-Notch Percent Shear vs. Temperature for St. Lucie Unit 1 Reactor Vessel Lower Shell Plate C-8-2 (Longitudinal Orientation).....	5-19
Figure 5-4	Charpy V-Notch Impact Energy vs. Temperature for St. Lucie Unit 1 Reactor Vessel Lower Shell Plate C-8-2 (Transverse Orientation).....	5-20
Figure 5-5	Charpy V-Notch Lateral Expansion vs. Temperature for St. Lucie Unit 1 Reactor Vessel Lower Shell Plate C-8-2 (Transverse Orientation).....	5-21
Figure 5-6	Charpy V-Notch Percent Shear vs. Temperature for St. Lucie Unit 1 Reactor Vessel Lower Shell Plate C-8-2 (Transverse Orientation).....	5-22
Figure 5-7	Charpy V-Notch Impact Energy vs. Temperature for St. Lucie Unit 1 Reactor Vessel Surveillance Weld Metal	5-23
Figure 5-8	Charpy V-Notch Lateral Expansion vs. Temperature for St. Lucie Unit 1 Reactor Vessel Surveillance Weld Metal	5-24
Figure 5-9	Charpy V-Notch Percent Shear vs. Temperature for St. Lucie Unit 1 Reactor Vessel Surveillance Weld Metal	5-25
Figure 5-10	Charpy V-Notch Impact Energy vs. Temperature for St. Lucie Unit 1 Reactor Vessel Heat Affected Zone Material.....	5-26

LIST OF FIGURES (CONTINUED)

Figure 5-11	Charpy V-Notch Lateral Expansion vs. Temperature for St. Lucie Unit 1 Reactor Vessel Heat Affected Zone Material.....	5-27
Figure 5-12	Charpy V-Notch Percent Shear vs. Temperature for St. Lucie Unit 1 Reactor Vessel Heat Affected Zone Material.....	5-28
Figure 5-13	Charpy Impact Specimen Fracture Surfaces for St. Lucie Unit 1 Reactor Vessel Lower Shell Plate C-8-2 (Transverse Orientation).....	5-29
Figure 5-14	Charpy Impact Specimen Fracture Surfaces for St. Lucie Unit 1 Reactor Vessel Lower Shell Plate C-8-2 (Longitudinal Orientation).....	5-30
Figure 5-15	Charpy Impact Specimen Fracture Surfaces for St. Lucie Unit 1 Reactor Vessel Weld Metal Specimens	5-31
Figure 5-16	Charpy Impact Specimen Fracture Surfaces for St. Lucie Unit 1 Reactor Vessel Heat Affected Zone (HAZ).....	5-32
Figure 5-17	Tensile Properties for St. Lucie Unit 1 Reactor Vessel Lower Shell Plate C-8-2 (Longitudinal Orientation)	5-33
Figure 5-18	Tensile Properties for St. Lucie Unit 1 Reactor Vessel Weld Metal.....	5-34
Figure 5-19	Tensile Properties for St. Lucie Unit 1 Reactor Vessel Heat-Affected-Zone (HAZ)	5-35
Figure 5-20	Fractured Tensile Specimens from St. Lucie Unit 1 Reactor Vessel Lower Shell Plate C-8-2 (Longitudinal Orientation).....	5-36
Figure 5-21	Fractured Tensile Specimens from St. Lucie Unit 1 Reactor Vessel Weld Metal	5-37
Figure 5-22	Fractured Tensile Specimens from St. Lucie Unit 1 Reactor Vessel Heat Affected Zone (HAZ).....	5-38
Figure 5-23	Engineering Stress-Strain Curves for Lower Shell Plate C-8-2 Tensile Specimens 1J4, 1JL and 1JM (Longitudinal Orientation).....	5-39
Figure 5-24	Engineering Stress-Strain Curve for Weld Metal Tensile Specimens 3J2, 3JJ, and 3JY	5-40
Figure 5-25	Engineering Stress-Strain Curves For Heat-Affected Zone (HAZ) Material Tensile Specimens 4KJ, 4KK, and 4KY	5-41

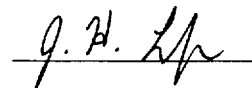
PREFACE

This report has been technically reviewed and verified by:

Reviewer:

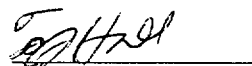
Sections 1 through 5, 7, 8, Appendices A, B, C and D

J. H. Ledger



Section 6

T.J. Hall



RECORD OF REVISION

Revision 1: This WCAP report is being revised to correct errors in the DORT models used in the original calculations. This issue was originally identified in Reference 35. The errors included a non-conservative assumption in the thickness of the core support barrel and a conservative assumption in the moderator density of the down-comer region. The incorrect thickness was present in the models used for Cycles 1 through 15, as well as the future projections. The incorrect moderator density was present only in Cycles 1 through 4. Additionally, some changes have been made (relative to the original issue) in the selection of the sensor measurements used in the neutron dosimetry analysis as a result of the updated DORT calculations.

Revision 1 to this WCAP report supersedes the original issue in its entirety.

EXECUTIVE SUMMARY

The purpose of this report is to document the results of the testing of surveillance capsule 284° from St. Lucie Unit 1. Capsule 284° was removed at 17.23 EFPY and post irradiation mechanical tests of the Charpy V-notch and tensile specimens was performed, along with a fluence evaluation based methodology and nuclear data including recently released neutron transport and dosimetry cross-section libraries derived from the ENDF/B-VI database. The calculated peak clad base/metal vessel fluence after 17.23 EFPY of plant operation was $1.45 \times 10^{19} \text{ n/cm}^2$ and the surveillance Capsule 284° calculated fluence was $1.45 \times 10^{19} \text{ n/cm}^2$. A brief summary of the Charpy V-notch testing results can be found in Section 1 and the updated capsule removal schedule can be found in Section 7. A supplement to this report is a credibility evaluation, which can be found in Appendix D, that shows the St. Lucie Unit 1 surveillance plate and weld data is credible.

1 SUMMARY OF RESULTS

The analysis of the reactor vessel materials contained in surveillance capsule 284° the third capsule to be removed from the St. Lucie Unit 1 reactor pressure vessel, led to the following conclusions: (General Note: Temperatures are reported to two significant digits only to match CVGraph output.)

- The capsule received an average fast neutron calculated fluence ($E > 1.0 \text{ MeV}$) of $1.45 \times 10^{19} \text{ n/cm}^2$ after 17.23 effective full power years (EFPY) of plant operation.
- Irradiation of the reactor vessel lower shell plate C-8-2 Charpy specimens, oriented with the longitudinal axis of the specimen parallel to the major working direction of the plate (longitudinal orientation), to $1.45 \times 10^{19} \text{ n/cm}^2$ ($E > 1.0 \text{ MeV}$) resulted in a 30 ft-lb transition temperature increase of 87.93°F and a 50 ft-lb transition temperature increase of 95.38°F. This results in an irradiated 30 ft-lb transition temperature of 95.18°F and an irradiated 50 ft-lb transition temperature of 130.62°F for the longitudinally oriented specimens
- Irradiation of the reactor vessel lower shell plate C-8-2 Charpy specimens, oriented with the longitudinal axis of the specimen normal to the major working direction of the plate (transverse orientation), to $1.45 \times 10^{19} \text{ n/cm}^2$ ($E > 1.0 \text{ MeV}$) resulted in a 30 ft-lb transition temperature increase of 84.99°F and a 50 ft-lb transition temperature increase of 97.55°F. This results in an irradiated 30 ft-lb transition temperature of 100.37°F and an irradiated 50 ft-lb transition temperature of 143.57°F for transversely oriented specimens.
- Irradiation of the weld metal Charpy specimens to $1.45 \times 10^{19} \text{ n/cm}^2$ ($E > 1.0 \text{ MeV}$) resulted in a 30 ft-lb transition temperature increase of 68.00°F and a 50 ft-lb transition temperature increase of 67.19°F. This results in an irradiated 30 ft-lb transition temperature of 10.01°F and an irradiated 50 ft-lb transition temperature of 31.58°F.
- Irradiation of the weld Heat-Affected-Zone (HAZ) metal Charpy specimens to $1.45 \times 10^{19} \text{ n/cm}^2$ ($E > 1.0 \text{ MeV}$) resulted in a 30 ft-lb transition temperature increase of 74.79°F and a 50 ft-lb transition temperature increase of 82.27°F. This results in an irradiated 30 ft-lb transition temperature of -4.87°F and an irradiated 50 ft-lb transition temperature of 44.91°F.
- The average upper shelf energy of the lower shell plate C-8-2 (longitudinal orientation) resulted in an average energy decrease of 29 ft-lb after irradiation to $1.45 \times 10^{19} \text{ n/cm}^2$ ($E > 1.0 \text{ MeV}$). This results in an irradiated average upper shelf energy of 110 ft-lb for the longitudinally oriented specimens.
- The average upper shelf energy of the lower shell plate C-8-2 (transverse orientation) resulted in an average energy decrease of 15 ft-lb after irradiation to $1.45 \times 10^{19} \text{ n/cm}^2$ ($E > 1.0 \text{ MeV}$). This results in an irradiated average upper shelf energy of 88 ft-lb for the transversely oriented specimens.
- The average upper shelf energy of the weld metal Charpy specimens resulted an average energy decrease of 34 ft-lb after irradiation to $1.45 \times 10^{19} \text{ n/cm}^2$ ($E > 1.0 \text{ MeV}$). Hence, this results in an irradiated average upper shelf energy of 110 ft-lb for the weld metal specimens.

- The average upper shelf energy of the weld HAZ metal Charpy specimens resulted an average energy decrease of 40 ft-lb after irradiation to $1.45 \times 10^{19} \text{ n/cm}^2$ ($E > 1.0 \text{ MeV}$). Hence, this results in an irradiated average upper shelf energy of 93 ft-lb for the weld HAZ metal.
- A comparison of the St. Lucie Unit 1 reactor vessel beltline material test results with the Regulatory Guide 1.99, Revision 2^[1], predictions led to the following conclusions:
 - The measured 30 ft-lb shift in transition temperature values for all the surveillance program materials (Weld and Plate) for capsule 284° is less than the Regulatory Guide 1.99, Revision 2, predictions.
 - The measured percent decrease in upper shelf energy of the Capsule 284° surveillance material is less than the Regulatory Guide 1.99, Revision 2, predictions.
- The peak calculated and best estimate end-of-license (32 EFPY) neutron fluence ($E > 1.0 \text{ MeV}$) at the core midplane for the St. Lucie Unit 1 reactor vessel using the Regulatory Guide 1.99, Revision 2 attenuation formula (ie. Equation # 3 in the guide; $f_{(\text{depth } x)} = f_{\text{surface}} * e^{(-0.24x)}$) is as follows:

<u>Calculated:</u>	Vessel inner radius*	=	$2.55 \times 10^{19} \text{ n/cm}^2$
	Vessel 1/4 thickness	=	$1.52 \times 10^{19} \text{ n/cm}^2$
	Vessel 3/4 thickness	=	$5.40 \times 10^{18} \text{ n/cm}^2$

<u>Best Estimate:</u>	Vessel inner radius*	=	$2.46 \times 10^{19} \text{ n/cm}^2$
	Vessel 1/4 thickness	=	$1.47 \times 10^{19} \text{ n/cm}^2$
	Vessel 3/4 thickness	=	$5.21 \times 10^{18} \text{ n/cm}^2$

- The credibility evaluation of the St. Lucie Unit 1 surveillance program presented in Appendix D of this report indicates that the surveillance results for lower shell plate C-8-2 and the weld metal are credible.
- All beltline materials exhibit a more than adequate upper shelf energy level for continued safe plant operation and are expected to maintain an upper shelf energy greater than 50 ft-lb throughout the life of the vessel (32 EFPY) as required by 10CFR50, Appendix G^[2].

2 INTRODUCTION

This report presents the results of the examination of the Capsule located at 284°, the third capsule to be removed from the reactor in the continuing surveillance program which monitors the effects of neutron irradiation on the St. Lucie Unit 1 reactor pressure vessel materials under actual operating conditions.

The surveillance program for the Florida Power and Light Company St. Lucie Unit 1 reactor pressure vessel materials was designed and recommended by Combustion Engineering. A description of the surveillance program and the preirradiation mechanical properties of the reactor vessel materials is presented in Reference 3. The surveillance program was planned to cover the 40-year design life of the reactor pressure vessel and was based on ASTM E185-70, "Standard Practice for conducting Surveillance for light-water cooled Nuclear Power Reactor Vessels". Capsule 284° was removed from the reactor after 17.23 EFPY of exposure and shipped to the Westinghouse Science and Technology Center Hot Cell Facility, where the postirradiation mechanical testing of the Charpy V-notch impact and tensile surveillance specimens was performed.

This report summarizes the testing of and the post-irradiation data obtained from surveillance capsule located at 284°, removed from the St. Lucie Unit 1 reactor vessel and discusses the analysis of the data.

3 BACKGROUND

The ability of the large steel pressure vessel containing the reactor core and its primary coolant to resist fracture constitutes an important factor in ensuring safety in the nuclear industry. The beltline region of the reactor pressure vessel is the most critical region of the vessel because it is subjected to significant fast neutron bombardment. The overall effects of fast neutron irradiation on the mechanical properties of low alloy, ferritic pressure vessel steels such as A533 Grade B Class 1 (base material of the Florida Power and Light Company St. Lucie Unit 1 reactor pressure vessel beltline) are well documented in the literature. Generally, low alloy ferritic materials show an increase in hardness and tensile properties and a decrease in ductility and toughness during high-energy irradiation.

A method for ensuring the integrity of reactor pressure vessels has been presented in "Fracture Toughness Criteria for Protection Against Failure," Appendix G to Section XI of the ASME Boiler and Pressure Vessel Code^[4]. The method uses fracture mechanics concepts and is based on the reference nil-ductility transition temperature (RT_{NDT}).

RT_{NDT} is defined as the greater of either the drop weight nil-ductility transition temperature (NDTT per ASTM E-208^[5]) or the temperature 60°F less than the 50 ft-lb (and 35-mil lateral expansion) temperature as determined from Charpy specimens oriented perpendicular (transverse) to the major working direction of the plate. The RT_{NDT} of a given material is used to index that material to a reference stress intensity factor curve (K_{Ia} curve) which appears in Appendix G to the ASME Code^[4]. The K_{Ia} curve is a lower bound of dynamic, crack arrest, and static fracture toughness results obtained from several heats of pressure vessel steel. When a given material is indexed to the K_{Ia} curve, allowable stress intensity factors can be obtained for this material as a function of temperature. Allowable operating limits can then be determined utilizing these allowable stress intensity factors. Note that Code Case N-640 now allows the use of the K_{Ic} curve as an alternative to the K_{Ia} curve.

RT_{NDT} and, in turn, the operating limits of nuclear power plants can be adjusted to account for the effects of radiation on the reactor vessel material properties. The changes in mechanical properties of a given reactor pressure vessel steel, due to irradiation, can be monitored by a reactor surveillance program, such as the St. Lucie Unit 1 reactor vessel radiation surveillance program^[6], in which a surveillance capsule is periodically removed from the operating nuclear reactor and the encapsulated specimens tested. The increase in the average Charpy V-notch 30 ft-lb temperature (ΔRT_{NDT}) due to irradiation is added to the initial RT_{NDT} , along with a margin (M) to cover uncertainties, to adjust the RT_{NDT} (ART) for radiation embrittlement. This ART ($RT_{NDT} \text{ initial} + M + \Delta RT_{NDT}$) is used to index the material to the K_{Ia} curve and, in turn, to set operating limits for the nuclear power plant that take into account the effects of irradiation on the reactor vessel materials.

4 DESCRIPTION OF PROGRAM

Six surveillance capsules for monitoring the effects of neutron exposure on the St. Lucie Unit 1 reactor pressure vessel core region (beltline) materials were inserted in the reactor vessel prior to initial plant start-up. The capsules were positioned in the reactor vessel between the thermal shield and the vessel wall at locations shown in Figure 4-1. The vertical center of the capsules is opposite the vertical center of the core.

Capsule 284° was removed after 17.23 effective full power years (EFPY) of plant operation. This capsule contained Charpy V-notch impact and tensile specimens made from reactor vessel lower shell course Plate C-8-2, submerged arc weld metal identical to the beltline region girth weld seam and heat-affected-zone (HAZ) metal. All HAZ specimens are obtained within the heat-affected-zone of Plate C-8-2. Standard Reference Material from HSST-01MY Plate was included in the program in addition to the reactor vessel materials, but not within capsule 284°.

Test specimens obtained from lower shell plate C-8-2 (after the thermal heat treatment and forming of the plate) was taken at least one plate thickness from the quenched ends of the plate. All test specimens were machined from the 1/4 thickness location of the plate after performing a simulated post-weld stress-relieving treatment on the test material and also from weld and HAZ metal of a stress-relieved weldment joining plates C-8-3 and C-8-1. All heat-affected-zone specimens were obtained from the weld heat-affected-zone of Plate C-8-2.

Charpy V-notch impact specimens from Plate C-8-2 were with the longitudinal axis of the specimen parallel to the major working direction of the plate (longitudinal orientation). Charpy V-notch impact specimens from Plate C-8-2 were with the transverse axis of the specimen perpendicular to the major working direction of the plate (transverse orientation). The Charpy V-notch specimens from the weld metal were machined with the longitudinal axis of the specimen transverse to the weld direction with the notch oriented in the direction of the weld.

Tensile specimens from Plate C-8-2 were machined in with the longitudinal axis of the specimen parallel to the major working direction of the plate (longitudinal orientation). Tensile specimens from the weld metal were oriented with the longitudinal axis of the specimen transverse to the weld direction.

Capsule 284° contained dosimeter wires of sulfur, iron, titanium, nickel (cadmium-shielded), aluminum-cobalt (cadmium-shielded and unshielded), copper (cadmium shielded) and uranium (cadmium-shielded and unshielded).

The capsule contained thermal monitors made from four low-melting-point eutectic alloys and sealed in glass capsules. These thermal monitors were used to define the maximum temperature attained by the test specimens during irradiation. The composition of the four eutectic alloys and their melting points are:

80% Au, 20% Sn	Melting Point 536°F (280°C)
90% Pb, 5% Sn, 5% Ag	Melting Point 558°F (292°C)
2.5% Ag, 97.5% Pb	Melting Point 580°F (304°C)
1.75% Ag, 0.75% Sn, 97.5% Ag	Melting Point 590°F (310°C)

The arrangement of the various mechanical test specimens, dosimeters and thermal monitors contained in capsule 284° is shown in Figure 4-2.

A typical St. Lucie Unit 1 surveillance capsule Charpy impact compartment assembly is shown in Figure 4-3.

A typical St. Lucie Unit 1 surveillance capsule tensile and flux-monitor compartment assembly is shown in Figure 4-4.

The heat treatment for the plate material consisted of austenitization at $1600^{\circ}\text{F} \pm 25^{\circ}\text{F}$ for 4 hours; water quenched and tempered at $1225^{\circ}\text{F} \pm 25^{\circ}\text{F}$ for 4 hours. After a 40 hour stress relief at $1150^{\circ}\text{F} \pm 25^{\circ}\text{F}$ the plates were furnace cooled to 600°F . The weldment received a final 41 hour and 45 minute stress relief at 1100 to 1150°F .

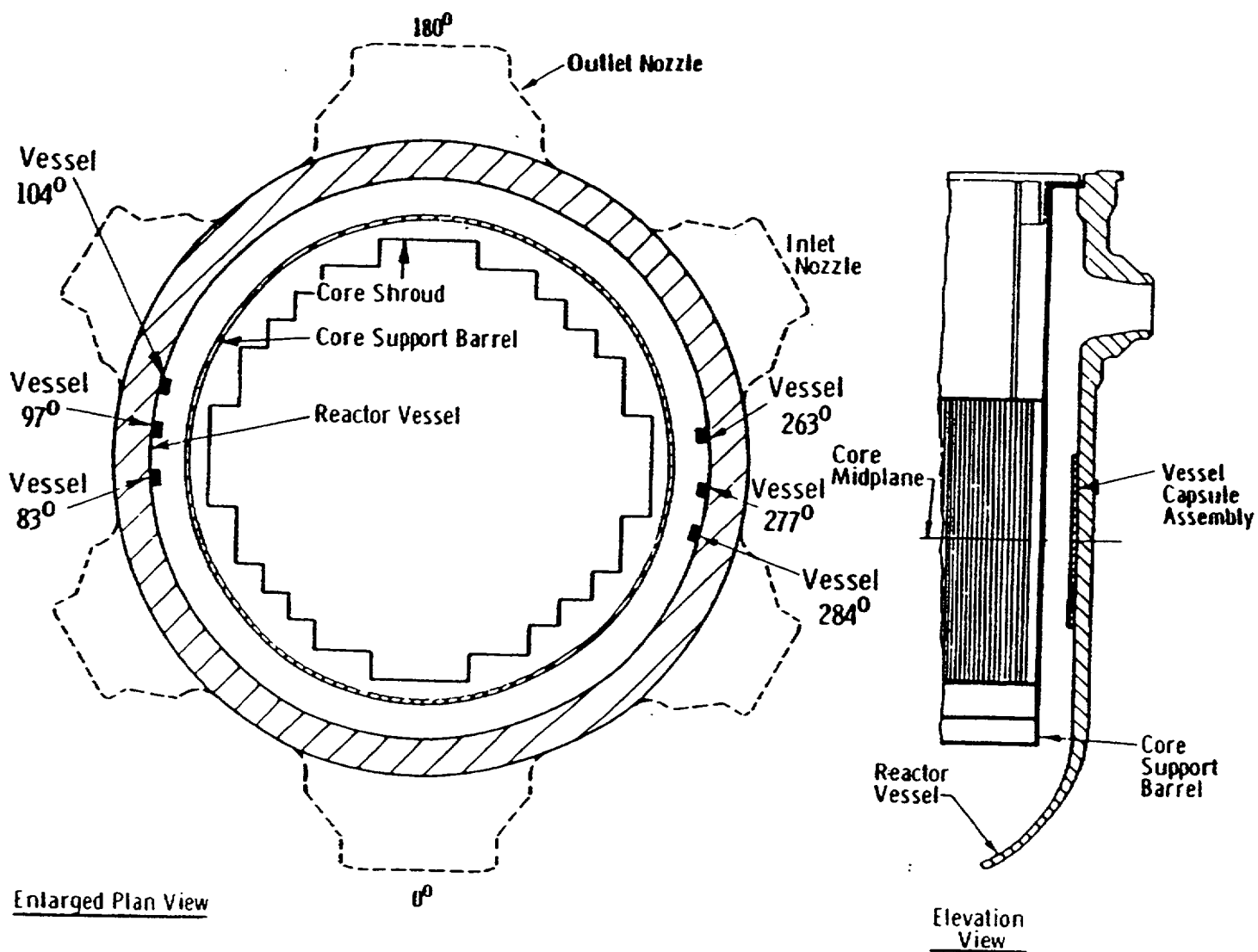


Figure 4-1. Arrangement of Surveillance Capsules in the St. Lucie Unit 1 Reactor Vessel

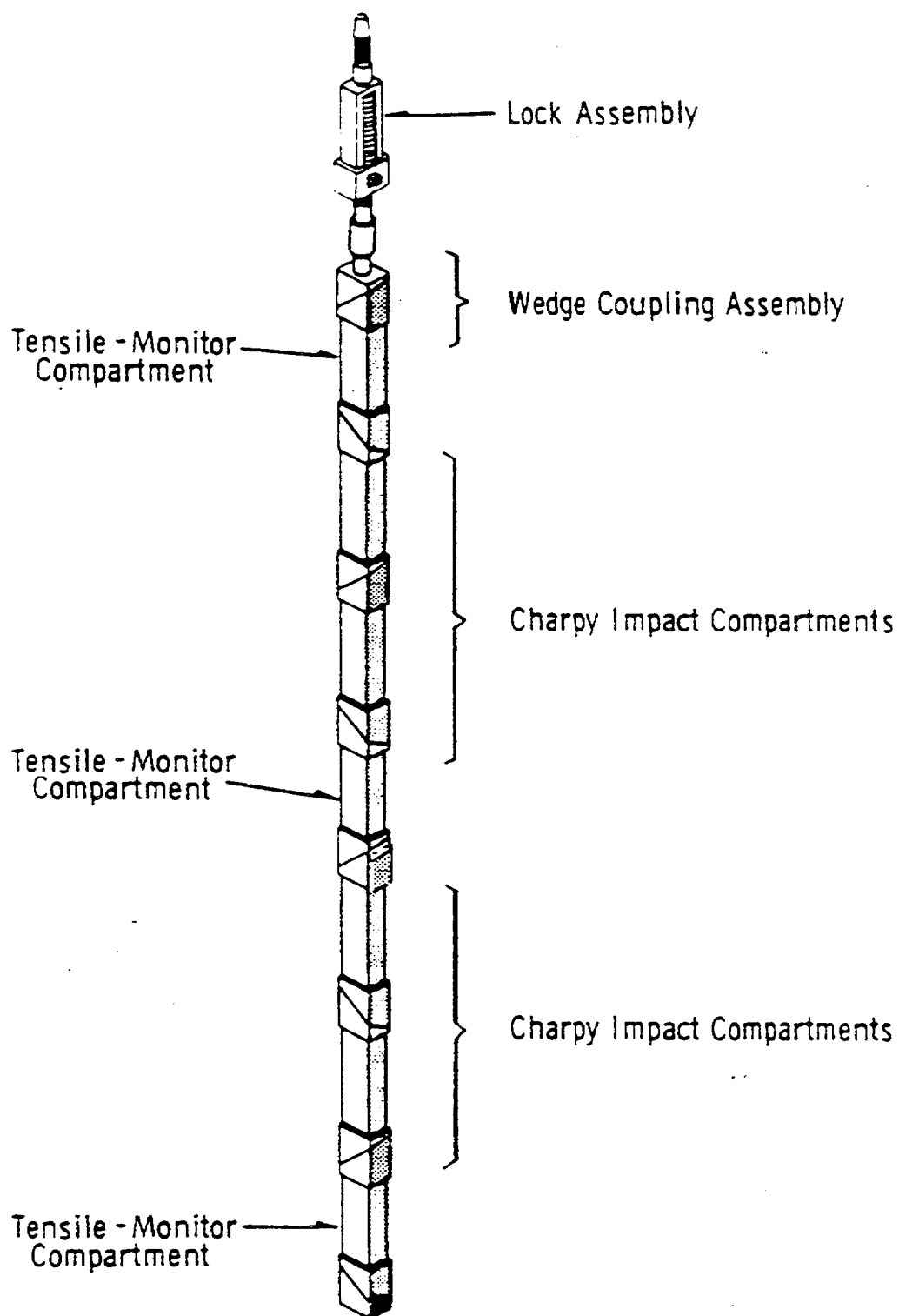


Figure 4-2 Typical St. Lucie Unit 1 Surveillance Capsule Assembly

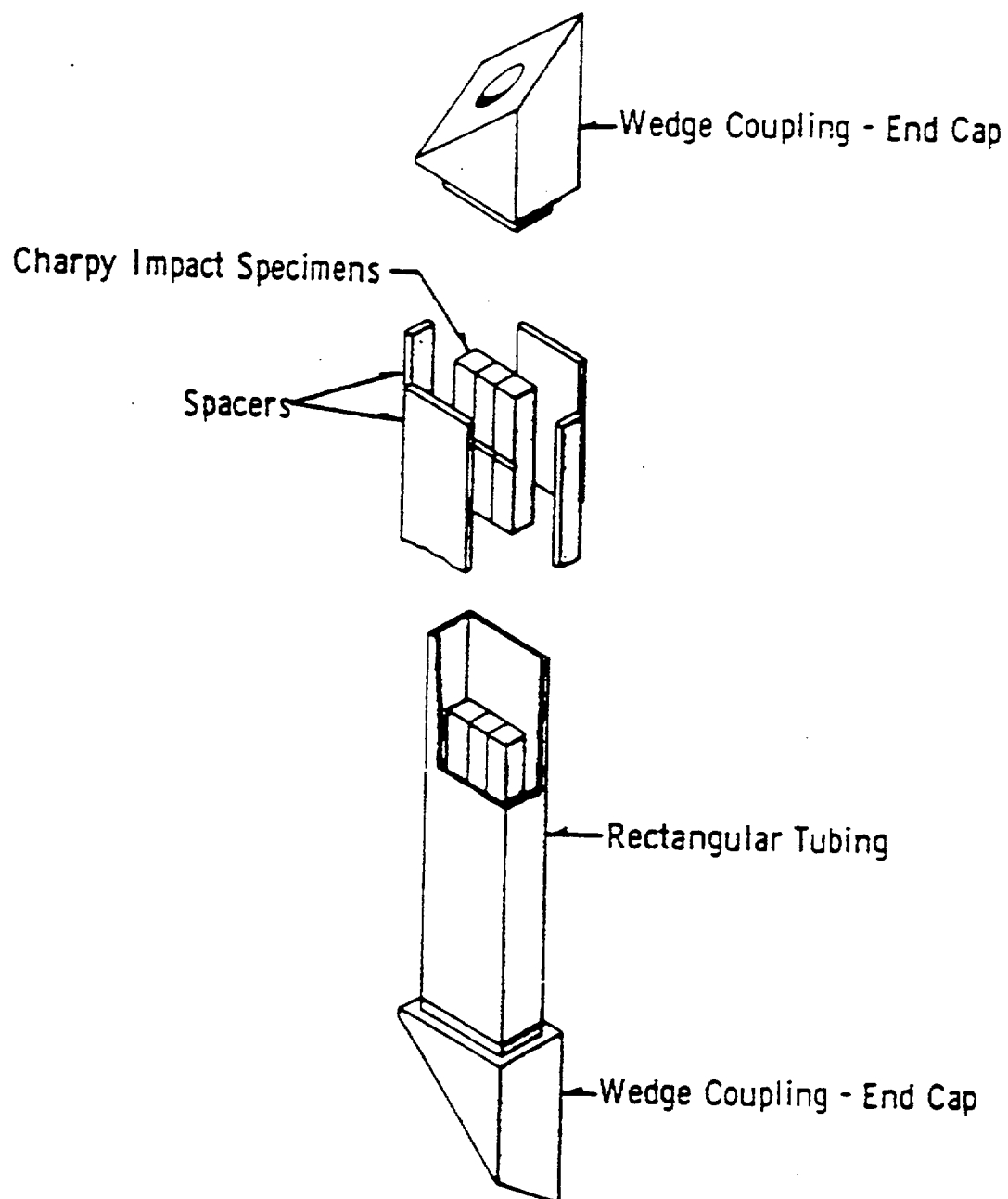


Figure 4-3 Typical St. Lucie Unit 1 Surveillance Capsule Charpy Impact Compartment Assembly

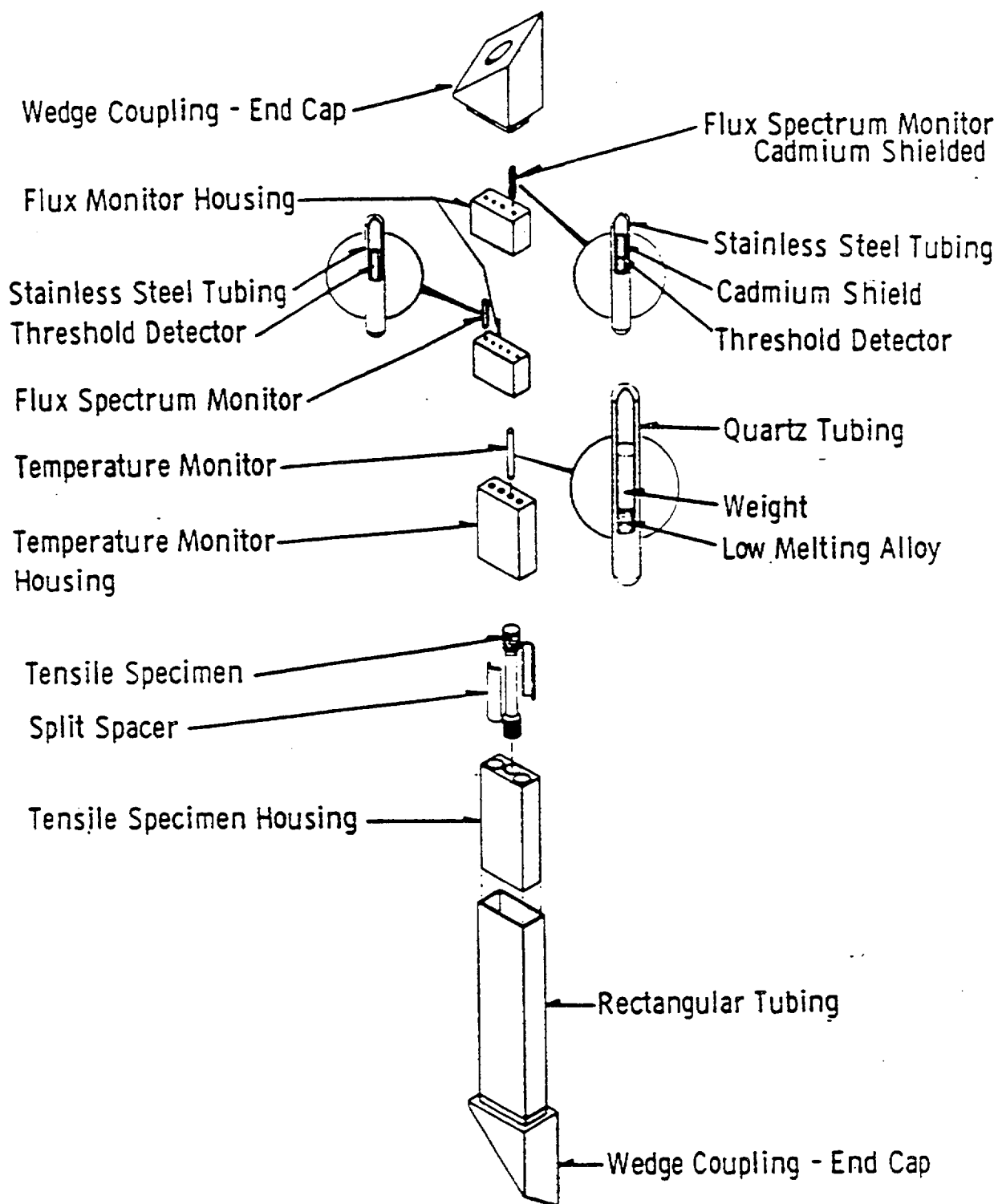


Figure 4-4 Typical St. Lucie Unit 1 Surveillance Capsule Tensile and Flux-Monitor Compartment Assembly

5 TESTING OF SPECIMENS FROM CAPSULE 284°

5.1 OVERVIEW

The post-irradiation mechanical testing of the Charpy V-notch impact specimens and tensile specimens was performed in the Remote Metallographic Facility (RMF) at the Westinghouse Science and Technology Center. Testing was performed in accordance with 10CFR50, Appendices G and H^[2], ASTM Specification E185-82^[7], and Westinghouse Procedure RMF 8402, Revision 2 as modified by Westinghouse RMF Procedures 8102, Revision 1, and 8103, Revision 1.

Upon receipt of the capsule at the hot cell laboratory, the specimens and spacer blocks were carefully removed, inspected for identification number, and checked against the master lists in TR-F-MCM-005^[3] and CENPD-39^[6]. No discrepancies were found.

Examination of the four low-melting, eutectic alloy thermal monitors indicated that the two lowest melting point monitors melted. Based on this examination, the maximum temperature to which the test specimens were exposed to was between 559°F and 579°F.

The Charpy impact tests were performed per ASTM Specification E23-98^[8] and RMF Procedure 8103, Revision 1, on a Tinius-Olsen Model 74, 358J machine. The tup (striker) of the Charpy impact test machine is instrumented with a GRC 930-I instrumentation system, feeding information into an IBM compatible computer. With this system, load-time and energy-time signals can be recorded in addition to the standard measurement of Charpy energy (E_D). From the load-time curve (Appendix A), the load of general yielding (P_{GY}), the time to general yielding (t_{GY}), the maximum load (P_M), and the time to maximum load (t_M) can be determined. Under some test conditions, a sharp drop in load indicative of fast fracture was observed. The load at which fast fracture was initiated is identified as the fast fracture load (P_F), and the load at which fast fracture terminated is identified as the arrest load (P_A). The energy at maximum load (E_M) was determined by comparing the energy-time record and the load-time record. The energy at maximum load is approximately equivalent to the energy required to initiate a crack in the specimen. Therefore, the propagation energy for the crack (E_p) is the difference between the total energy to fracture (E_D) and the energy at maximum load (E_M).

The yield stress (σ_Y) was calculated from the three-point bend formula having the following expression:

$$\sigma_Y = (P_{GY} * L) / [B * (W - a)^2 * C] \quad (1)$$

where: L = distance between the specimen supports in the impact machine
 B = the width of the specimen measured parallel to the notch
 W = height of the specimen, measured perpendicularly to the notch
 a = notch depth

The constant C is dependent on the notch flank angle (ϕ), notch root radius (ρ) and the type of loading (i.e., pure bending or three-point bending). In three-point bending, for a Charpy specimen in which $\phi = 45^\circ$ and $\rho = 0.010$ inch, Equation 1 is valid with $C = 1.21$. Therefore, (for $L = 4W$),

$$\sigma_y = (P_{GY} * L) / [B * (W - a)^2 * 1.21] = (3.33 * P_{GY} * W) / [B * (W - a)^2] \quad (2)$$

For the Charpy specimen, $B = 0.394$ inch, $W = 0.394$ inch and $a = 0.079$ inch. Equation 2 then reduces to:

$$\sigma_y = 33.3 * P_{GY} \quad (3)$$

where σ_y is in units of psi and P_{GY} is in units of lbs. The flow stress was calculated from the average of the yield and maximum loads, also using the three-point bend formula.

The symbol A in columns 4, 5, and 6 of Tables 5-5 through 5-8 is the cross-section area under the notch of the Charpy specimens:

$$A = B * (W - a) = 0.1241 \text{ sq. in.} \quad (4)$$

Percent shear was determined from post-fracture photographs using the ratio-of-areas methods in compliance with ASTM Specification A370-97^[9]. The lateral expansion was measured using a dial gage rig similar to that shown in the same specification.

Tensile tests were performed on a 20,000-pound Instron, split-console test machine (Model 1115) per ASTM Specification E8-99^[10] and E21-92^[11], and RMF Procedure 8102, Revision 1. All pull rods, grips, and pins were made of Inconel 718. The upper pull rod was connected through a universal joint to improve axiality of loading. The tests were conducted at a constant crosshead speed of 0.05 inches per minute throughout the test.

Extension measurements were made with a linear variable displacement transducer extensometer. The extensometer knife edges were spring-loaded to the specimen and operated through specimen failure. The extensometer gage length was 1.00 inch. The extensometer is rated as Class B-2 per ASTM E83-93^[12].

Elevated test temperatures were obtained with a three-zone electric resistance split-tube furnace with a 9-inch hot zone. All tests were conducted in air. Because of the difficulty in remotely attaching a thermocouple directly to the specimen, the following procedure was used to monitor specimen temperatures. Chromel-Alumel thermocouples were positioned at the center and at each end of the gage section of a dummy specimen and in each tensile machine gripper. In the test configuration, with a slight load on the specimen, a plot of specimen temperature versus upper and lower tensile machine gripper and controller temperatures was developed over the range from room temperature to 550°F. During the actual testing, the grip temperatures were used to obtain desired specimen temperatures. Experiments have indicated that this method is accurate to $\pm 2^\circ\text{F}$.

The yield load, ultimate load, fracture load, total elongation, and uniform elongation were determined directly from the load-extension curve. The yield strength, ultimate strength, and fracture strength were calculated using the original cross-sectional area. The final diameter and final gage length were determined from post-fracture photographs. The fracture area used to calculate the fracture stress (true stress at fracture) and percent reduction in area was computed using the final diameter measurement.

5.2 CHARPY V-NOTCH IMPACT TEST RESULTS

The results of the Charpy V-notch impact tests performed on the various materials contained in capsule 284°, which received a fluence of 1.45×10^{19} n/cm² ($E > 1.0$ MeV) in 17.23 EFPY of operation, are presented in Tables 5-1 through 5-8 and are compared with unirradiated results as shown in Figures 5-1 through 5-12.

The transition temperature increases and upper shelf energy decreases for the capsule 284° materials are summarized in Table 5-9. These results led to the following conclusions:

Irradiation of the reactor vessel lower shell plate C-8-2 Charpy specimens, oriented with the longitudinal axis of the specimen parallel to the major working direction of the plate (longitudinal orientation), to 1.45×10^{19} n/cm² ($E > 1.0$ MeV) resulted in a 30 ft-lb transition temperature increase of 87.93°F and a 50 ft-lb transition temperature increase of 95.38°F. This results in an irradiated 30 ft-lb transition temperature of 95.18°F and an irradiated 50 ft-lb transition temperature of 130.62°F for the longitudinally oriented specimens.

Irradiation of the reactor vessel lower shell plate C-8-2 Charpy specimens, oriented with the longitudinal axis of the specimen normal to the major working direction of the plate (transverse orientation), to 1.45×10^{19} n/cm² ($E > 1.0$ MeV) resulted in a 30 ft-lb transition temperature increase of 84.99°F and a 50 ft-lb transition temperature increase of 97.55°F. This results in an irradiated 30 ft-lb transition temperature of 100.37°F and an irradiated 50 ft-lb transition temperature of 143.57°F for transversely oriented specimens.

Irradiation of the weld metal Charpy specimens to 1.45×10^{19} n/cm² ($E > 1.0$ MeV) resulted in a 30 ft-lb transition temperature increase of 68.00°F and a 50 ft-lb transition temperature increase of 67.19°F. This results in an irradiated 30 ft-lb transition temperature of 10.01°F and an irradiated 50 ft-lb transition temperature of 31.58°F.

Irradiation of the weld Heat-Affected-Zone (HAZ) metal Charpy specimens to 1.45×10^{19} n/cm² ($E > 1.0$ MeV) resulted in a 30 ft-lb transition temperature increase of 74.79°F and a 50 ft-lb transition temperature increase of 82.27°F. This results in an irradiated 30 ft-lb transition temperature of -4.87°F and an irradiated 50 ft-lb transition temperature of 44.91°F.

The average upper shelf energy of the lower shell plate C-8-2 (longitudinal orientation) resulted in an average energy decrease of 29 ft-lb after irradiation to 1.45×10^{19} n/cm² ($E > 1.0$ MeV). This results in an irradiated average upper shelf energy of 110 ft-lb for the longitudinally oriented specimens.

The average upper shelf energy of the lower shell plate C-8-2 (transverse orientation) resulted in an average energy decrease of 15 ft-lb after irradiation to 1.45×10^{19} n/cm² ($E > 1.0$ MeV). This results in an irradiated average upper shelf energy of 88 ft-lb for the transversely oriented specimens.

The average upper shelf energy of the weld metal Charpy specimens resulted an average energy decrease of 34 ft-lb after irradiation to 1.45×10^{19} n/cm² ($E > 1.0$ MeV). Hence, this results in an irradiated average upper shelf energy of 110 ft-lb for the weld metal specimens.

The average upper shelf energy of the weld HAZ metal Charpy specimens resulted an average energy decrease of 40 ft-lb after irradiation to 1.45×10^{19} n/cm² ($E > 1.0$ MeV). Hence, this results in an irradiated average upper shelf energy of 93 ft-lb for the weld HAZ metal.

A comparison, as presented in Table 5-10, of the St. Lucie Unit 1 reactor vessel beltline material test results with the Regulatory Guide 1.99, Revision 2^[1], predictions led to the following conclusions:

- The measured 30 ft-lb shift in transition temperature values for all the surveillance program materials (Weld and Plate) for capsule 284° is less than the Regulatory Guide 1.99, Revision 2, predictions.
- The measured percent decrease in upper shelf energy of the Capsule 284° surveillance material is less than the Regulatory Guide 1.99, Revision 2, predictions.
- Further comparisons are made in the credibility evaluation presented in Appendix D

The fracture appearance of each irradiated Charpy specimen from the various surveillance capsule 284° materials is shown in Figures 5-13 through 5-16 and show an increasingly ductile or tougher appearance with increasing test temperature.

All beltline materials exhibit a more than adequate upper shelf energy level for continued safe plant operation and are expected to maintain an upper shelf energy of no less than 50 ft-lb throughout the life of the vessel (32 EFY) as required by 10CFR50, Appendix G.

The load-time records for individual instrumented Charpy specimen tests are shown in Appendix A.

The Charpy V-notch data presented in this report is based on a re-plot of all capsule data using CVGRAPH, Version 4.1, which is a hyperbolic tangent curve-fitting program. Hence, Appendix C contains a comparison of the Charpy V-notch shift results for each surveillance material (hand-fitting versus hyperbolic tangent curve-fitting). Additionally, Appendix B presents the CVGRAPH, Version 4.1, Charpy V-notch plots and the program input data.

5.3 TENSILE TEST RESULTS

The results of the tensile tests performed on the various materials contained in capsule 284° irradiated to 1.45×10^{19} n/cm² ($E > 1.0$ MeV) are presented in Table 5-11 and are compared with unirradiated results as shown in Figures 5-17 through 5-19.

The results of the tensile tests performed on the lower shell plate C-8-2 (longitudinal orientation) indicated that irradiation to 1.45×10^{19} n/cm² ($E > 1.0$ MeV) caused an approximate increase of 9 to 11 ksi in the 0.2 percent offset yield strength and approximately a 9 to 12 ksi increase in the ultimate tensile strength when compared to unirradiated data^[1] (Figure 5-17).

The results of the tensile tests performed on the surveillance weld metal indicated that irradiation to 1.45×10^{19} n/cm² ($E > 1.0$ MeV) caused a 10 to 17 ksi increase in the 0.2 percent offset yield strength and a 7 to 9 ksi increase in the ultimate tensile strength when compared to unirradiated data (Figure 5-18).

The results of the tensile tests performed on the surveillance HAZ metal indicated that irradiation to 1.45×10^{19} n/cm² ($E > 1.0$ MeV) caused a 12 to 16 ksi increase in the 0.2 percent offset yield strength and a 10 to 13 ksi increase in the ultimate tensile strength when compared to unirradiated data (Figure 5-19).

The fractured tensile specimens for the lower shell plate C-8-2 material are shown in Figure 5-20, while the fractured tensile specimens for the surveillance weld metal and heat-affected-zone material are shown in Figures 5-21 and 5-22, respectively.

The engineering stress-strain curves for the tensile tests are shown in Figures 5-23 through 5-25.

Table 5-1 Charpy V-notch Data for the St. Lucie Unit 1 Lower Shell Plate C-8-2 Irradiated to a Fluence of 1.45×10^{19} n/cm² (E > 1.0 MeV) (Longitudinal Orientation)

Sample Number	Temperature		Impact Energy		Lateral Expansion		Shear
	F	C	ft-lbs	Joules	mils	mm	%
155	5	-15	8	11	3	0.08	3
136	25	-4	12	16	12	0.30	10
14M	50	10	7	9	9	0.23	5
145	72	22	16	22	9	0.23	15
16D	80	27	19	26	14	0.36	20
146	100	38	40	54	28	0.71	30
164	120	49	55	75	40	1.02	35
157	135	57	49	66	32	0.81	40
143	150	66	56	76	40	1.02	40
117	200	93	88	119	59	1.50	70
14U	275	135	107	145	78	1.98	100
14E	325	163	112	152	75	1.91	100

Table 5-2 Charpy V-notch Data for the St. Lucie Unit 1 Lower Shell Plate C-8-2 Irradiated to a Fluence of 1.45×10^{19} n/cm² (E> 1.0 MeV) (Transverse Orientation)

Sample Number	Temperature		Impact Energy		Lateral Expansion		Shear
	F	C	ft-lbs	Joules	mils	mm	%
252	10	-12	15	20	10	0.25	10
25M	50	10	14	19	11	0.28	10
25L	90	32	28	38	24	0.61	20
25C	100	38	27	37	19	0.48	20
26C	115	46	37	50	24	0.61	20
26A	125	52	42	57	28	0.71	25
25J	135	57	37	50	34	0.86	30
251	150	66	57	77	43	1.09	40
253	175	79	66	89	49	1.24	50
26B	220	104	77	104	60	1.52	95
25P	275	135	92	125	69	1.75	100
24Y	325	163	83	113	62	1.57	100

Table 5-3 Charpy V-notch Data for the St. Lucie Unit 1 Surveillance Weld Metal Irradiated to a Fluence of 1.45×10^{19} n/cm² (E > 1.0 MeV)

Sample Number	Temperature		Impact Energy		Lateral Expansion		Shear
	F	C	ft-lbs	Joules	mils	mm	%
31C	-50	-46	5	7	4	0.10	10
36L	-10	-23	12	16	8	0.20	15
343	0	-18	26	35	20	0.51	20
325	10	-12	18	24	13	0.33	20
317	15	-9	36	49	25	0.64	30
33K	25	-4	34	46	26	0.66	40
35J	30	-1	63	85	46	1.17	50
367	40	4	65	88	47	1.19	50
31D	100	38	87	118	63	1.60	85
34M	150	66	107	145	75	1.91	95
32T	200	93	115	156	83	2.11	100
353	250	121	107	145	81	2.06	100

Table 5-4 Charpy V-notch Data for the St. Lucie Unit 1 Heat Affected Zone Metal Irradiated to a Fluence of 1.45×10^{19} n/cm² (E> 1.0 MeV)

Sample Number	Temperature		Impact Energy		Lateral Expansion		Shear %
	F	C	ft-lbs	Joules	mils	mm	
45L	-40	-40	9	12	6	0.15	20
46C	-5	-21	21	28	20	0.51	40
46B	10	-12	31	42	20	0.51	30
421	20	-7	55	75	37	0.94	50
45M	30	-1	41	56	35	0.89	60
461	40	4	62	84	40	1.02	65
463	60	16	36	49	30	0.76	40
46D	72	22	85	115	57	1.45	90
45U	100	38	73	99	49	1.24	75
45T	135	57	57	77	41	1.04	60
462	200	93	79	107	59	1.50	95
464	250	121	107	145	74	1.88	100

**Table 5-5 Instrumented Charpy Impact Test Results for the St. Lucie Unit 1 Lower Shell Plate C-8-2
Irradiated to a Fluence of 1.45×10^{19} n/cm² (E>1.0 MeV) (Longitudinal Orientation)**

Sample No.	Test Temp. (°F)	Charpy Energy E _D (ft-lb)	Normalized Energies (ft-lb/in ²)			Yield Load P _{GY} (lb)	Time to Yield t _{GY} (msec)	Max. Load P _M (lb)	Time to Max. T _m (msec)	Fast Fract. Load P _F (lb)	Arrest Load P _A (lb)	Yield Stress S _Y (ksi)	Flow Stress (ksi)
			Charpy E _D /A	Max. E _M /A	Prop. E _P /A								
155	5	8	64	33	32	3435	0.16	3452	0.16	3435	0	114	115
136	25	12	97	56	40	4133	0.17	4340	0.20	4340	0	138	141
14M	50	7	56	28	29	3138	0.15	3138	0.15	3138	0	104	104
145	72	16	129	69	59	4025	0.17	4395	0.22	4395	0	134	140
16D	80	19	153	75	78	3764	0.17	4298	0.24	4156	82	125	134
146	100	40	322	239	83	3974	0.17	4791	0.51	4738	166	132	146
164	120	55	443	337	106	3906	0.17	4854	0.68	4732	234	130	146
157	135	49	395	240	155	3950	0.17	4786	0.52	4641	682	132	145
143	150	56	451	333	118	3931	0.17	4848	0.67	4647	866	131	146
117	200	88	709	330	379	3891	0.17	4819	0.67	4141	2230	130	145
14U	275	107	862	311	552	3262	0.17	4471	0.69	n/a	n/a	109	129

**Table 5-6 Instrumented Charpy Impact Test Results for the St. Lucie Unit 1 Lower Shell Plate C-8-2
Irradiated to a Fluence of 1.45×10^{19} n/cm² (E>1.0 MeV) (Transverse Orientation)**

Sample No.	Test Temp. (°F)	Charpy Energy E _D (ft-lb)	Normalized Energies (ft-lb/in ²)			Yield Load P _{GY} (lb)	Time to Yield t _{GY} (msec)	Max. Load P _M (lb)	Time to Max. T _m (msec)	Fast Fract. Load P _F (lb)	Arrest Load P _A (lb)	Yield Stress S _Y (ksi)	Flow Stress (ksi)
			Charpy E _D /A	Max. E _M /A	Prop. E _p /A								
252	10	15	121	68	53	4076	0.17	4580	0.22	4563	0	136	144
25M	50	14	113	64	49	4244	0.17	4571	0.21	4571	0	141	147
25L	90	28	226	146	80	3683	0.17	4412	0.37	4403	372	123	135
25C	100	27	218	70	148	4124	0.17	4427	0.22	4389	674	137	142
26C	115	37	298	152	146	3746	0.17	4389	0.38	4378	446	125	135
26A	125	42	338	201	138	3861	0.17	4592	0.46	4530	908	129	141
25J	135	37	298	222	76	3807	0.17	4633	0.5	4606	1022	127	141
251	150	57	459	234	225	3921	0.17	4711	0.51	4592	2560	131	144
253	175	66	532	248	284	3986	0.17	4910	0.52	4649	2294	133	148
26B	220	77	620	233	387	3471	0.17	4558	0.54	4407	3181	116	134
25P	275	92	741	307	435	3590	0.17	4595	0.65	n/a	n/a	120	136
24Y	325	83	669	231	438	3537	0.17	4455	0.53	n/a	n/a	118	133

**Table 5-7 Instrumented Charpy Impact Test Results for the St. Lucie Unit 1 Surveillance Weld Metal
Irradiated to a Fluence of 1.45×10^{19} n/cm² (E>1.0 MeV)**

Sample No.	Test Temp. (°F)	Charpy Energy E _D (ft-lb)	Normalized Energies (ft-lb/in ²)			Yield Load P _{GY} (lb)	Time to Yield t _{GY} (msec)	Max. Load P _M (lb)	Time to Max. T _m (msec)	Fast Fract. Load P _F (lb)	Arrest Load P _A (lb)	Yield Stress S _Y (ksi)	Flow Stress (ksi)
			Charpy E _D /A	Max. E _M /A	Prop. E _P /A								
31C	-50	5	40	17	23	2056	0.15	2231	0.13	2056	0	68	71
36L	-10	12	97	38	59	3739	0.17	3757	0.17	3739	291.38	125	125
343	0	26	209	72	138	4130	0.17	4522	0.23	4393	128	138	144
325	10	18	145	69	76	4209	0.17	4655	0.22	4620	126	140	148
317	15	36	290	213	77	4350	0.17	4779	0.45	4773	321	145	152
33K	25	34	274	69	205	4193	0.17	4536	0.22	4295	881	140	145
35J	30	63	508	242	266	4183	0.17	4642	0.52	4417	492	139	147
367	40	65	524	237	286	3904	0.17	4449	0.53	4054	1015	130	139
31D	100	87	701	321	380	3915	0.17	4589	0.67	3786	2385	130	142
34M	150	107	862	314	549	3687	0.17	4381	0.69	3200	2328	123	134
32T	200	115	927	315	611	3279	0.17	4371	0.71	n/a	n/a	109	127
353	250	107	862	295	567	3342	0.17	4172	0.69	n/a	n/a	111	125

**Table 5-8 Instrumented Charpy Impact Test Results for the St. Lucie Unit 1 Heat Affected Zone Material
Irradiated to a Fluence of 1.45×10^{19} n/cm² (E>1.0 MeV)**

Sample No.	Test Temp. (°F)	Charpy Energy E _D (ft-lb)	Normalized Energies (ft-lb/in ²)			Yield Load P _{GY} (lb)	Time to Yield t _{GY} (msec)	Max. Load P _M (lb)	Time to Max. T _m (msec)	Fast Fract. Load P _F (lb)	Arrest Load P _A (lb)	Yield Stress S _Y (ksi)	Flow Stress (ksi)
			Charpy E _D /A	Max. E _M /A	Prop. E _p /A								
45L	-40	9	73	31	41	3411	0.16	3420	0.16	3411	108	114	114
46C	-5	21	169	73	96	4445	0.17	4882	0.22	4677	1497	148	155
46B	10	31	250	180	70	4213	0.18	4648	0.41	4635	467	140	148
421	20	55	443	254	189	4268	0.17	4843	0.52	4671	677	142	152
45M	30	41	330	72	259	4296	0.17	4661	0.22	4356	2461	143	149
461	40	62	500	249	250	4123	0.17	4749	0.53	4579	1924	137	148
463	60	36	290	70	220	4198	0.17	4574	0.22	4367	1486	140	146
46D	72	85	685	353	332	4187	0.17	4920	0.69	4738	3500	139	152
45U	100	73	588	328	260	4030	0.17	4750	0.67	4260	1516	134	146
45T	135	57	459	243	217	4029	0.17	4686	0.52	4151	1826	134	145
462	200	79	637	315	322	3540	0.17	4491	0.69	4262	3189	118	134
464	250	107	862	324	539	3695	0.17	4653	0.68	n/a	n/a	123	139

Table 5-9 Effect of Irradiation to 1.45×10^{19} n/cm² (E>1.0 MeV) on the Notch Toughness Properties of the St. Lucie Unit 1 Reactor Vessel Surveillance Materials

Material	Average 30 (ft-lb) ^(a) Transition Temperature (°F)			Average 35 mil Lateral ^(b) Expansion Temperature (°F)			Average 50 ft-lb ^(a) Transition Temperature (°F)			Average Energy Absorption ^(a) at Full Shear (ft-lb)		
	Unirradiated	Irradiated	ΔT	Unirradiated	Irradiated	ΔT	Unirradiated	Irradiated	ΔT	Unirradiated	Irradiated	ΔE
Lower Shell Plate C-8-2 (Longitudinal)	7.25	95.18	87.93	35.58	131.61	96.03	35.23	130.62	95.38	139	110	-29
Lower Shell Plate C-8-2 (Transverse)	15.37	100.37	84.99	44.98	136.08	91.1	46.01	143.57	97.55	103	88	-15
Weld Metal	-57.99	10.01	68	-32.8	28.64	61.44	-35.6	31.58	67.19	144	110	-34
HAZ Metal	-79.66	-4.87	74.79	-22.74	42.01	64.76	-37.36	44.91	82.27	133	93	-40

- a. "Average" is defined as the value read from the curve fit through the data points of the Charpy tests (see Figures 5-1, 5-4, 5-7 and 5-10).
- b. "Average" is defined as the value read from the curve fit through the data points of the Charpy tests (see Figures 5-2, 5-5, 5-8 and 5-11)

Table 5-10 Comparison of the St. Lucie Unit 1 Surveillance Material 30 ft-lb Transition Temperature Shifts and Upper Shelf Energy Decrease with Regulatory Guide 1.99, Revision 2, Predictions

Material	Capsule	Fluence ($\times 10^{19}$ n/cm ²) ^(a)	30 ft-lb Transition Temperature Shift			Upper Shelf Energy Decrease	
			Predicted (°F) ^(d)	Predicted (°F) ^(e)	Measured (°F)	Predicted (%) ^(b, d)	Measured (%)
Lower Shell Plate C-8-2 (Longitudinal)	97°	0.591	88.6	65.3	68.7	21	23
	104°	0.918	105.8	78.0	79.87	24	17
	284°	1.45	119.2	87.9	87.93	27	21
Lower Shell Plate C-8-2 (Transverse)	97°	0.591	88.6	65.3	63.83	21	24
	104°	0.918	105.8	78.0	N/A ^(c)	24	N/A ^(c)
	284°	1.45	119.2	87.9	84.99	27	15
Surveillance Program Weld Metal	97°	0.591	87.1	57.7	72.34	32	31
	104°	0.918	104.0	68.9	67.4	37	25
	284°	1.45	117.3	77.7	68.0	42	24
Heat Affected Zone Material	97°	0.591	---	---	19.48	---	14
	104°	0.918	---	---	59.8	---	22
	284°	1.45	---	---	74.79	---	30

Notes:

- (a) Calculated Fluences from capsule 284° dosimetry analysis results ($E > 1.0$ MeV)
- (b) From Figure 2 of Regulatory Guide 1.99, Revision 2, using the Cu wt. Percent and capsule fluence values. See note (d).
- (c) No Transverse Material in Capsule 104°
- (d) The Lower Shell Plate weight percent copper/nickel was 0.15 and 0.57, while the surveillance weld weight percent copper/nickel was 0.23 and 0.07. The copper and nickel values were used to determine the chemistry factor, which in turn is used to calculate the predicted ΔRT_{NDT} .
- (e) Based on Reg. Guide 1.99, Rev. 2, methodology using chemistry factor calculated from Surveillance data (Plate CF = 79.9, Weld CF = 70.6). See credibility evaluation in Appendix D.

Table 5-11 Tensile Specimens From Lower Shell Course Plate C-8-2, Weld, and Heat Affected Zone Material

Sample		Test	0.2% Yield	Ultimate	Fracture	Fracture	Fracture	Uniform	Total	Reduction
Number	Material	Temperature	Strength	Strength	Load	Stress	Strength	Elongation	Elongation	in Area
		(F)	(ksi)	(ksi)	(kip)	(ksi)	(ksi)	(%)	(%)	(%)
1J4	PLATE	125	82.5	103.3	3.45	173.6	70.2	11.2	23.6	60
1JL	PLATE	250	77.4	98.4	3.23	192.8	65.7	10.7	23.1	66
1JM	PLATE	550	73.3	98.6	3.58	167.4	72.9	10.7	22.2	56
3J2	WELD	35	82.5	97.4	3.08	202.9	62.7	12.9	28.4	69
3JJ	WELD	150	78.9	91.6	2.90	173.2	59.1	12.0	25.9	66
3JY	WELD	550	79.5	93	3.54	176.2	72.2	11.8	22.7	59
4KJ	HAZ	72	83	99.4	3.33	193.6	67.9	9.0	30.6	65
4KK	HAZ	225	75.4	91.5	3.14	166.6	64	7.8	27.0	62
4KY	HAZ	550	74.9	94.4	3.48	113.1	71	10.1	13.8	37

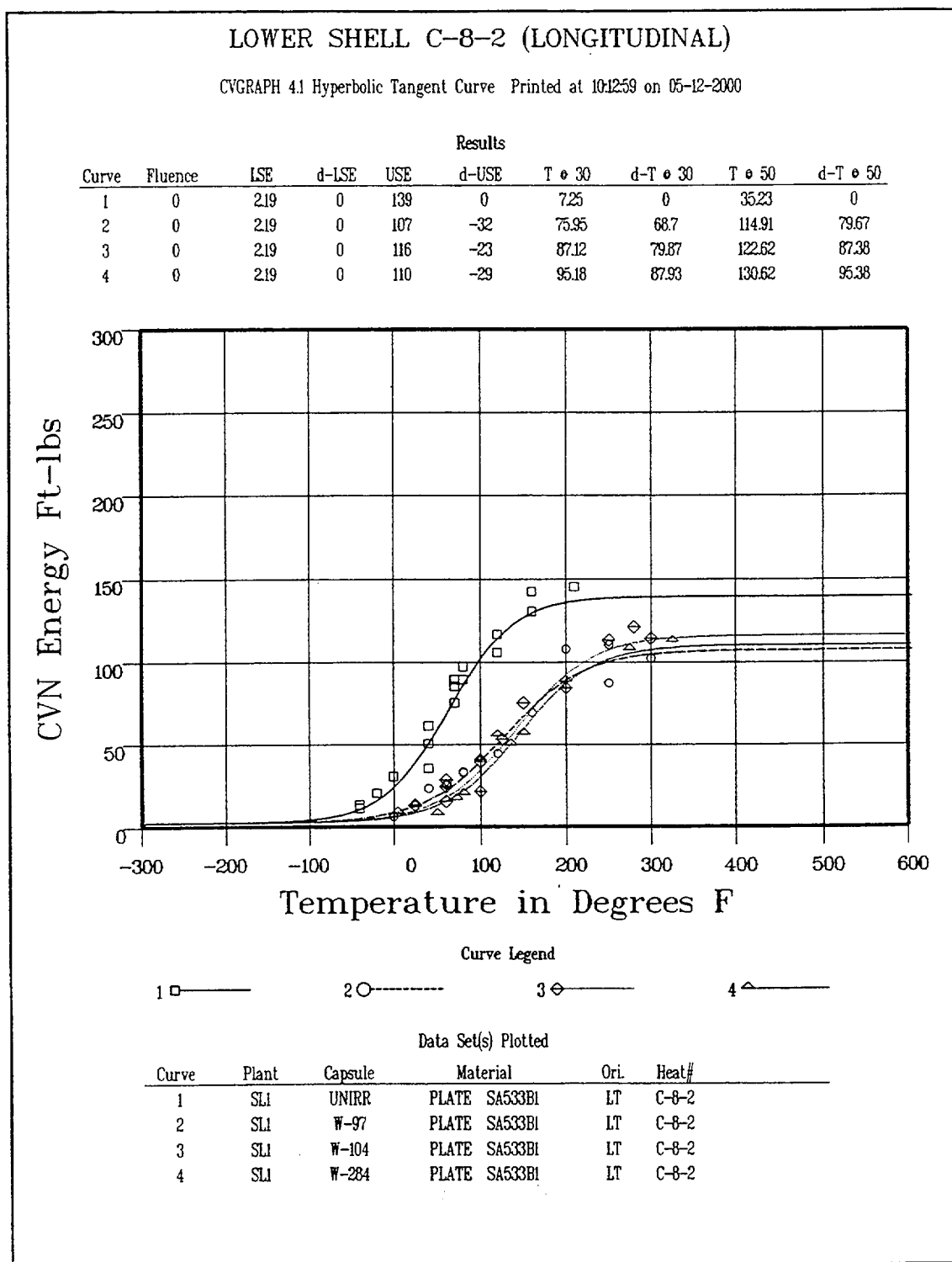


**Figure 5-1 Charpy V-Notch Impact Energy vs. Temperature for St. Lucie Unit 1 Reactor Vessel
Lower Shell Plate C-8-2 (Longitudinal Orientation)**

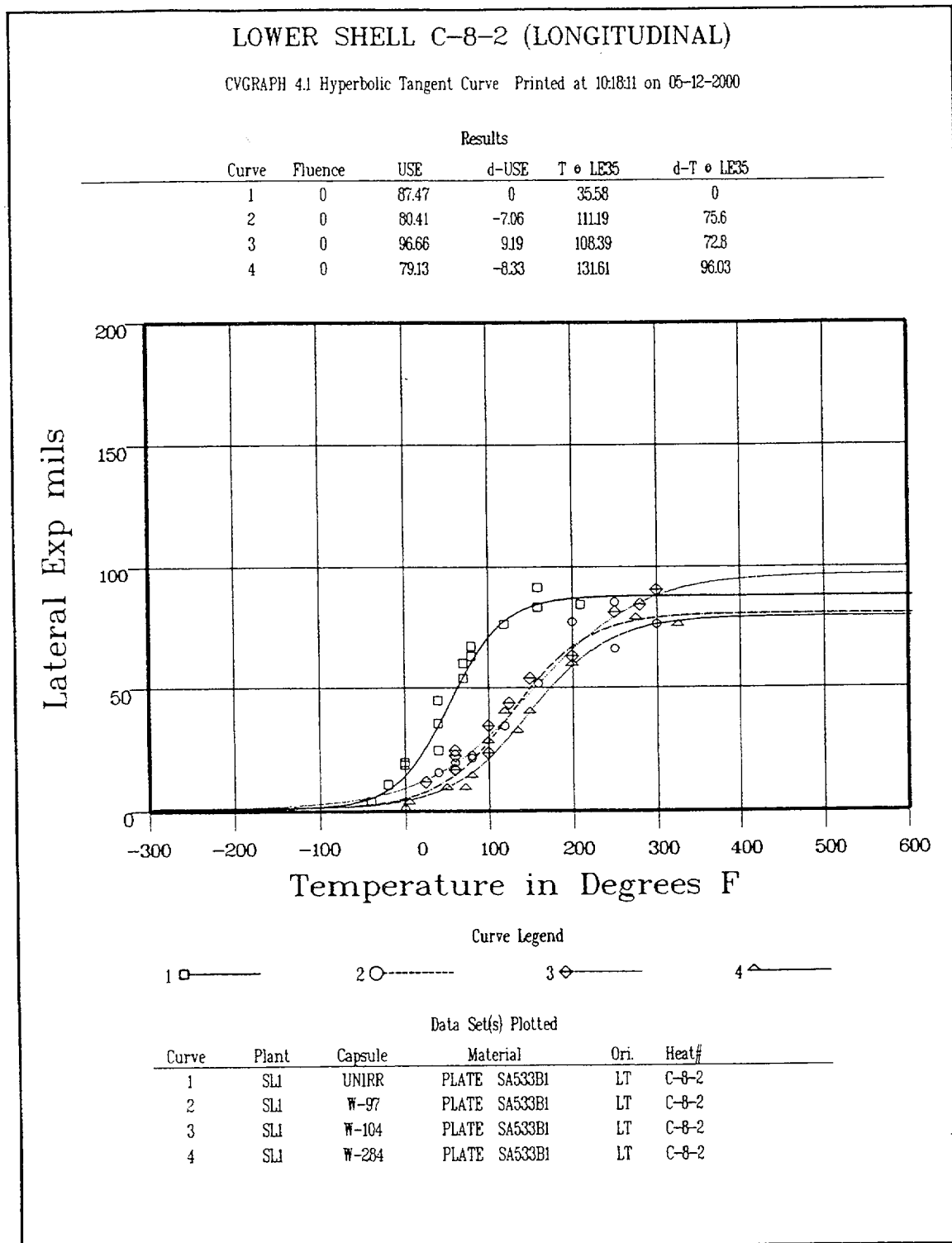
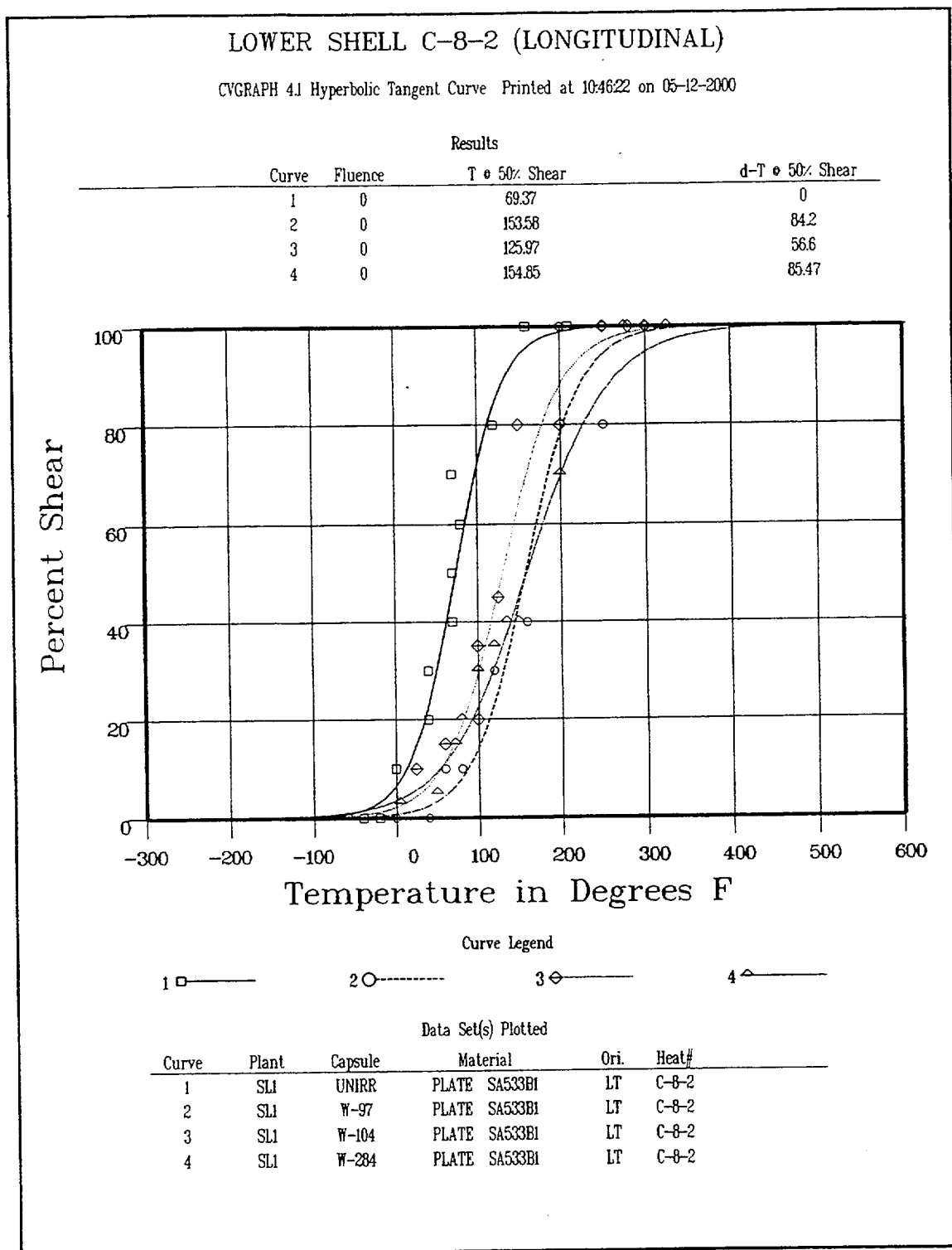
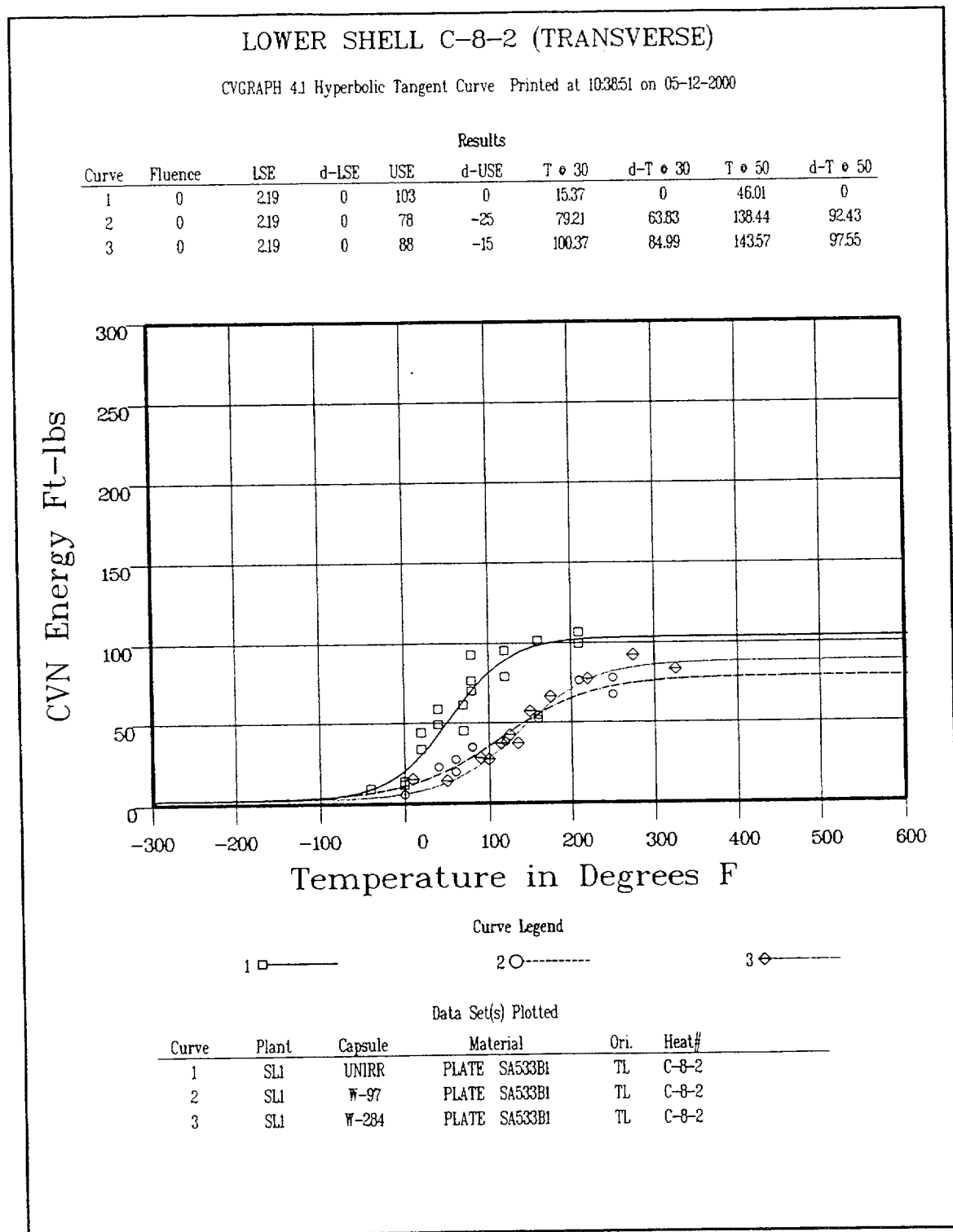


Figure 5-2 Charpy V-Notch Lateral Expansion vs. Temperature for St. Lucie Unit 1 Reactor Vessel Lower Shell Plate C-8-2 (Longitudinal Orientation)



**Figure 5-3 Charpy V-Notch Percent Shear vs. Temperature for St. Lucie Unit 1 Reactor Vessel
Lower Shell Plate C-8-2 (Longitudinal Orientation)**



**Figure 5-4 Charpy V-Notch Impact Energy vs. Temperature for St. Lucie Unit 1 Reactor Vessel
Lower Shell Plate C-8-2 (Transverse Orientation)**

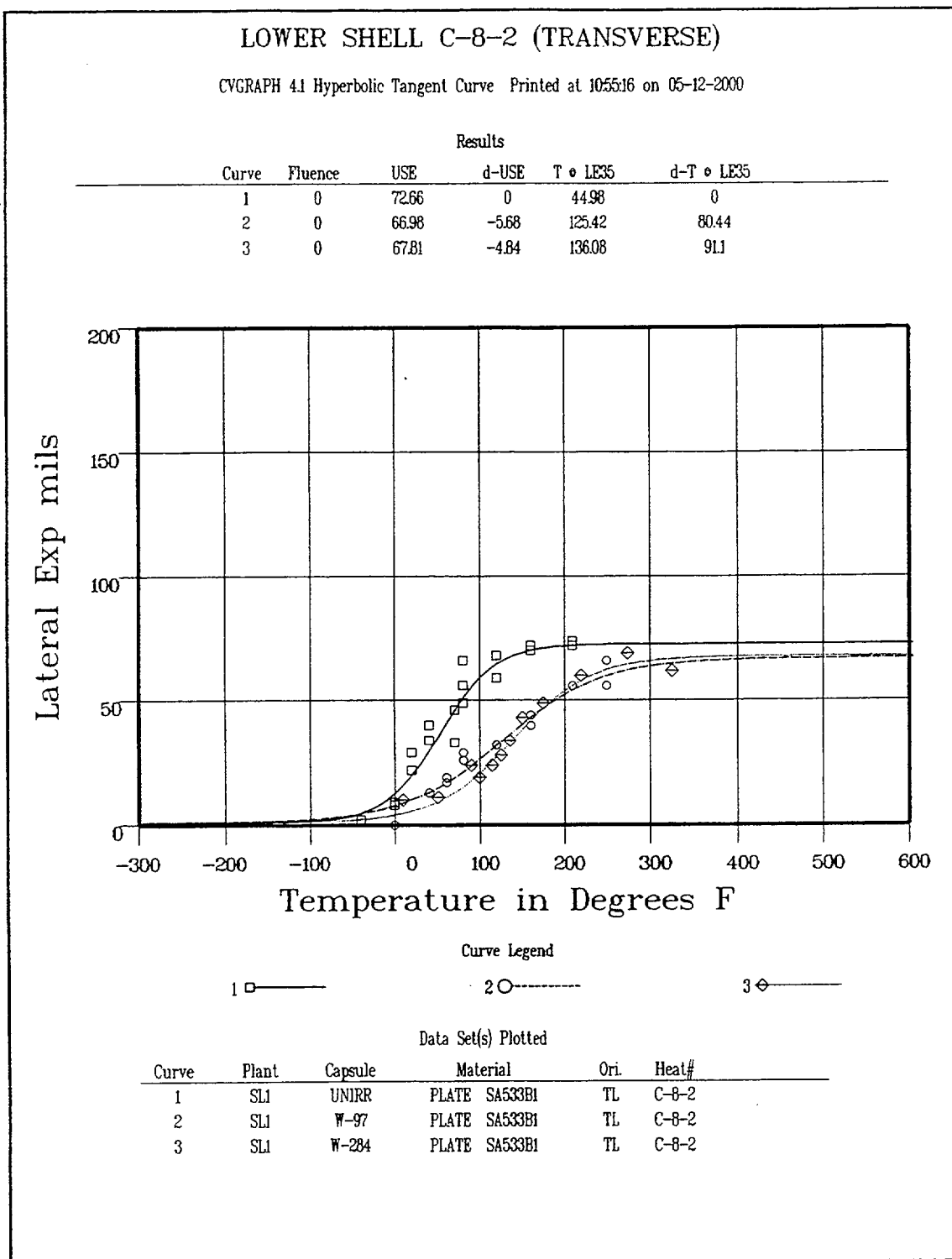


Figure 5-5 Charpy V-Notch Lateral Expansion vs. Temperature for St. Lucie Unit 1 Reactor Vessel Lower Shell Plate C-8-2 (Transverse Orientation)

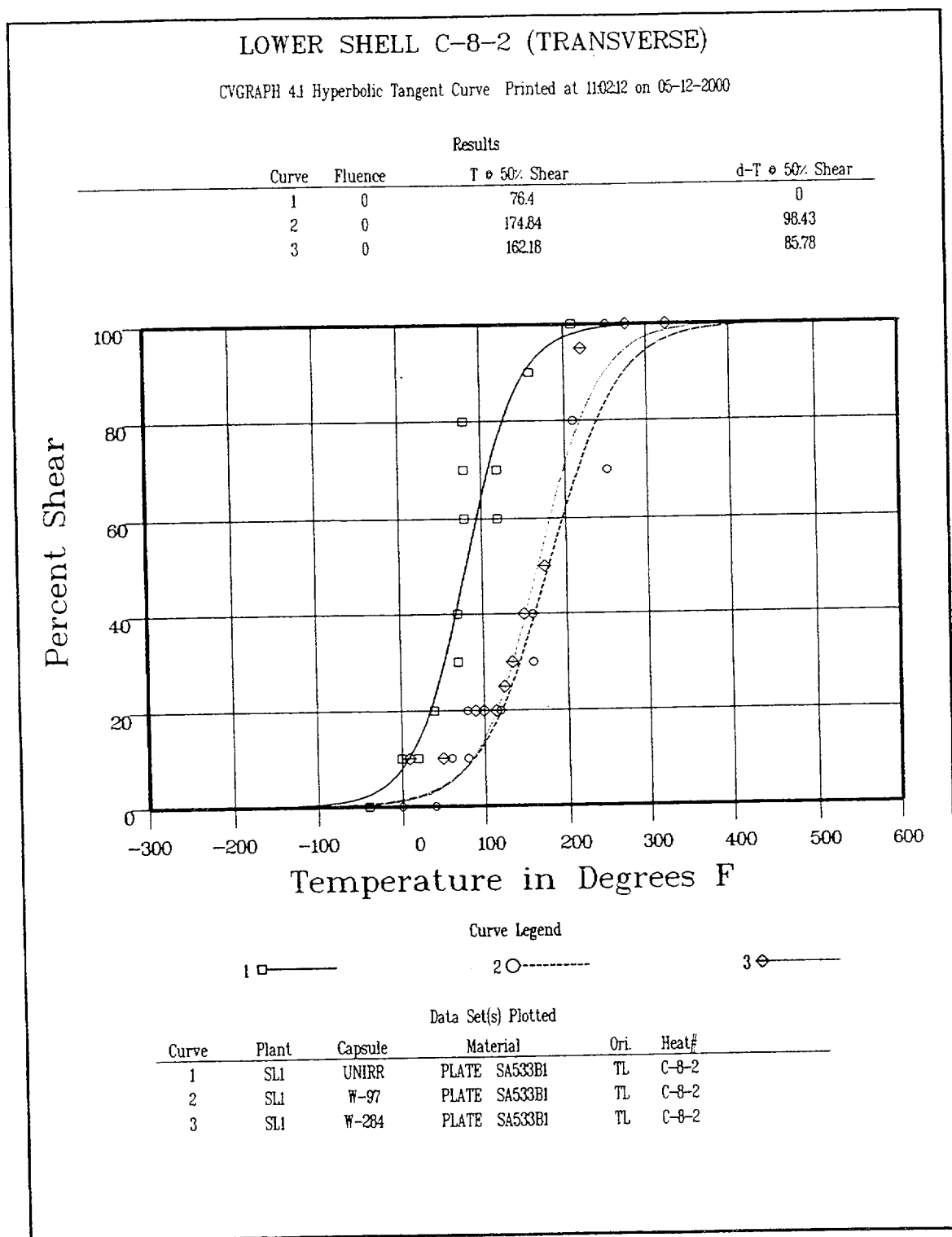


Figure 5-6 Charpy V-Notch Percent Shear vs. Temperature for St. Lucie Unit 1 Reactor Vessel
Lower Shell Plate C-8-2 (Transverse Orientation)

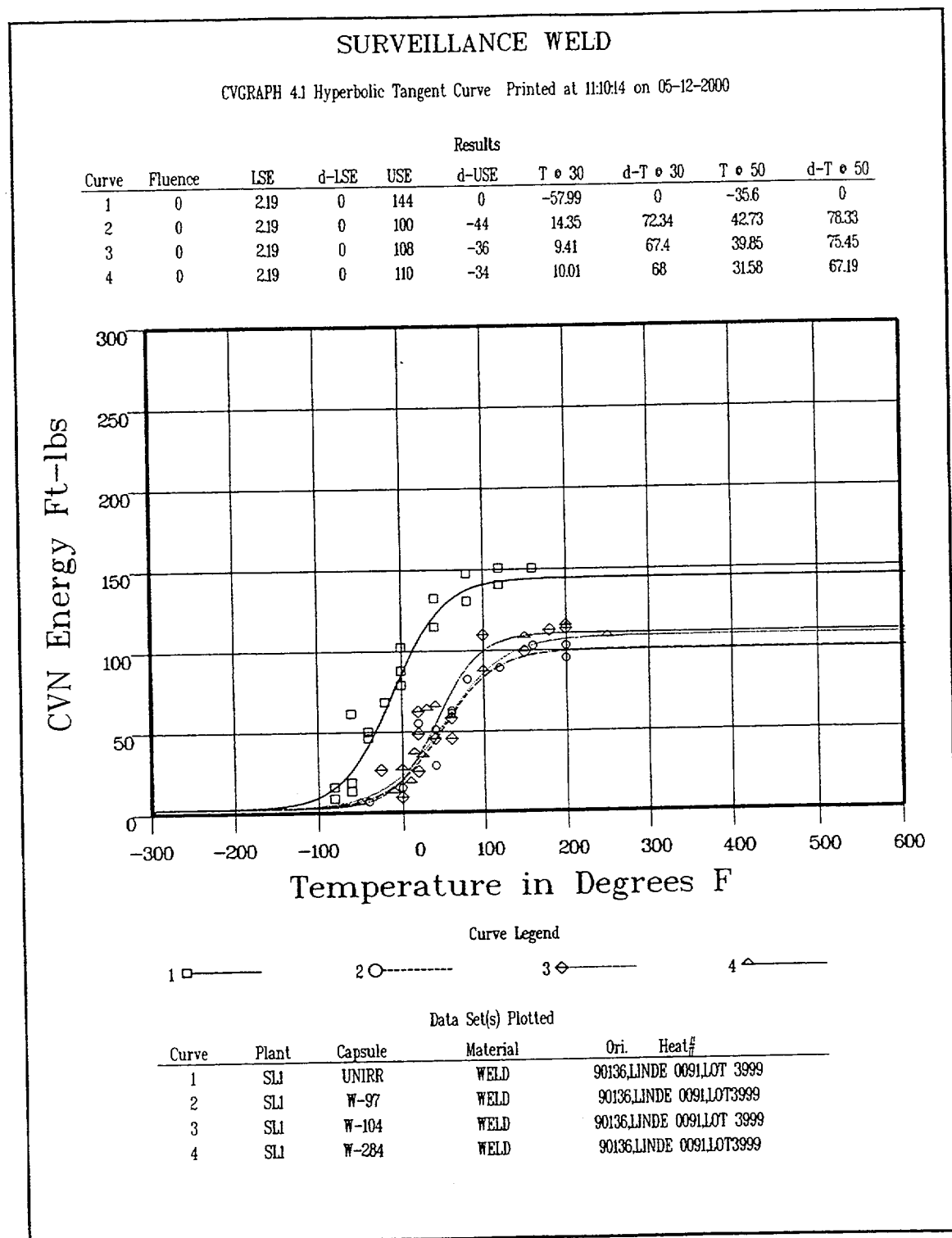


Figure 5-7 Charpy V-Notch Impact Energy vs. Temperature for St. Lucie Unit 1 Reactor Vessel Surveillance Weld Material

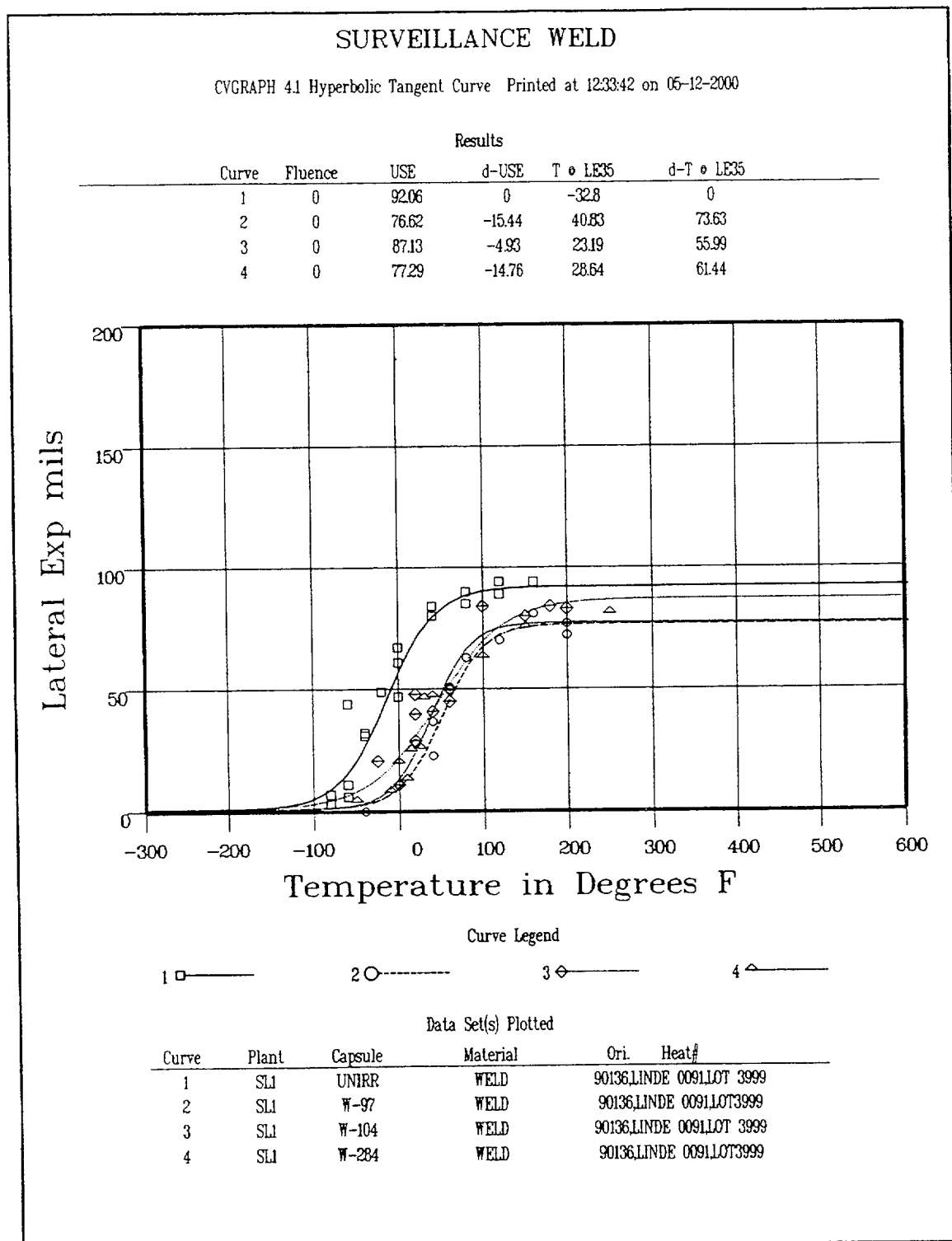


Figure 5-8 Charpy V-Notch Lateral Expansion vs. Temperature for St. Lucie Unit 1 Reactor Vessel Surveillance Weld Metal

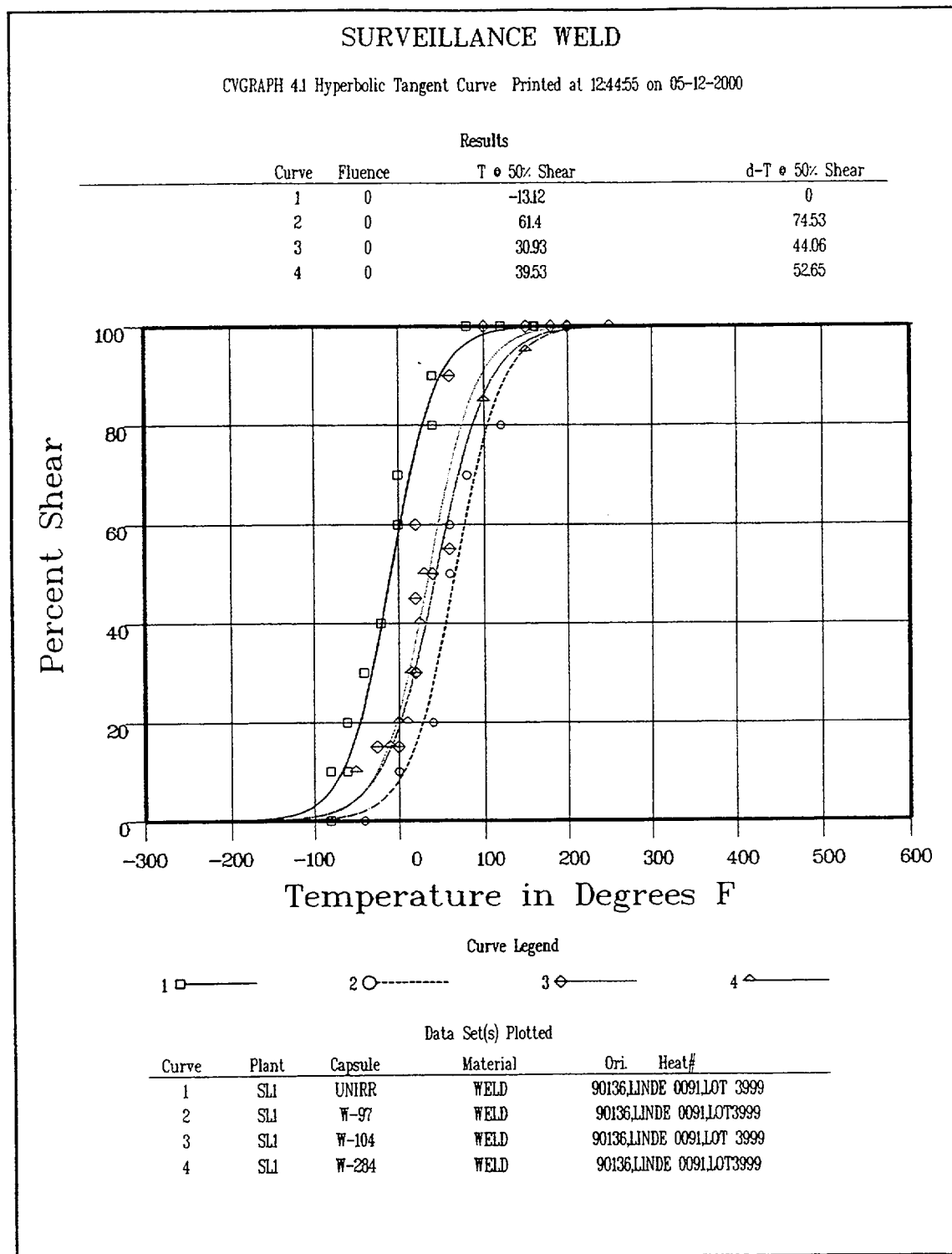


Figure 5-9 Charpy V-Notch Percent Shear vs. Temperature for St. Lucie Unit 1 Reactor Vessel Surveillance Weld Metal

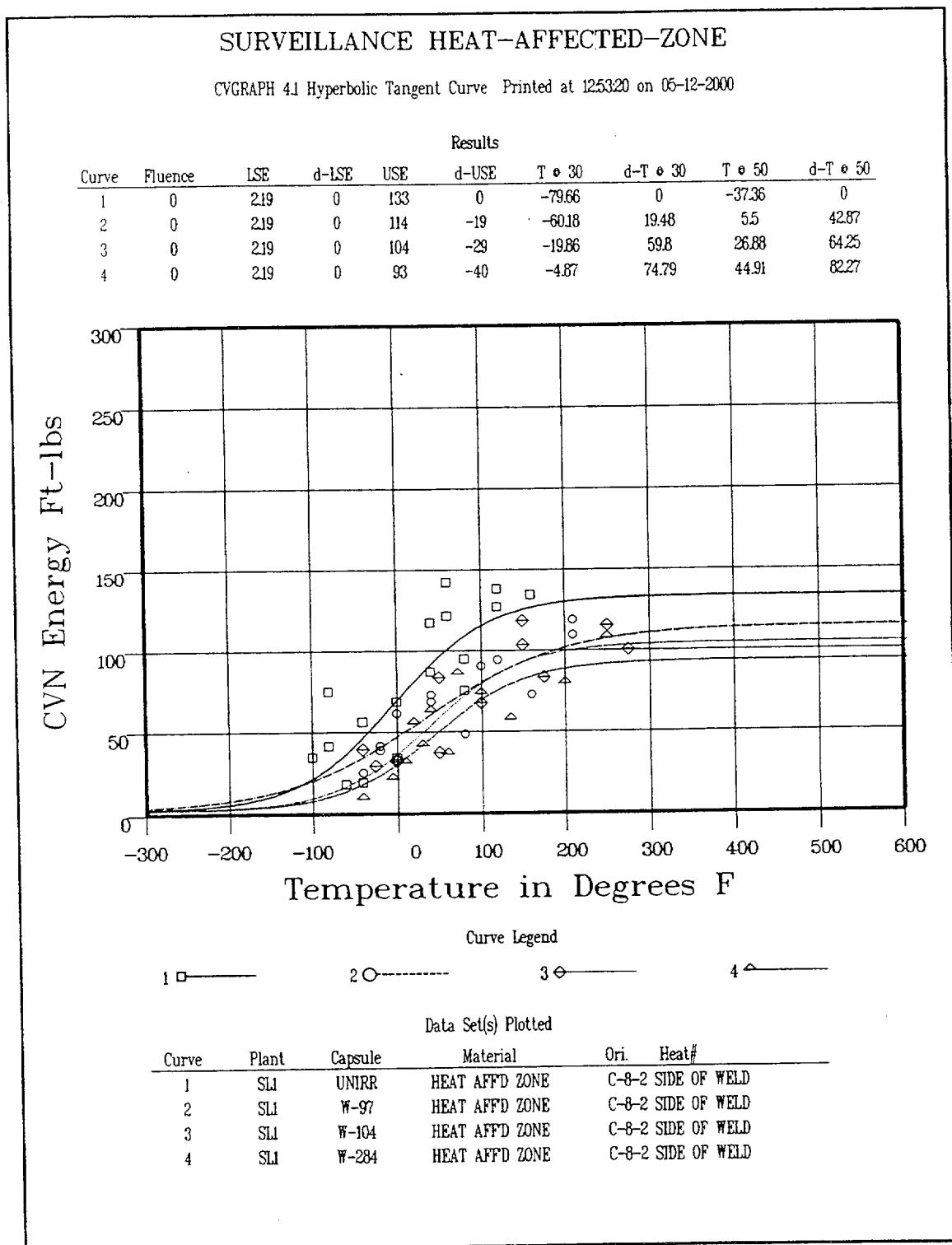


Figure 5-10 Charpy V-Notch Impact Energy vs. Temperature for St. Lucie Unit 1 Reactor Vessel Heat Affected Zone Material

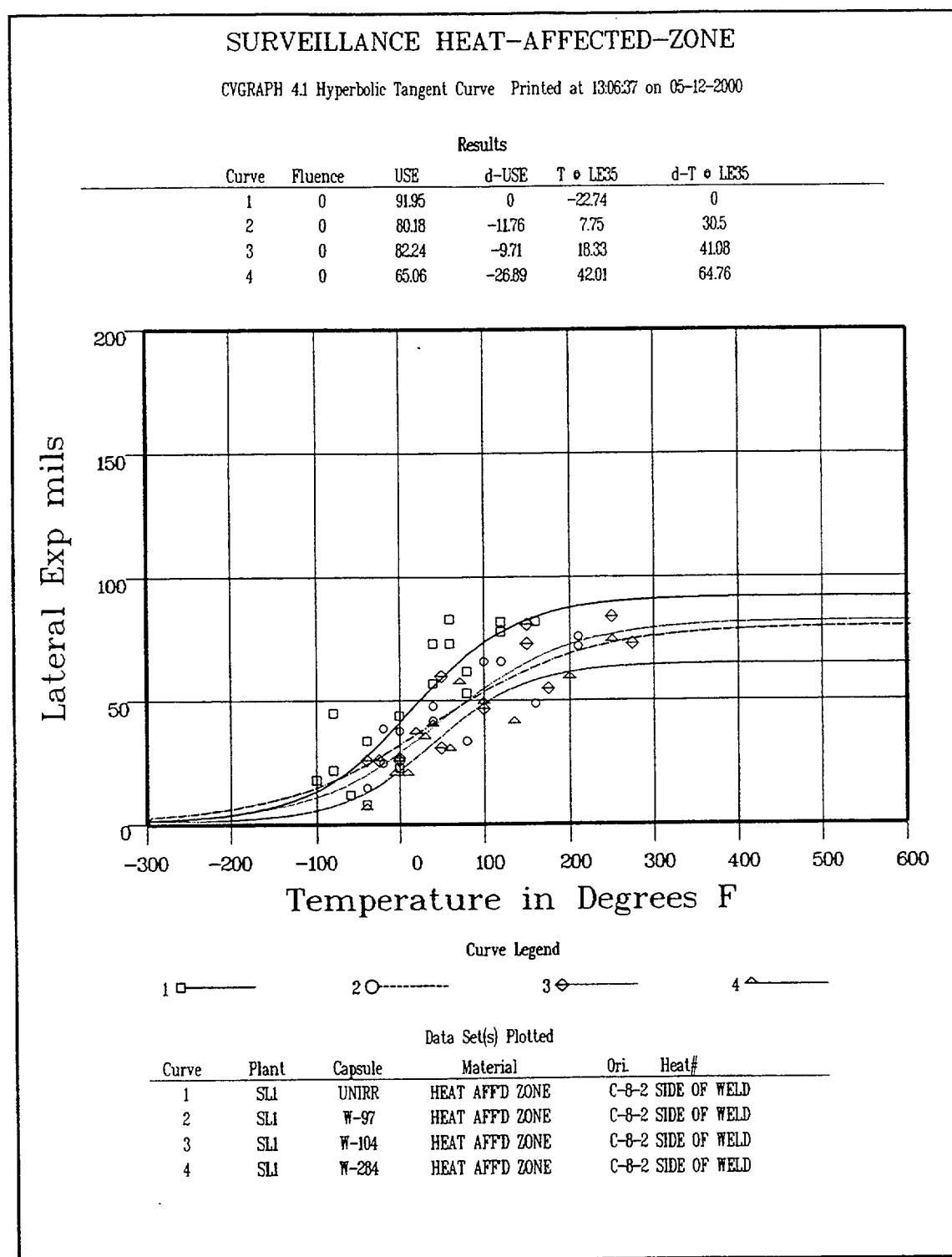


Figure 5-11 Charpy V-Notch Lateral Expansion vs. Temperature for St. Lucie Unit 1 Reactor Vessel Heat Affected Zone Material

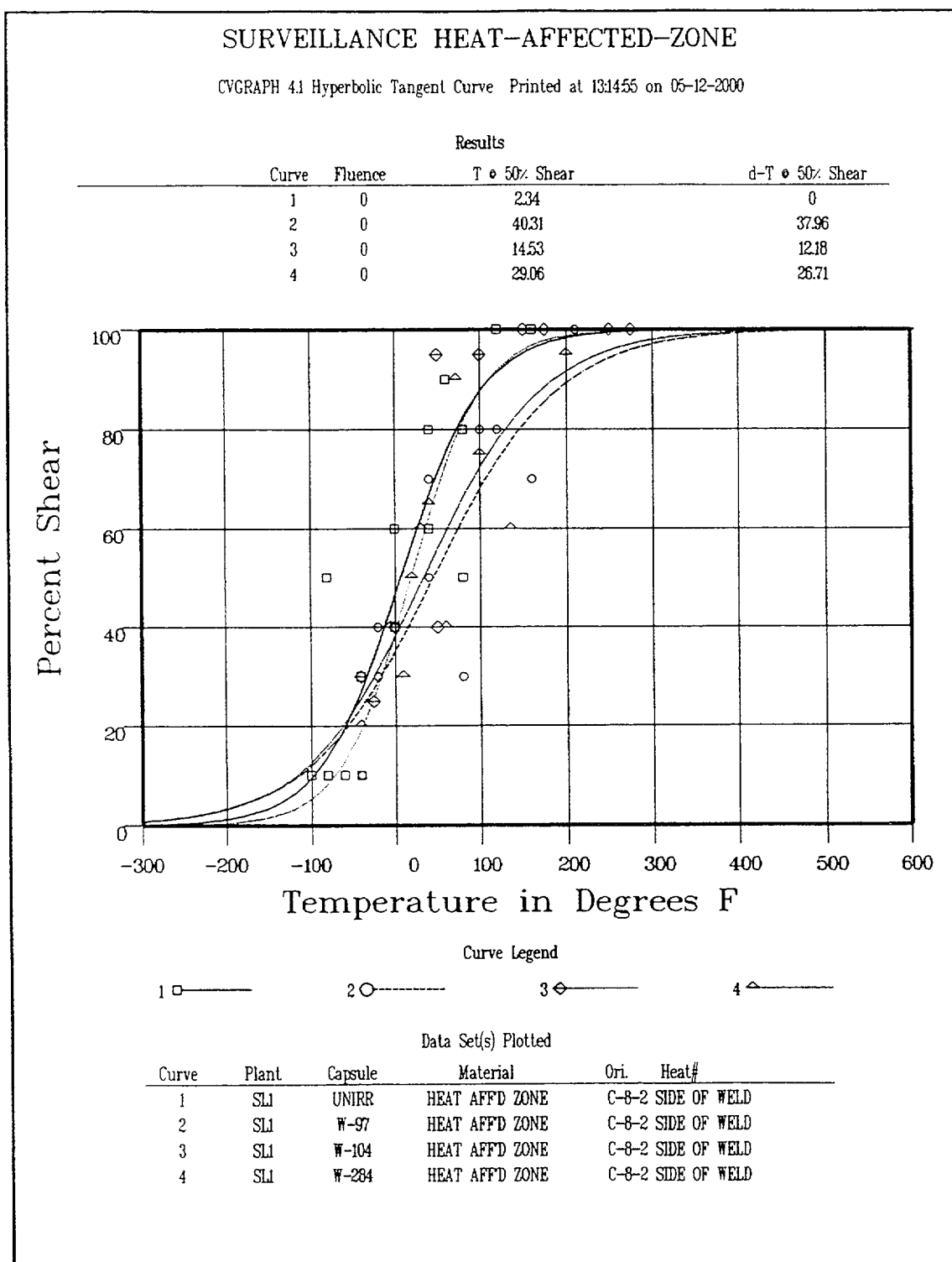


Figure 5-12 Charpy V-Notch Percent Shear vs. Temperature for St. Lucie Unit 1 Reactor Vessel Heat Affected Zone Material

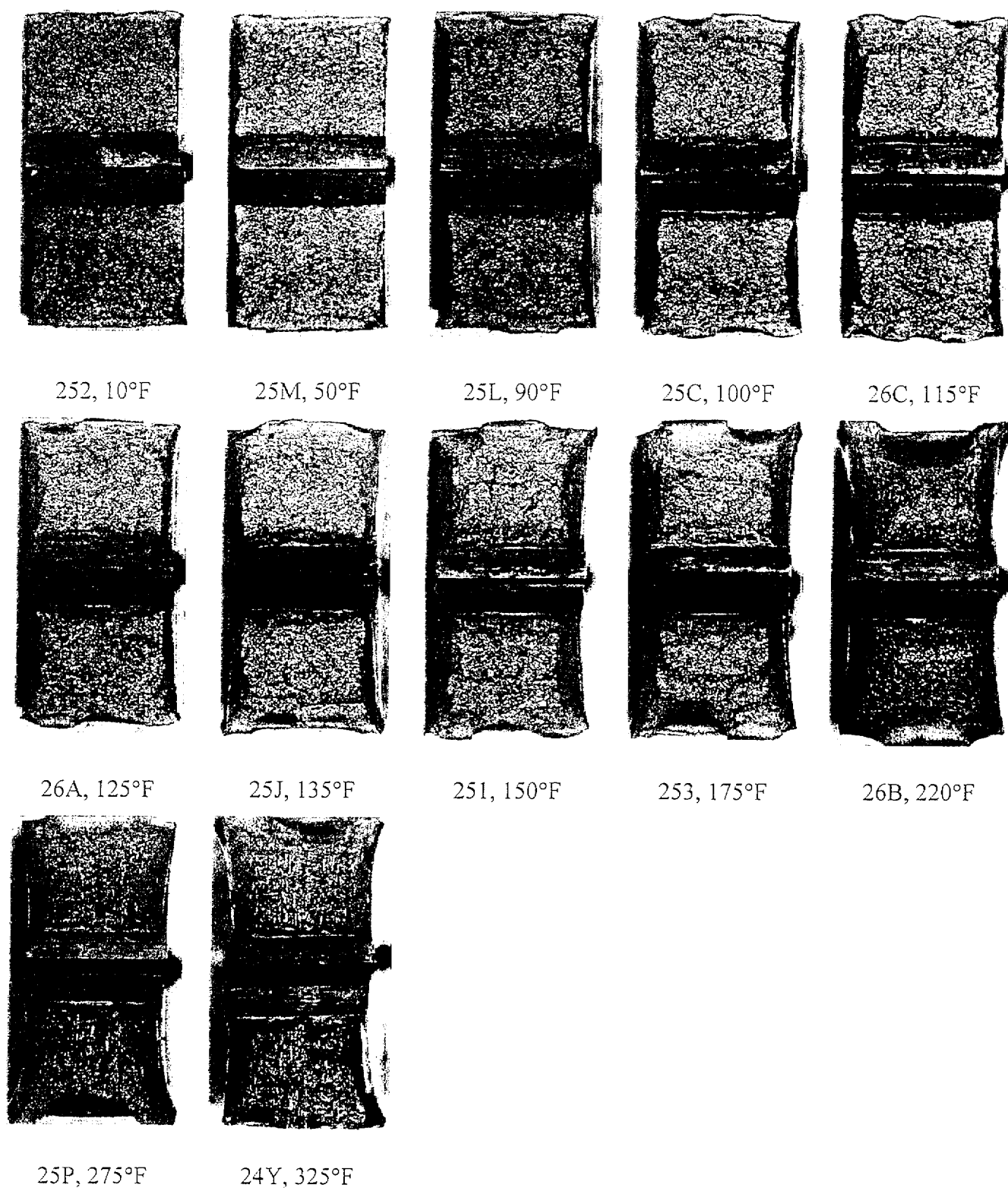


Figure 5-13 Charpy Impact Specimen Fracture Surfaces for St. Lucie Unit 1 Reactor Vessel Lower Shell Plate C-8-2 (Transverse Orientation)

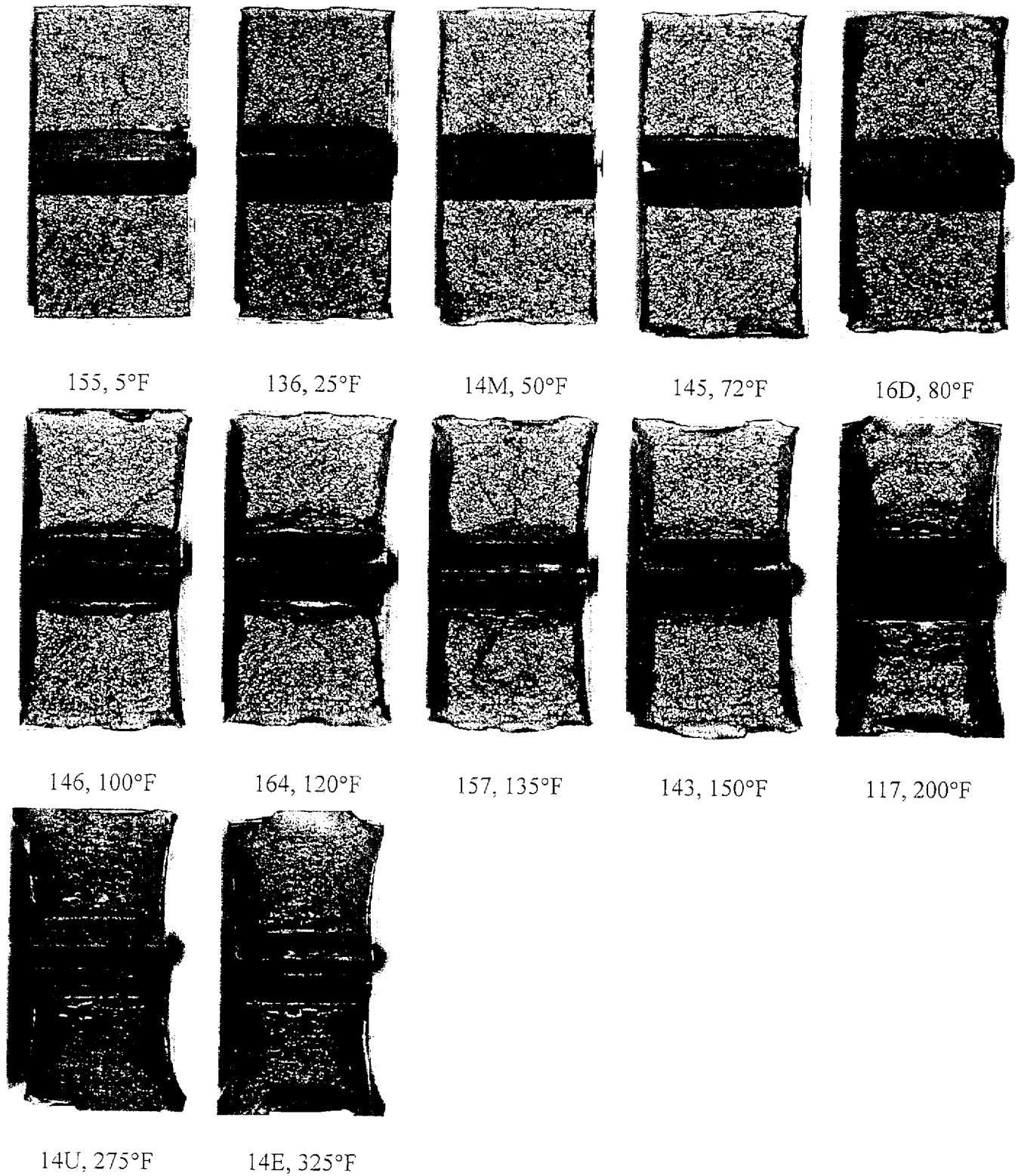


Figure 5-14 Charpy Impact Specimen Fracture Surfaces for St. Lucie Unit 1 Reactor Vessel Lower Shell Plate C-8-2 (Longitudinal Orientation)

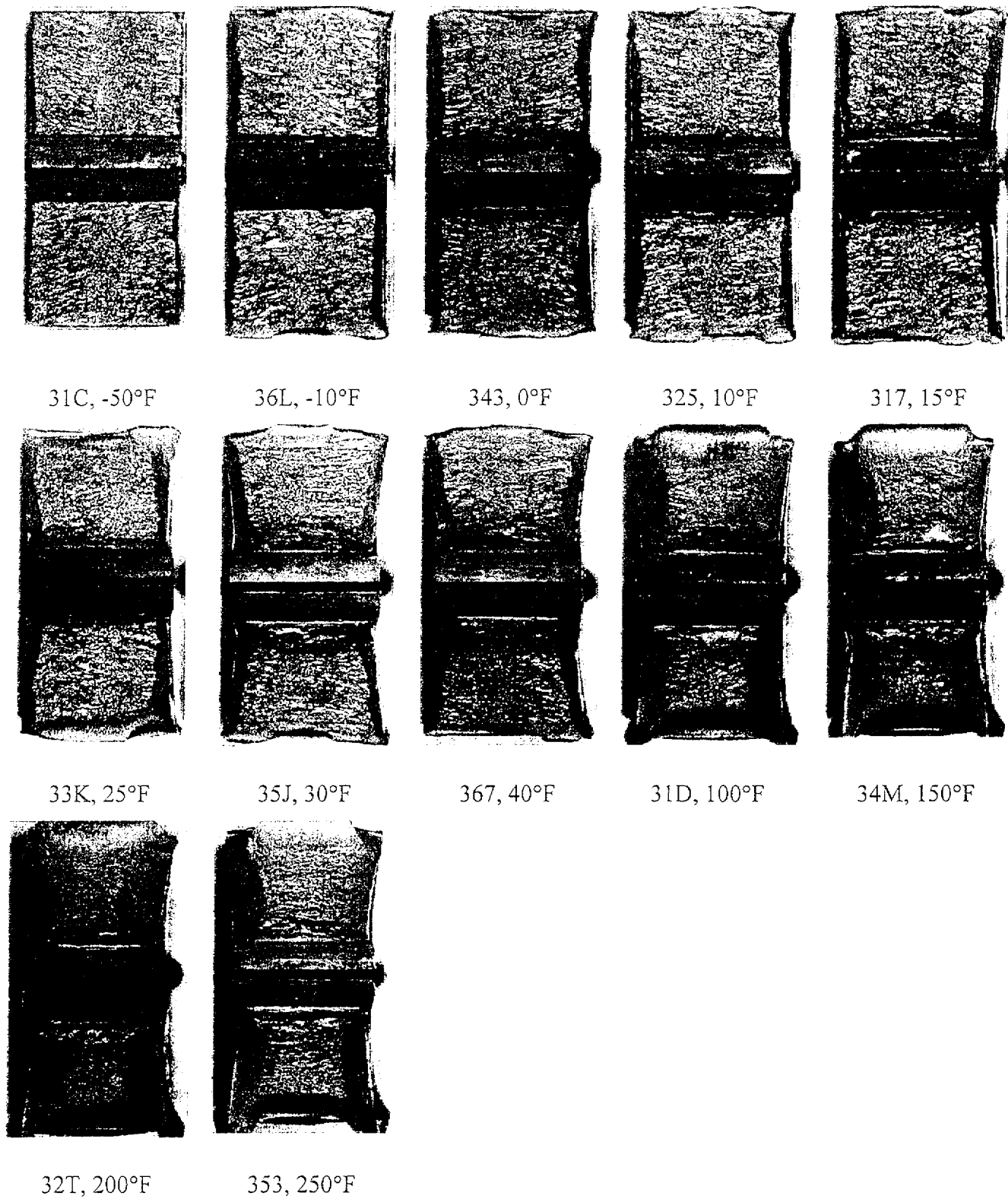


Figure 5-15 Charpy Impact Specimen Fracture Surfaces for St. Lucie Unit 2 Reactor Vessel Weld Metal Specimens

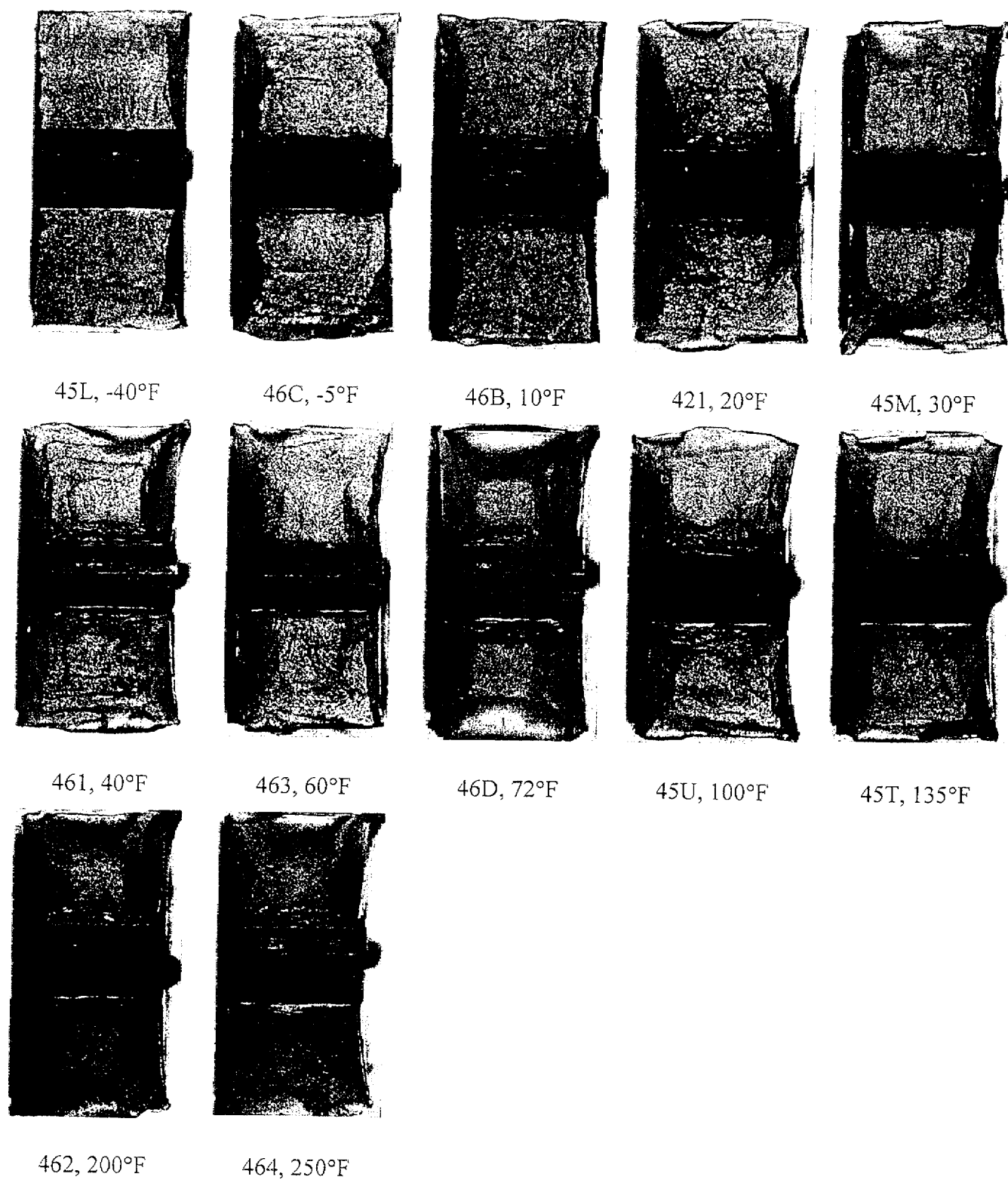
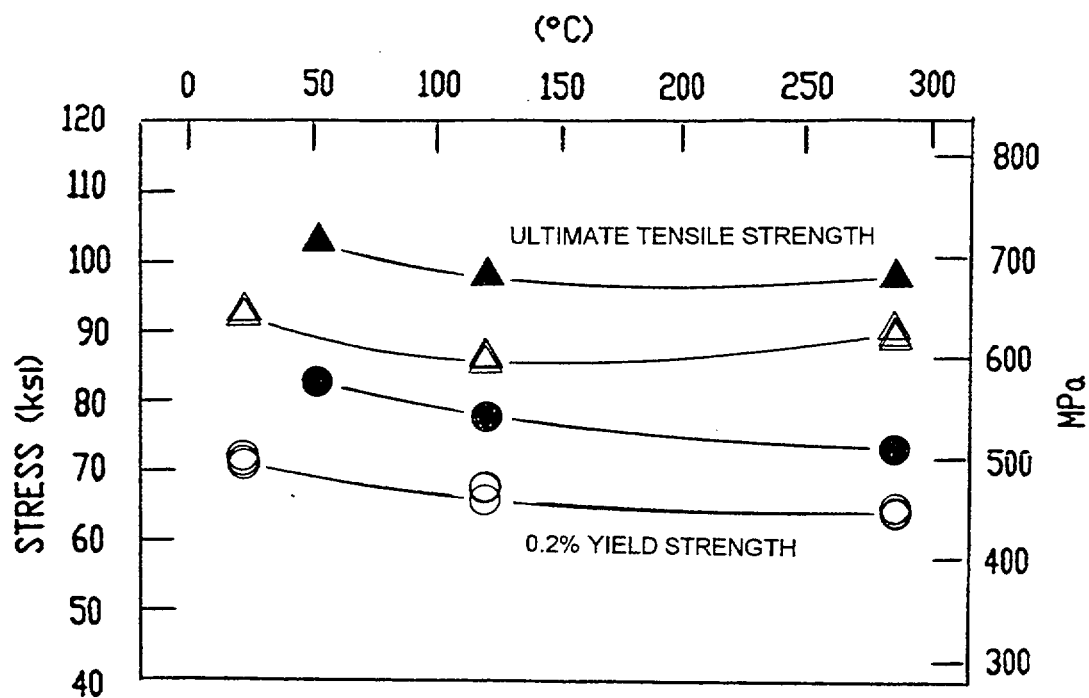


Figure 5-16 Charpy Impact Specimen Fracture Surfaces for St. Lucie Unit 1 Reactor Vessel Heat Affected Zone (HAZ)



LEGEND:

○ △ UNIRRADIATED

● ▲ IRRADIATED TO A FLUENCE OF 1.45×10^{19} n/cm² (E>1.0MeV) AT 550°F

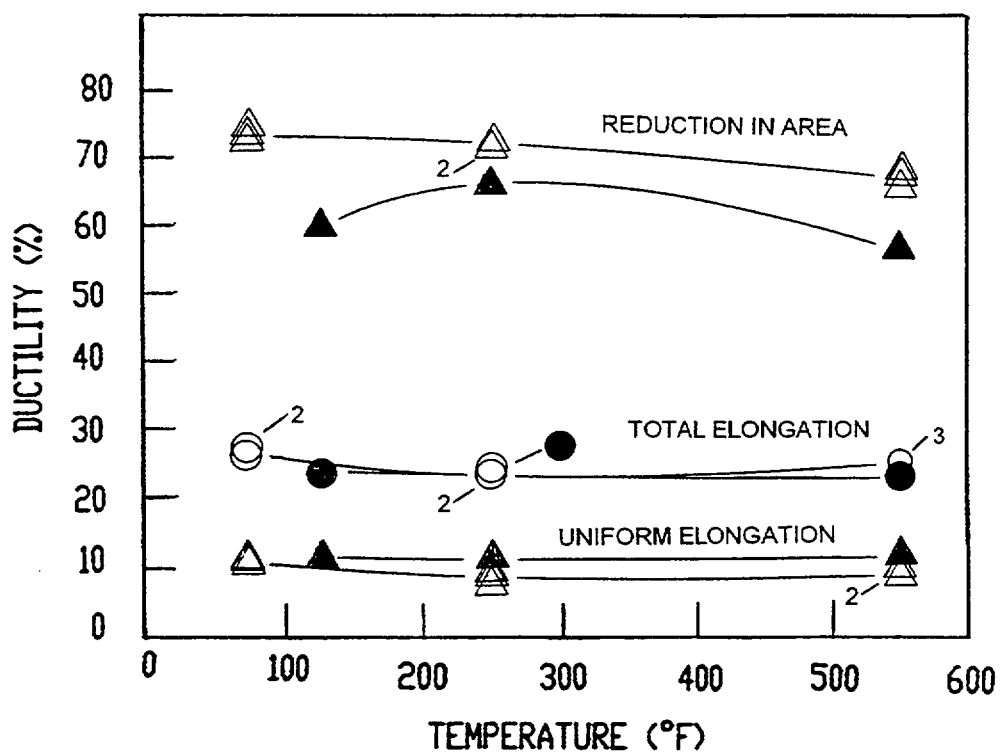


Figure 5-17 Tensile Properties for St. Lucie Unit 1 Reactor Vessel Lower Shell Plate C-8-2 (Longitudinal Orientation)

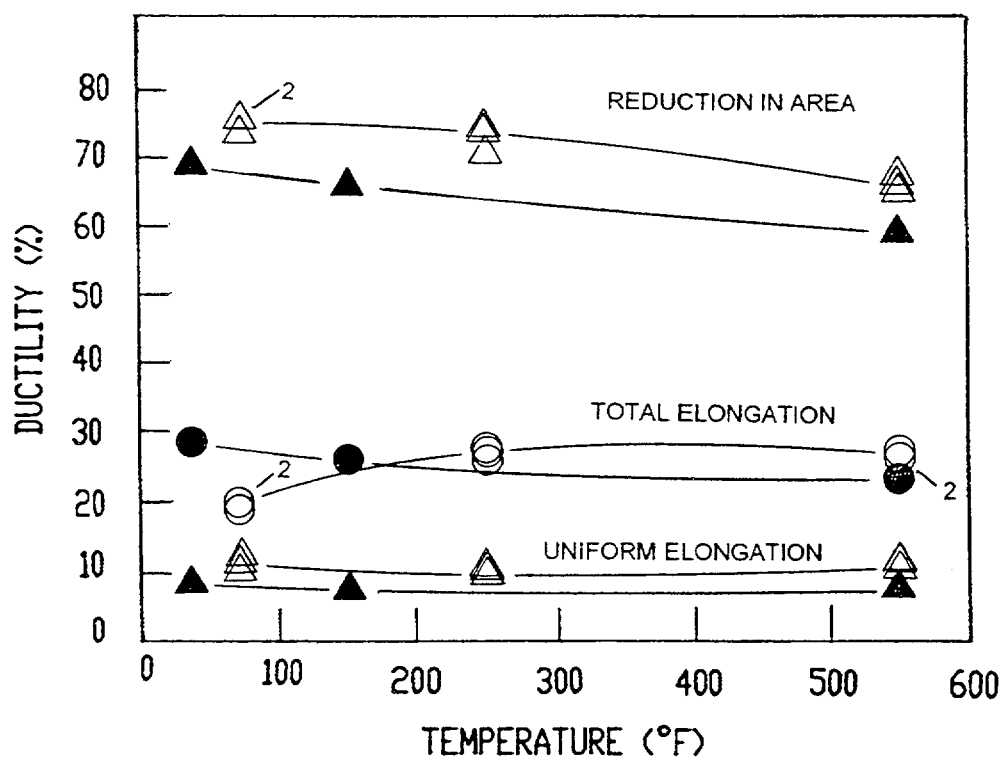
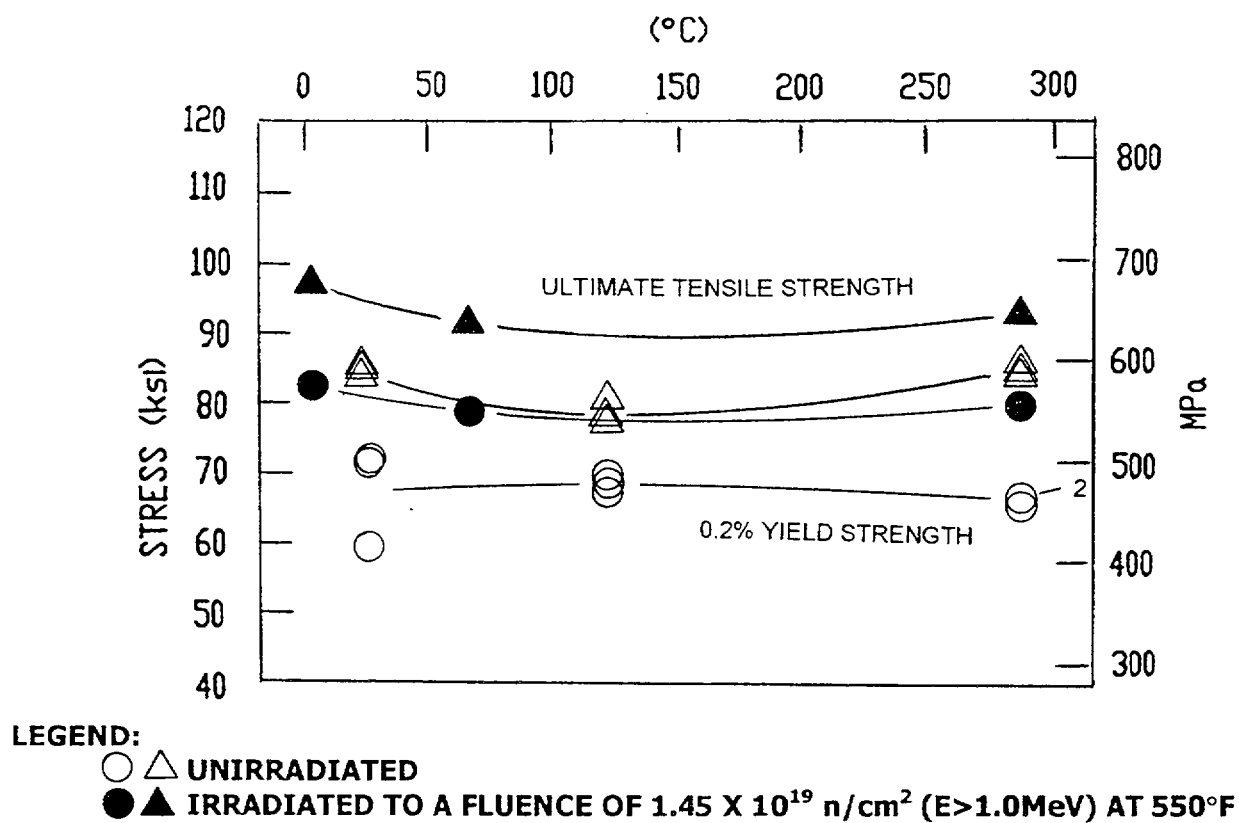
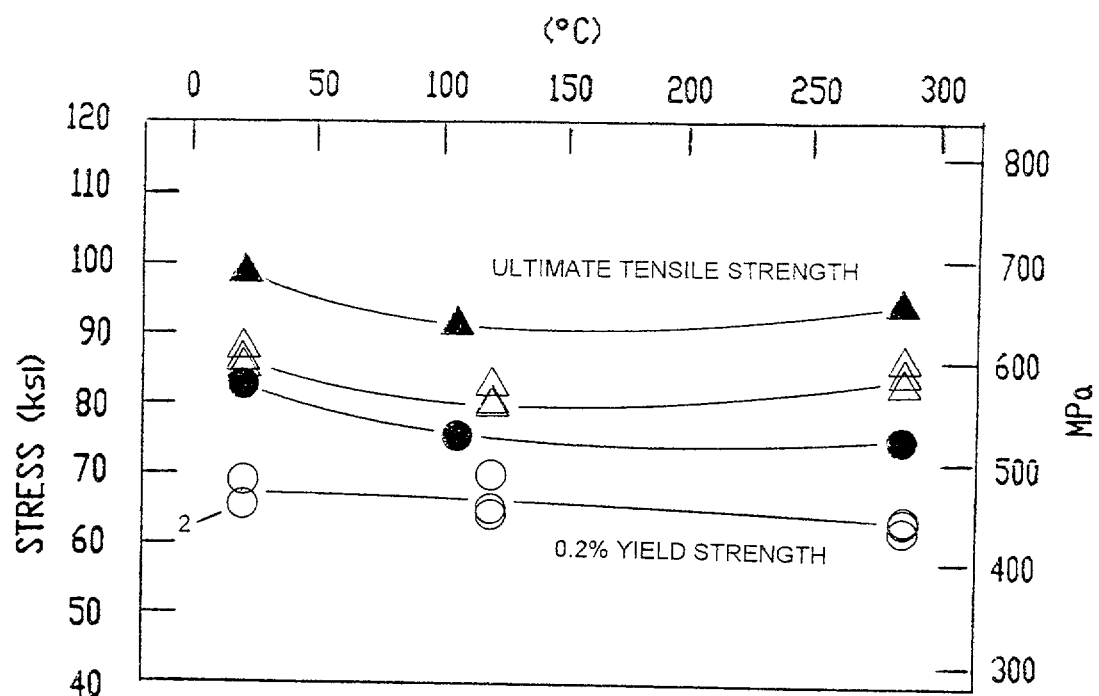


Figure 5-18 Tensile Properties for St. Lucie Unit 1 Reactor Vessel Weld Metal



LEGEND:

○ △ UNIRRADIATED

● ▲ IRRADIATED TO A FLUENCE OF 1.45×10^{19} n/cm² (E>1.0MeV) AT 550°F

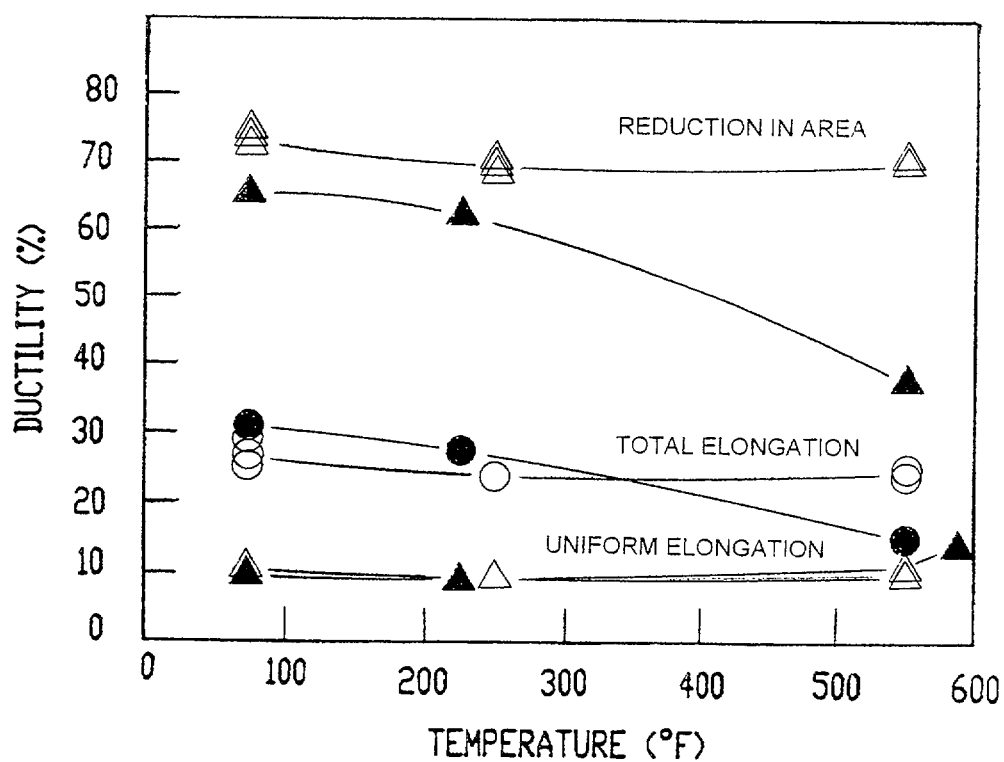
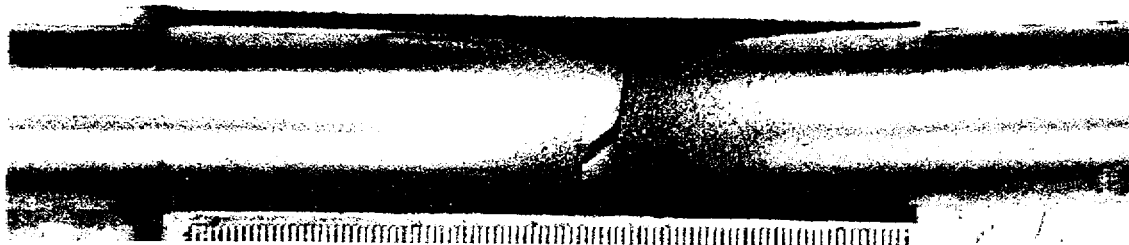
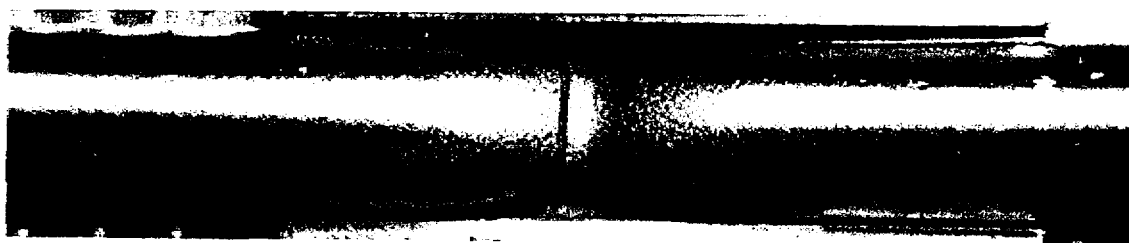


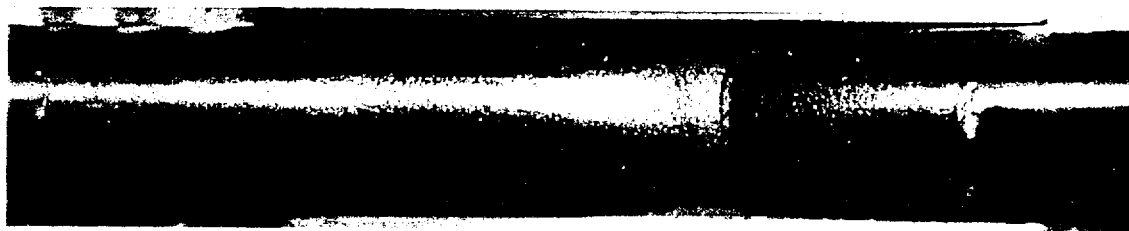
Figure 5-19 Tensile Properties for St. Lucie Unit 1 Reactor Vessel Heat-Affected-Zone (HAZ)



Specimen 1J4 Tested at 125°F

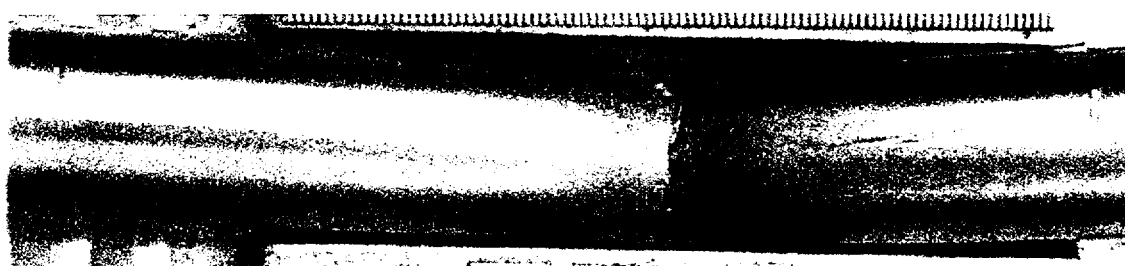


Specimen 1JL Tested at 250°F



Specimen 1JM Tested at 550°F

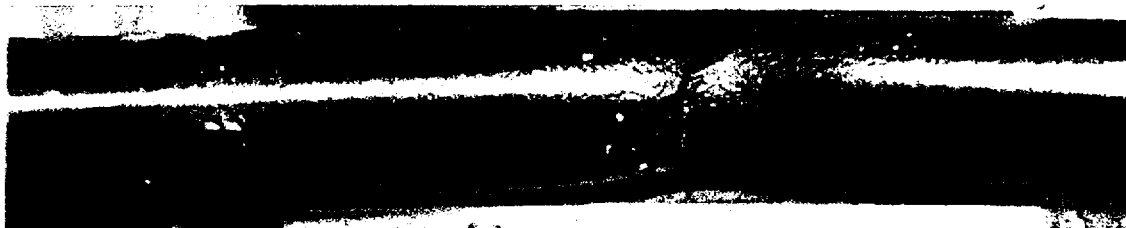
Figure 5-20 Fractured Tensile Specimens from St. Lucie Unit 1 Reactor Vessel Lower Shell C-8-2 (Longitudinal Orientation)



Specimen 3J2 Tested at 35°F

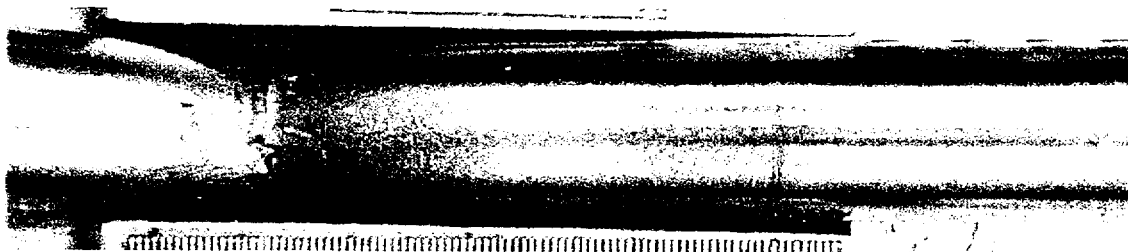


Specimen 3JJ Tested at 150°F



Specimen 3JY Tested at 550°F

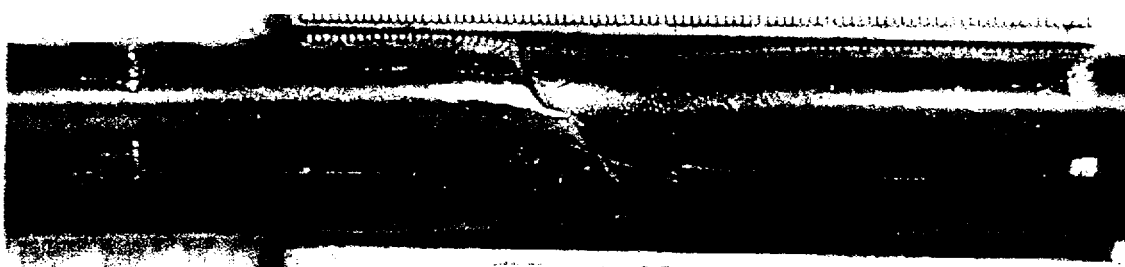
Figure 5-21 Fractured Tensile Specimens from St. Lucie Unit 1 Reactor Vessel Weld Metal



Specimen 4KJ Tested at 72°F



Specimen 4KK Tested at 225°F



Specimen 4KY Tested at 550°F

Figure 5-22 Fractured Tensile Specimens from St. Lucie Unit 1 Reactor Vessel Heat-Affected-Zone (HAZ)

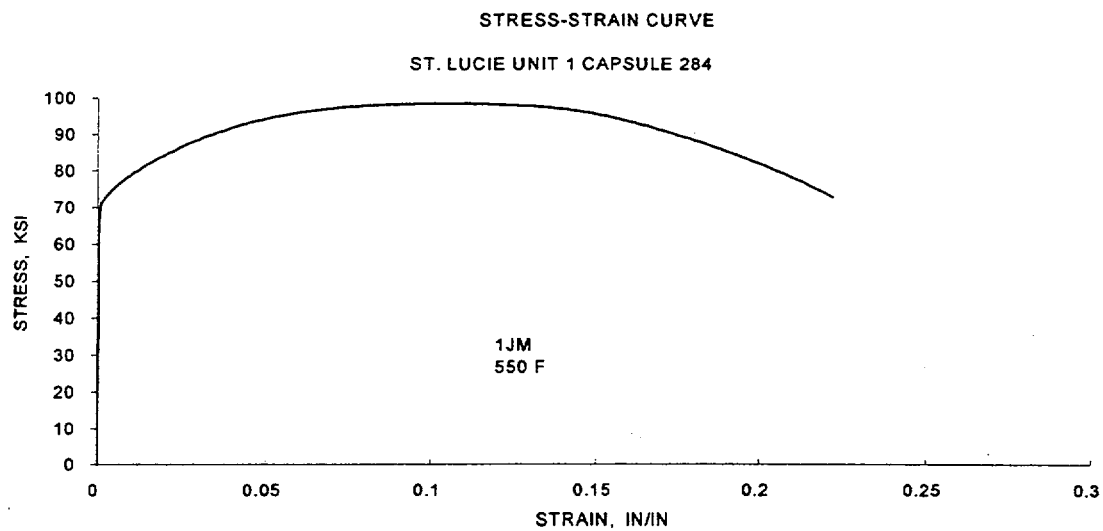
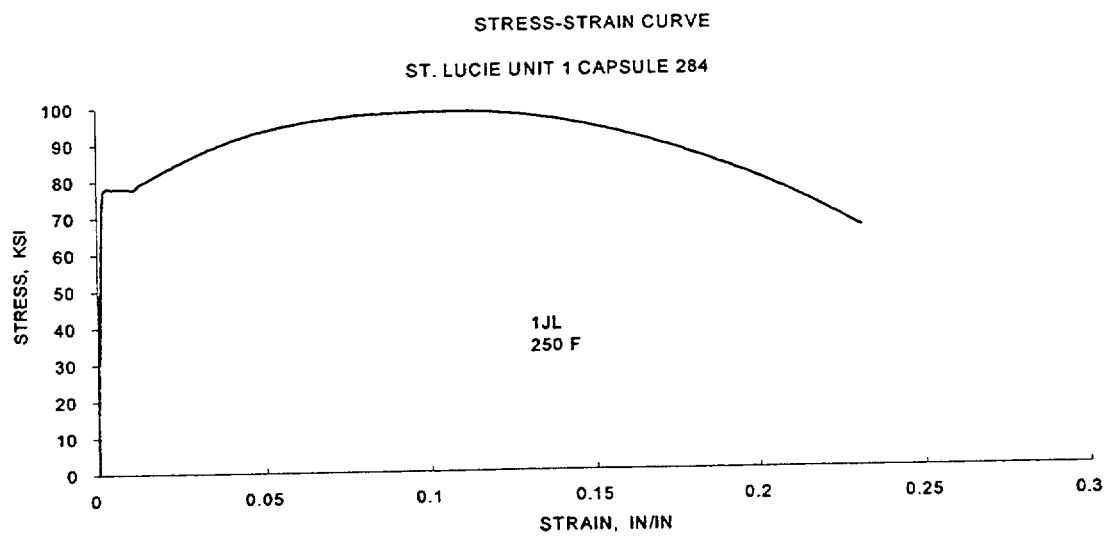
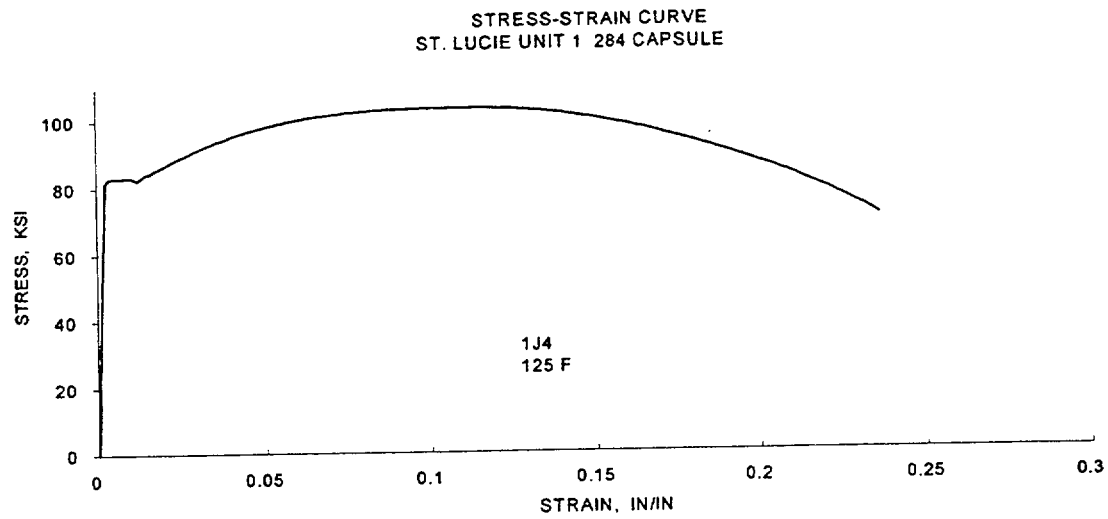


**Figure 5-23 Engineering Stress-Strain Curves for Lower Shell Plate C-8-2 Tensile Specimens
1J4, 1JL and 1JM (Longitudinal Orientation)**

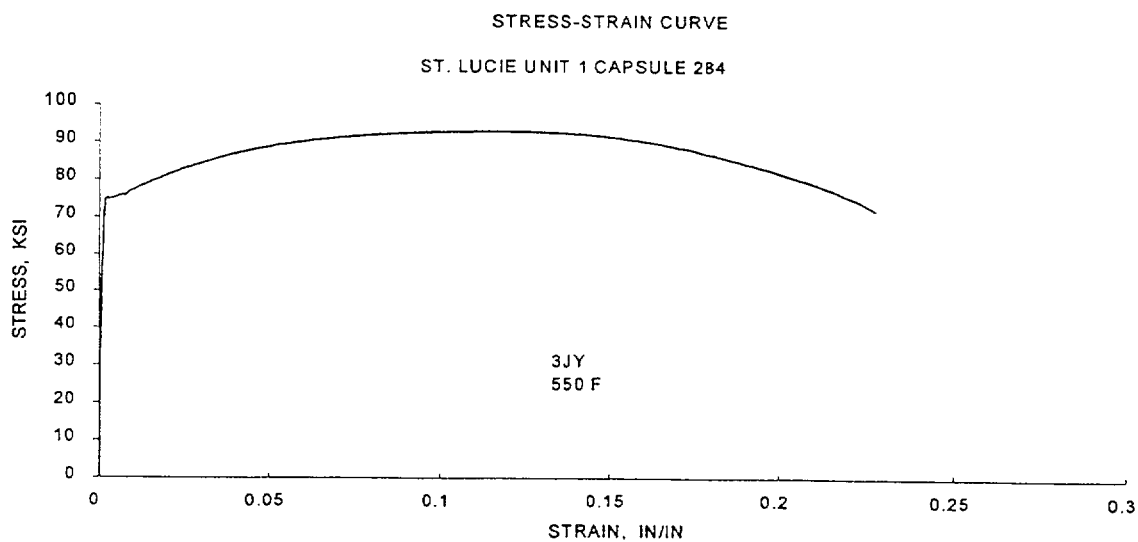
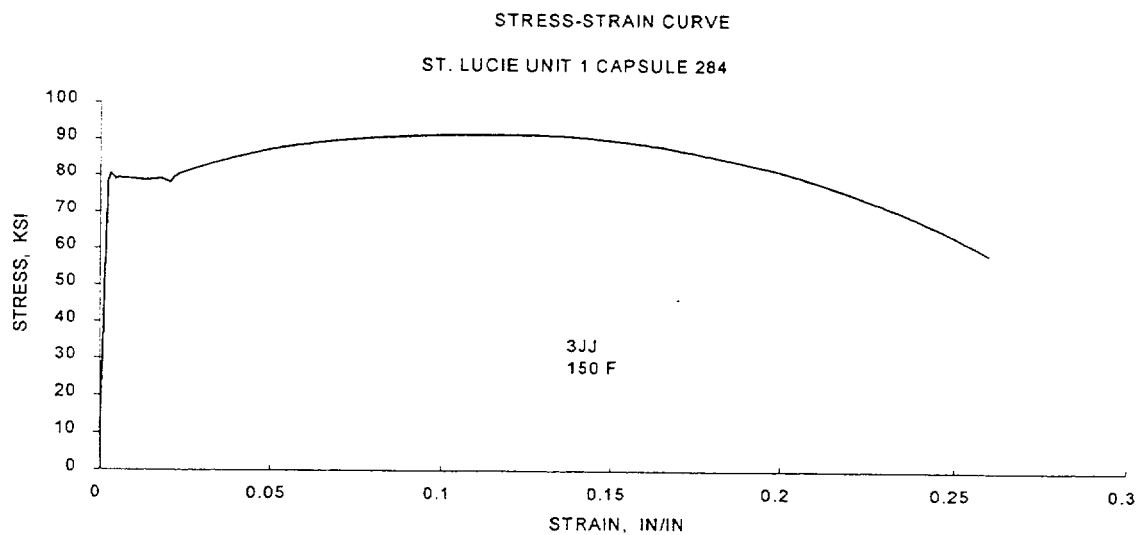
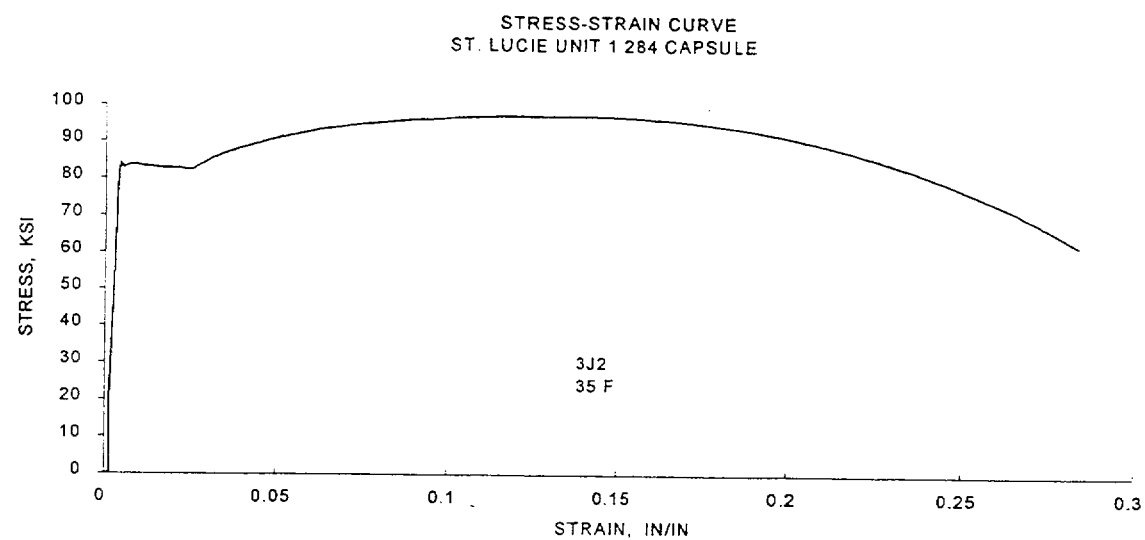


Figure 5-24 Engineering Stress-Strain Curves Weld Metal Tensile Specimens 3J2, 3JJ, and 3JY

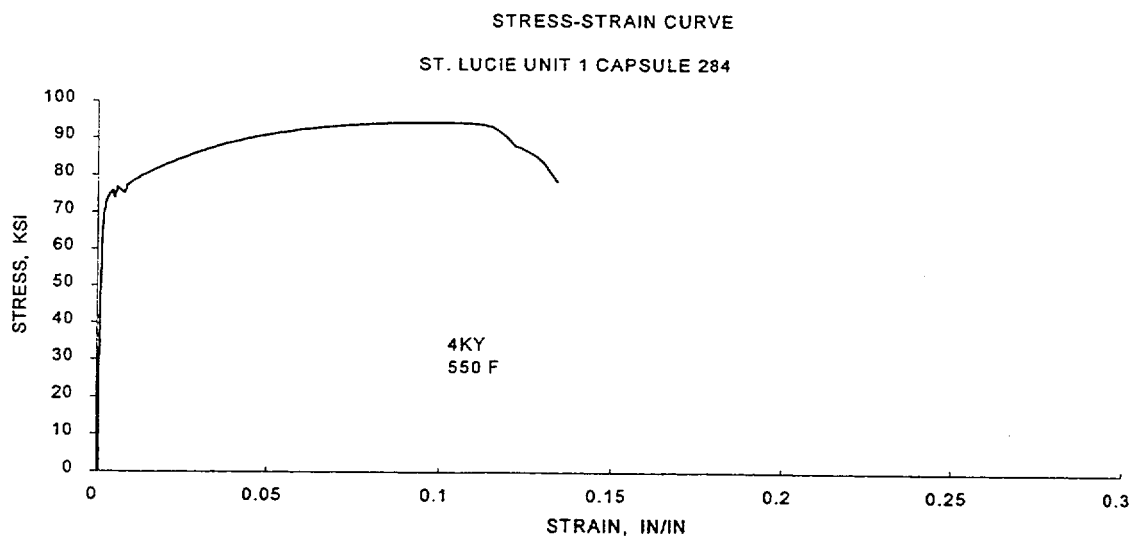
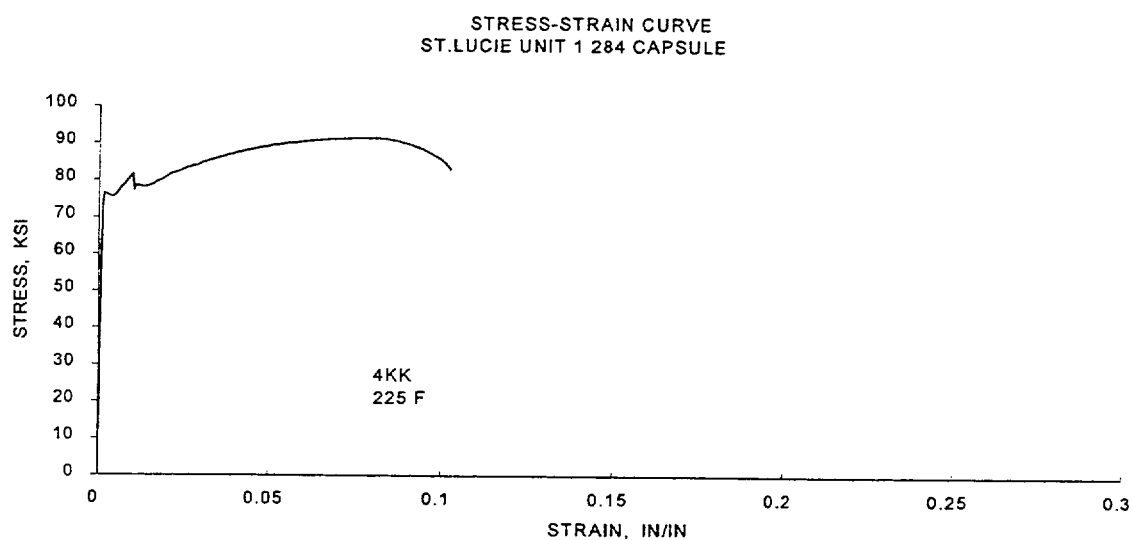
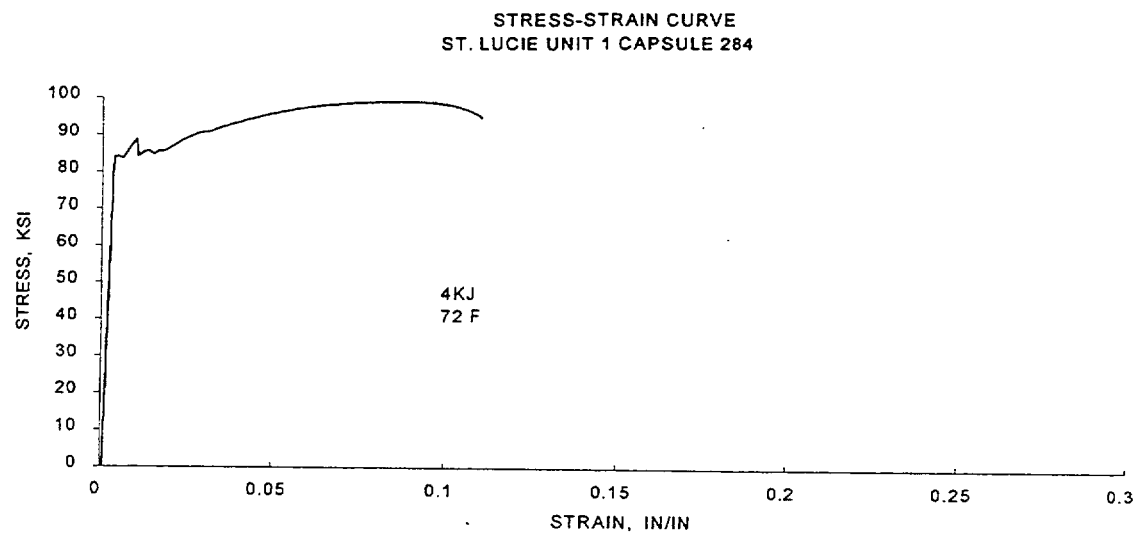


Figure 5-25 Engineering Stress-Strain Curves for Heat-Affected-Zone (HAZ) Material Tensile Specimens 4KJ, 4KK, and 4KY

6 RADIATION ANALYSIS AND NEUTRON DOSIMETRY

6.1 INTRODUCTION

Knowledge of the neutron environment within the reactor vessel and surveillance capsule geometry is required as an integral part of LWR reactor vessel surveillance programs for two reasons. First, in order to interpret the neutron radiation induced material property changes observed in the test specimens, the neutron environment (energy spectrum, flux, fluence) to which the test specimens were exposed must be known. Second, in order to relate the changes observed in the test specimens to the present and future condition of the reactor vessel, a relationship must be established between the neutron environment at various positions within the reactor vessel and that experienced by the test specimens. The former requirement is normally met by employing a combination of rigorous analytical techniques and measurements obtained with passive neutron flux monitors contained in each of the surveillance capsules. The latter information is generally derived solely from analysis.

The use of fast neutron fluence ($E > 1.0$ MeV) to correlate measured material property changes to the neutron exposure of the material has traditionally been accepted for development of damage trend curves as well as for the implementation of trend curve data to assess vessel condition. In recent years, however, it has been suggested that an exposure model that accounts for differences in neutron energy spectra between surveillance capsule locations and positions within the vessel wall could lead to an improvement in the uncertainties associated with damage trend curves as well as to a more accurate evaluation of damage gradients through the reactor vessel wall.

Because of this potential shift away from a threshold fluence toward an energy dependent damage function for data correlation, ASTM Standard Practice E853, "Analysis and Interpretation of Light-Water Reactor Surveillance Results," recommends reporting displacements per iron atom (dpa) along with fluence ($E > 1.0$ MeV) to provide a data base for future reference. The energy dependent dpa function to be used for this evaluation is specified in ASTM Standard Practice E693, "Characterizing Neutron Exposures in Iron and Low Alloy Steels in Terms of Displacements per Atom." The application of the dpa parameter to the assessment of embrittlement gradients through the thickness of the reactor vessel wall has already been promulgated in Revision 2 to Regulatory Guide 1.99, "Radiation Embrittlement of Reactor Vessel Materials."

This section provides the results of the neutron dosimetry evaluations performed in conjunction with the analysis of test specimens contained in the 97°, 104°, and 284° surveillance capsules which were withdrawn at the end of the fifth, ninth, and fifteenth fuel cycles, respectively. This evaluation is based on current state-of-the-art methodology and nuclear data including neutron transport and dosimetry cross-section libraries derived from the ENDF/B-VI data base. This report provides a consistent up-to-date neutron exposure data base for use in evaluating the material properties of the St. Lucie Unit 1 reactor vessel.

In each capsule dosimetry evaluation, fast neutron exposure parameters in terms of neutron fluence ($E > 1.0$ MeV), neutron fluence ($E > 0.1$ MeV), and iron atom displacements (dpa) are established for the capsule irradiation history. The analytical formalism relating the measured capsule exposure to the exposure of the vessel wall is described and used to project the integrated exposure of the vessel wall. Also, uncertainties associated with the derived exposure parameters at the surveillance capsules and with the projected exposure of the reactor vessel are provided.

All of the calculations and dosimetry evaluations presented in this section have been based on the latest available nuclear cross-section data derived from ENDF/B-VI and the latest available calculational tools and are consistent with the requirements of Regulatory Guide 1.190, "Calculational and Dosimetry Methods for Determining Pressure Vessel Neutron Fluence." Additionally, the methods used to develop the best estimate pressure vessel fluence are consistent with the NRC approved methodology described in WCAP-14040-NP-A, "Methodology Used to Develop Cold Overpressure Mitigating System Setpoints and RCS Heatup and Cooldown Limit Curves," January 1996.

6.2 DISCRETE ORDINATES ANALYSIS

A plan view of the reactor geometry at the core midplane is shown in Figure 4-1. Six irradiation capsules attached to the reactor vessel wall are included in the reactor design to constitute the reactor vessel surveillance program. The capsules are located at azimuthal angles of 83°, 97°, 104°, 263°, 277°, and 284° relative to the core cardinal axis as shown in Figure 4-1.

A view of a surveillance capsule assembly is shown in Figure 4-2. A total of seven stainless steel specimen containers hold the charpy and tensile monitors. The assembly is positioned axially centered on the core midplane, thus spanning the central portion of the active fuel zone.

From a neutronic standpoint, the surveillance capsules and associated support structures are significant. The presence of these materials has a marked effect on both the spatial distribution of neutron flux and the neutron energy spectrum in the water annulus and on the inside of the vessel wall near the capsule locations. In order to determine the neutron environment at the test specimen location, the capsules themselves must be included in the analytical model.

In performing the fast neutron exposure evaluations for the surveillance capsules and reactor vessel, several transport calculations were needed to accommodate changes in geometry, loading patterns, and downcomer temperature. Each is described in the table below.

Cycles 1-4:	Out-In Loading Pattern, Thermal Shield in Place
Cycle 5:	In-Out Loading Pattern at Uprated Power
Cycles 6-9:	Thermal Shield Permanently Removed
Cycles 11,13:	Fresh Fuel Assemblies Containing full length Hafnium rods in Peripheral Locations
Cycles 12,14:	Once Burned Fuel Assemblies Containing full length Hafnium rods in Peripheral Locations
Cycles 10,15:	No Hafnium rods in Peripheral Assemblies

These calculations were combined to produce average relative neutron energy distributions throughout the reactor geometry as well as to establish relative radial distributions of exposure parameters $\{\phi(E > 1.0 \text{ MeV}), \phi(E > 0.1 \text{ MeV}), \text{ and } \text{dpa/sec}\}$ through the vessel wall integrated over time. The neutron spectral information was required for the interpretation of neutron dosimetry withdrawn from the surveillance capsules as well as for the determination of exposure parameter ratios, i.e., $[\text{dpa/sec}]/[\phi(E > 1.0 \text{ MeV})]$, within the reactor vessel

geometry. The relative radial gradient information was required to permit the projection of measured exposure parameters to locations interior to the reactor vessel wall, i.e., the $\frac{1}{4}T$ and $\frac{3}{4}T$ locations.

Two-dimensional r, θ forward transport calculations for the reactor models were carried out using the DORT two-dimensional discrete ordinates code Version 3.1^[13] and the BUGLE-96 cross-section library^[14]. The BUGLE-96 library is a 47 energy group ENDF/B-VI based data set produced specifically for light water reactor applications. In these analyses, anisotropic scattering was treated with a P_3 expansion of the scattering cross-sections and the angular discretization was modeled with an S_8 order of angular quadrature.

The core power distribution utilized in the reference forward transport calculations were generated from input relative pin-by-pin and assembly power data through the SORCERY program. Cycle specific axial power distributions provided axial peaking factors for the core midplane and peak vessel locations that were applied to the results of the forward calculations.

Selected results from the neutron transport analyses are provided in Tables 6-1 through 6-5. The data listed in these tables establish the means for absolute comparisons of analysis and measurement for the 97° , 104° , and 284° capsule irradiation periods and provide the means to correlate dosimetry results with the corresponding exposure of the reactor vessel wall.

In Table 6-1, the calculated exposure parameters [$\phi(E > 1.0 \text{ MeV})$, $\phi(E > 0.1 \text{ MeV})$, and dpa/sec] are given at the geometric center of the two 14° surveillance capsule positions (104° and 284°) and for the 7° capsule position (97°) for the cycle specific core power distributions. Similar data are given in Table 6-2 for the reactor vessel inner radius. It is important to note that the data for the vessel inner radius were taken at the clad/base metal interface, thus representing the maximum predicted exposure levels of the vessel plates and welds.

Radial gradient information applicable to $\phi(E > 1.0 \text{ MeV})$, $\phi(E > 0.1 \text{ MeV})$, and dpa/sec is given in Tables 6-3, 6-4, and 6-5, respectively. The data obtained from the reference forward neutron transport calculations are presented on a relative basis for each exposure parameter at key azimuthal locations. Exposure distributions through the vessel wall may be obtained by normalizing the calculated or projected exposure at the vessel inner radius to the gradient data listed in Tables 6-3 through 6-5.

For example, the neutron flux $\phi(E > 1.0 \text{ MeV})$ at the $\frac{1}{4}T$ depth in the reactor vessel wall along the 0° azimuth is given by:

$$\phi_{1/4T}(0^\circ) = \phi(221.55, 0^\circ) F(227.03, 0^\circ)$$

where:

$\phi_{1/4T}(0^\circ) =$ Projected neutron flux at the $\frac{1}{4}T$ position on the 0° azimuth.

$\phi(221.55, 0^\circ) =$ Projected or calculated neutron flux at the vessel inner radius on the 0° azimuth.

$F(227.03, 0^\circ) =$ Ratio of the neutron flux at the $\frac{1}{4}T$ position to the flux at the vessel inner radius for the 0° azimuth. This data is obtained from Table 6-3.

Similar expressions apply for exposure parameters expressed in terms of $\phi(E > 0.1 \text{ MeV})$ and dpa/sec where the attenuation function F is obtained from Tables 6-4 and 6-5, respectively.

6.3 NEUTRON DOSIMETRY

The passive neutron sensors included in the St. Lucie Unit 1 surveillance program are listed in Table 6-6. Also given in Table 6-6 are the primary nuclear reactions and associated nuclear constants that were used in the evaluation of the neutron energy spectrum within the surveillance capsules and in the subsequent determination of the various exposure parameters of interest [$\phi(E > 1.0 \text{ MeV})$, $\phi(E > 0.1 \text{ MeV})$, dpa/sec]. The relative locations of the neutron sensors within the capsules are shown in Figure 4-4.

The use of passive monitors such as those listed in Table 6-6 does not yield a direct measure of the energy dependent neutron flux at the point of interest. Rather, the activation or fission process is a measure of the integrated effect that the time and energy dependent neutron flux has on the target material over the course of the irradiation period. An accurate assessment of the average neutron flux level incident on the various monitors may be derived from the activation measurements only if the irradiation parameters are well known. In particular, the following variables are of interest:

- The measured specific activity of each monitor,
- The physical characteristics of each monitor,
- The operating history of the reactor,
- The energy response of each monitor, and
- The neutron energy spectrum at the monitor location.

The specific activity of each of the neutron monitors was determined using established ASTM procedures^[16 through 28]. Following sample preparation and weighing, the activity of each monitor was determined by means of a lithium-drifted germanium, Ge(Li), gamma spectrometer. The irradiation history of the St. Lucie Unit 1 reactor was obtained from plant personnel^[29 and 30] and data reported in NUREG-0020, "Licensed Operating Reactors Status Summary Report," for the Cycles 1 to 15 operating periods. The irradiation history applicable to the exposure of the 97°, 104°, and 284° capsules is given in Table 6-7.

Having the measured specific activities, the physical characteristics of the sensors, and the operating history of the reactor, reaction rates referenced to full-power operation were determined from the following equation:

$$R = \frac{A}{N_0 F Y \sum \frac{P_j}{P_{ref}} C_j [1 - e^{-\lambda t_j}] [e^{-\lambda t_d}]}$$

where:

- R = Reaction rate averaged over the irradiation period and referenced to operation at a core power level of P_{ref} (rps/nucleus).
- A = Measured specific activity (dps/gm).
- N_0 = Number of target element atoms per gram of sensor.
- F = Weight fraction of the target isotope in the sensor material.
- Y = Number of product atoms produced per reaction.

P_j	=	Average core power level during irradiation period j (MW).
P_{ref}	=	Maximum or reference power level of the reactor (MW).
C_j	=	97° Capsule: Calculated ratio of $\phi(E > 1.0 \text{ MeV})$ during irradiation period j to the time weighted average $\phi(E > 1.0 \text{ MeV})$ over the entire irradiation period.
		104° and 284° Capsules: Determined as the ratio of the calculated reaction rate during period j to the spectrum average reaction rate over the irradiation period for each reaction. This was done to account for the spectrum changes due to removal of the thermal shield.
λ	=	Decay constant of the product isotope (1/sec).
t_j	=	Length of irradiation period j (sec).
t_d	=	Decay time following irradiation period j (sec).

and the summation is carried out over the total number of monthly intervals comprising the irradiation period.

In the equation describing the reaction rate calculation, the ratio $[P_j]/[P_{ref}]$ accounts for month-by-month variation of reactor core power level within any given fuel cycle as well as over multiple fuel cycles. The ratio C_j , which can be calculated for each fuel cycle, accounts for the change in sensor reaction rates caused by variations in flux level induced by changes in core spatial power distributions from fuel cycle to fuel cycle. The actual C_j values that were used to assess the sensor reaction rates from the 97°, 104°, and 284° St. Lucie Unit 1 surveillance capsules are presented in Table 6-16.

These C_j values are typically derived from the information provided in Table 6-1 and they are determined on a fuel cycle-specific basis in order to account for core spatial power distribution differences in each cycle. The rationale behind this approach is that the impact of changing flux levels for constant power operation can be quite significant for sensor sets that have been irradiated for many cycles in a reactor that has transitioned from non-low leakage to low leakage fuel management, for sensor sets contained in surveillance capsules that have been moved from one capsule location to another, or when major changes to the reactor internals occur, such as removal of the thermal shield. This latter effect may be observed from the C_j data that has been provided in Table 6-16. Furthermore, since the neutron transport calculations are steady-state approximations of each fuel cycle, the radial power distribution change is not modeled explicitly. Hence, an average assembly power is used for the calculation. This is an adequate approximation since the effect of the relative radial power shift in the peripheral assemblies over a fuel cycle is small compared to cycle-to-cycle loading pattern changes.

The cycle-average flux values are used in the calculation of C_j assuming that the neutron energy spectrum at the capsule is unchanged. The irradiation period of the 104° and the 284° capsules encompassed the removal of the thermal shield following Cycle 5 which would have a marked change in the neutron energy spectrum at the capsule. The spectrum change affects each of the dosimeters differently since the response functions of the dosimeters are different, as shown below:

Monitor	Reaction of	Detector
<u>Material</u>	<u>Interest</u>	<u>Response</u>
Copper	$^{63}\text{Cu} (n,\gamma)$	$E > 4.7 \text{ MeV}$
Titanium	$^{46}\text{Ti} (n,p)$	$E > 4.4 \text{ MeV}$
Iron	$^{54}\text{Fe} (n,p)$	$E > 1.0 \text{ MeV}$
Nickel	$^{58}\text{Ni} (n,p)$	$E > 1.0 \text{ MeV}$
Uranium-238	$^{238}\text{U} (n,f)$	$E > 0.4 \text{ MeV}$
Neptunium-237	$^{237}\text{Np} (n,f)$	$E > 0.08 \text{ MeV}$
Cobalt-Al	$^{59}\text{Co} (n,\gamma)$	$E > 0.015 \text{ MeV}$

To account for the spectrum change for the 104° and the 284° capsule irradiations, the C_j terms were derived from the calculated reaction rates provided in the cycle-specific neutron transport calculations.

Measured and saturated reaction product specific activities as well as the derived full power reaction rates are listed in Table 6-8. The reaction rates of the ^{238}U sensors provided in Table 6-8 include corrections for ^{235}U impurities, plutonium build-in, and gamma ray induced fissions.

In the determination of the Best Estimate fast neutron exposures of the surveillance capsules, least squares analysis is used to combine the plant-specific calculation and available measurements within the constraints of the respective uncertainties to produce a Best Estimate of the radiation field at each measurement location. These Best Estimate values have associated uncertainties less than those associated with the input parameters. The overall data base of [Best Estimate]/[Calculation] (BE/C) comparisons is then used to bias the plant-specific calculation to produce Best Estimate values at the pressure vessel wall with an associated uncertainty less than that applicable to the stand-alone calculation.

Least squares adjustment methods provide the capability of combining the measurement data with the neutron transport calculation resulting in a Best Estimate neutron energy spectrum with associated uncertainties. Best Estimates for key exposure parameters such as $\phi(E > 1.0 \text{ MeV})$ or dpa/s along with their uncertainties are then easily obtained from the adjusted spectrum. The use of measurements in combination with the analytical results reduces the uncertainty in the calculated spectrum and acts to remove biases that may be present in the analytical technique.

In general, the least squares methods, as applied to pressure vessel fluence evaluations, act to reconcile the measured sensor reaction rate data, dosimetry reaction cross-sections, and the calculated neutron energy spectrum within their respective uncertainties. For example,

$$R_i \pm \delta_{R_i} = \sum_g (\sigma_{ig} \pm \delta_{\sigma_{ig}})(\phi_g \pm \delta_{\phi_g})$$

relates a set of measured reaction rates, R_i , to a single neutron spectrum, ϕ_g , through the multigroup dosimeter reaction cross-section, σ_{ig} , each with an uncertainty δ .

The primary objective of the least squares evaluation is to produce unbiased estimates of the neutron exposure parameters at the location of the measurement. The analytical method alone may be deficient because it inherently contains uncertainty due to the input assumptions to the calculation. Typically these assumptions include parameters such as the temperature of the water in the peripheral fuel assemblies, bypass region, and downcomer regions, component dimensions, and peripheral core source. Industry consensus indicates that the use of calculation alone results in overall uncertainties in the neutron exposure parameters in the range of 15-20% (1σ).

By combining the calculated results with available measurements, the uncertainties associated with the key neutron exposure parameters can be reduced. Specifically ASTM Standard E 944 states:

“The algorithms of the adjustment codes tend to decrease the variances of the adjusted data compared to the corresponding input values. The least squares adjustment codes yield estimates for the output data with minimum variances, that is, the “best estimates”. This is the primary reason for using these adjustment procedures”.

In the current analysis, the FERRET^[31] code was employed to combine the results of plant specific neutron transport calculations and multiple foil reaction rate measurements to determine best estimate values of exposure parameters ($\phi(E > 1.0 \text{ MeV})$ and dpa) along with associated uncertainties at the surveillance capsule measurement locations.

The application of the least squares methodology requires the following input:

- 1 - The calculated neutron energy spectrum and associated uncertainties at the measurement location.
- 2 - The measured reaction rate and associated uncertainty for each sensor contained in the multiple foil set.
- 3 - The energy dependent dosimetry reaction cross-sections and associated uncertainties for each sensor contained in the multiple foil sensor set.

The calculated neutron spectrum is obtained from the results of plant specific neutron transport calculations applicable to the irradiation period experienced by the dosimetry sensor set. This calculation is based on the application of the benchmarked transport calculational methodology using the DORT discrete ordinates transport code. The sensor reaction rates are derived from the measured specific activities obtained from the counting laboratory using the specific irradiation history of the sensor set to perform the radioactive decay corrections. The dosimetry reaction cross-sections and uncertainties are obtained from the SNLRML dosimetry cross-section library^[33]. The SNLRML library is an evaluated dosimetry reaction cross-section compilation recommended for use in LWR evaluations by ASTM Standard E1018, “Application of ASTM Evaluated Cross-Section Data File, Matrix E 706 (IIB)”. There are no additional data or data libraries built into the FERRET code system. All of the required input is supplied externally at the time of the analysis.

The uncertainties associated with the measured reaction rates, dosimetry cross-sections, and calculated neutron spectrum are input to the least squares procedure in the form of variances and covariance's. The assignment of the input uncertainties also follows the guidance provided in ASTM Standard E 944.

The following provides a summary of the uncertainties associated with the least squares evaluation of the surveillance capsule dosimetry sets.

Reaction Rate Uncertainties

The overall uncertainty associated with the measured reaction rates includes components due to the basic measurement process, the irradiation history corrections, and the corrections for competing reactions. A high level of accuracy in the reaction rate determinations is assured by utilizing laboratory procedures that conform to ASTM National Consensus Standards. In all cases, the latest available versions of the applicable standard are used in the dosimetry evaluations.

From these standards, it is noted that the achievable uncertainties in the measured specific activities of each of the sensors comprising typical multiple foil sensor sets are as follows:

<u>Reaction</u>	<u>Precision</u>	<u>Bias</u>
$^{63}\text{Cu}(\text{n},\alpha)^{60}\text{Co}$	1%	3%
$^{46}\text{Ti}(\text{n},\text{p})^{46}\text{Sc}$	1%	3%
$^{54}\text{Fe}(\text{n},\text{p})^{54}\text{Mn}$	1%	3%
$^{58}\text{Ni}(\text{n},\text{p})^{58}\text{Co}$	1%	3%
$^{238}\text{U}(\text{n},\text{f})\text{FP}$	1%	5%
$^{59}\text{Co}(\text{n},\gamma)^{60}\text{Co}$	1%	5%

These uncertainties include the impacts of counting statistics, sample weighing, detector calibration, source/detector geometry corrections, and product nuclide branching ratios.

In determining reaction rates from the measured specific activities, the following additional uncertainties are incurred:

<u>Reaction</u>	<u>Fission Yield</u>	<u>Product Half-Life</u>	<u>Competing Reactions</u>
$^{63}\text{Cu}(\text{n},\alpha)^{60}\text{Co}$		0.02%	
$^{46}\text{Ti}(\text{n},\text{p})^{46}\text{Sc}$		0.2%	
$^{54}\text{Fe}(\text{n},\text{p})^{54}\text{Mn}$		0.2%	
$^{58}\text{Ni}(\text{n},\text{p})^{58}\text{Co}$		0.2%	
$^{238}\text{U}(\text{n},\text{f})\text{FP}$	1%	0.1%	4%
$^{59}\text{Co}(\text{n},\gamma)^{60}\text{Co}$		0.02%	

After combining all of these uncertainty components, the sensor reaction rates derived from the counting and data evaluation procedures result in the following net uncertainties associated with the sensor reaction rates that are input to the least squares evaluation:

<u>Reaction</u>	<u>Reaction Rate Uncertainty</u>
$^{63}\text{Cu}(n,\alpha)^{60}\text{Co}$	5%
$^{46}\text{Ti}(n,p)^{46}\text{Sc}$	5%
$^{54}\text{Fe}(n,p)^{54}\text{Mn}$	5%
$^{58}\text{Ni}(n,p)^{58}\text{Co}$	5%
$^{238}\text{U}(n,f)\text{FP}$	10%
$^{59}\text{Co}(n,\gamma)^{60}\text{Co}$	5%

The listed uncertainty values are at the 1σ level.

In addition to the use of ASTM National Consensus Standards in the evaluation of sensor reaction rates, these procedures have been periodically tested via round robin counting exercises included as a part of the NRC Sponsored Light Water Reactor Surveillance Dosimetry Improvement Program (LWR-SDIP) as well as by evaluation of fluence counting standards provided by the National Institute of Science and Technology (NIST).

Dosimetry Cross-Section Uncertainties

The reaction rate cross-sections used in the neutron fluence evaluations are taken from the SNLRML library^[33]. This data library provides reaction cross-sections and associated uncertainties, including covariances, for 66 dosimetry sensors in common use. Both cross-sections and uncertainties are provided in a fine multigroup structure for use in least squares adjustment applications. These cross-sections were compiled from the most recent cross-section evaluations and they have been tested with respect to their accuracy and consistency for least squares evaluations. Further, the library has been empirically tested for use in fission spectra determination as well as in the fluence and energy characterization of 14 MeV neutron sources. Detailed discussions of the contents of the SNLRML library along with the evaluation process for each of the sensors is provided in Reference 33.

For sensors of interest to LWR dosimetry applications, the following uncertainties in the fission spectrum averaged cross-sections are provided in the SNLRML documentation package.

<u>Reaction</u>	<u>Uncertainty</u>
$^{63}\text{Cu}(n,\alpha)^{60}\text{Co}$	4.08-4.16%
$^{46}\text{Ti}(n,p)^{46}\text{Sc}$	4.51-4.87%
$^{54}\text{Fe}(n,p)^{54}\text{Mn}$	3.05-3.11%
$^{58}\text{Ni}(n,p)^{58}\text{Co}$	4.49-4.56%
$^{238}\text{U}(n,f)\text{FP}$	0.54-0.64%
$^{59}\text{Co}(n,\gamma)^{60}\text{Co}$	0.79-3.59%

These tabulated ranges provide an indication of the dosimetry cross-section uncertainties associated with typical sensor sets used in LWR irradiations.

Calculated Neutron Spectrum

The neutron spectrum input to the least squares adjustment procedure is obtained directly from the results of plant specific transport calculations for each sensor location. The spectrum at each location is input in an absolute sense (rather than as simply a relative spectral shape). Therefore, within the constraints of the assigned uncertainties, the calculated data are treated equally with the measurements.

While the uncertainties associated with the reaction rates are obtained from the measurement procedures and counting benchmarks and the dosimetry cross-section uncertainties are supplied directly with the SNLRML library, the uncertainty matrix for the calculated spectrum is constructed from the following relationship:

$$M_{gg'} = R_n^2 + R_g R_{g'} P_{gg'}$$

where R_n specifies an overall fractional normalization uncertainty and the fractional uncertainties, R_g and $R_{g'}$, specify additional random groupwise uncertainties that are correlated with a correlation matrix given by:

$$P_{gg'} = [1 - \theta] \delta_{gg'} + \theta e^{-H}$$

where

$$H = \frac{(g - g')^2}{2\gamma^2}$$

The first term in the correlation matrix equation specifies purely random uncertainties, while the second term describes the short range correlation's over a group range γ (θ specifies the strength of the latter term). The value of δ is 1.0 when $g = g'$ and 0.0 otherwise. For the trial spectrum used in the current evaluations, a short range correlation of $\gamma = 6$ groups was used. This choice implies that neighboring groups are strongly correlated when θ is close to 1. Strong long-range correlation's (or anti-correlation's) were justified based on information presented by R. E. Maerker^[34]. The uncertainties associated with the measured reaction rates included both statistical (counting) and systematic components. The systematic component of the overall uncertainty accounts for counter efficiency, counter calibrations, irradiation history corrections, and corrections for competing reactions in the individual sensors.

The set of parameters defining the input uncertainties for the calculated spectrum is as follows:

Flux Normalization Uncertainty (R_n)	15%
Flux Group Uncertainties ($R_g, R_{g'}$)	
($E > 0.0055$ MeV)	15%
(0.68 eV $< E < 0.0055$ MeV)	29%
($E < 0.68$ eV)	52%

Short Range Correlation (θ)

($E > 0.0055$ MeV)	0.9
($0.68 \text{ eV} < E < 0.0055$ MeV)	0.5
($E < 0.68 \text{ eV}$)	0.5

Flux Group Correlation Range (γ)

($E > 0.0055$ MeV)	6
($0.68 \text{ eV} < E < 0.0055$ MeV)	3
($E < 0.68 \text{ eV}$)	2

Having the reaction rate, dosimetry cross-section, and calculated spectrum input with associated uncertainties, the overall least squares evaluation of the data set can be conveniently divided into the following two components:

- 1 - A pre-adjustment procedure performed by the SAND ^[32] module that processes the calculated neutron spectrum and SNLRML dosimetry cross-sections into the 53 energy group structure required by FERRET
- 2 - The subsequent application of the least squares algorithm in the FERRET module itself.

The pre-adjustment processing can be summarized as follows:

- 1 - The calculated neutron energy spectrum in the BUGLE-96 group structure is input to the SAND module.
- 2 - The input spectrum is expanded to 620 energy groups to provide compatibility with the SNLRML dosimetry cross-section library.
- 3 - The 620 group spectrum is combined with the dosimetry cross-section library to compute spectrum weighted cross-sections in the 53 energy group structure used in the FERRET module.
- 4 - The 620 group spectrum is likewise collapsed to the 53 energy group structure used in FERRET.

The application of this pre-processing procedure allows the fine group dosimetry cross-sections to be spectrally weighted by a calculated spectrum representative of the actual measurement location in the reactor. This approach, if executed properly, is superior to the use of broad group cross-sections that have been collapsed with an arbitrary spectrum.

The second step in the least squares adjustment procedure may be summarized as follows:

- 1 - The 53 group neutron energy spectrum and dosimetry reaction cross-sections output from the SAND module are input to the FERRET module along with the measured reaction rate for each sensor included in the multiple foil set. This input includes uncertainty estimates for the neutron spectrum, the dosimetry cross-sections, and the sensor reaction rates.

- 2 - The least squares evaluation of the input data is performed by the FERRET module.
- 3 - Best Estimate values of neutron exposure parameters [$\phi(E > 1.0 \text{ MeV})$ and dpa/s] along with associated uncertainties are output from the FERRET module.

Results of the least squares evaluation of the 97°, 104°, and 284° capsule dosimetry sets are given in Table 6-9. The data summarized in that table include fast neutron exposure evaluations in terms of $\Phi(E > 1.0 \text{ MeV})$, $\Phi(E > 0.1 \text{ MeV})$, and dpa. In general, good results were achieved in the fits of the best estimate spectra to the individual measured reaction rates. The measured, calculated, and best estimate reaction rates for each foil reaction are given in Table 6-10. The best estimate neutron spectra from the least squares evaluations of the capsule dosimetry sets are given in Table 6-11 in the FERRET 53 energy group structure.

The resultant uncertainties (1σ) associated with the Best Estimate fast neutron exposure of the three St. Lucie surveillance capsules are summarized as follows:

Quantity	Percent Standard Deviation		
	284° Capsule	104° Capsule	97° Capsule
$\Phi(E > 1.0 \text{ MeV})$	6	6	6
dpa	6	6	6
$\Phi(E > 0.1 \text{ MeV})$	9	9	10

It is important to note that the least squares adjustment procedure performed by the FERRET code is limited to the data evaluation at the measurement location. The purpose of this stage of the overall fluence evaluation methodology is to obtain the best estimates of the neutron exposure at the measurement location in terms of $\phi(E > 1.0 \text{ MeV})$ and dpa as well as to estimate the uncertainty associated with each of these capsule exposures. The FERRET code does not perform an adjustment of the neutron spectrum at the pressure vessel wall.

In Table 6-12, absolute comparisons of the best estimate and calculated fluence at the center of the 97°, 104°, and 284° capsules are presented. The results for the dosimetry evaluation (BE/C ratio of 0.96 for $\Phi(E > 1.0 \text{ MeV})$) are consistent with results obtained from similar evaluations of dosimetry from other reactors using methodologies based on ENDF/B-VI cross-sections.

6.4 PROJECTIONS OF REACTOR VESSEL EXPOSURE

The best estimate exposure of the St. Lucie Unit 1 reactor vessel was developed using a combination of absolute plant specific transport calculations and all available plant specific measurement data. In the case of St. Lucie Unit 1, the measurement data base contains measurements from the three surveillance capsules discussed in this report.

Combining this measurement data base with the plant-specific calculations, the best estimate vessel exposure is obtained from the following relationship:

$$\Phi_{Best\ Est.} = K \Phi_{Calc.}$$

where:

- $\Phi_{Best\ Est.}$ = The best estimate fast neutron exposure at the location of interest.
- K = The plant specific best estimate/calculation (BE/C) bias factor derived from the surveillance capsule dosimetry data.
- $\Phi_{Calc.}$ = The absolute calculated fast neutron exposure at the location of interest.

A distinction should be made between the Best Estimate/Calculation, or [BE]/[C], ratios and the Measurement/Calculation, or [M]/[C], ratios. In this case, Best Estimate values refer to the combination of calculation and measurement via a least squares adjustment procedure to arrive at the best estimate of the neutron flux ($E > 1.0$ MeV) with an associated uncertainty. The least squares procedure provides a weighting of calculated and measured input based on the energy response and uncertainty associated with each input parameter. The [BE]/[C] ratios, therefore, represent a comparison of the results of the least squares adjustment with the analytical prediction of the neutron flux ($E > 1.0$ MeV). The [M]/[C] ratios, on the other hand, provide a direct comparison of actual calculated and measured individual foil reaction rates. Using the [M]/[C] data, a direct comparison of calculated and measured neutron flux ($E > 1.0$ MeV) can not be made without a suitable weighting of the individual foil results.

The approach defined in the above equation is based on the premise that the measurement data represent the most accurate plant-specific information available at the locations of the dosimetry; and, further that the use of the measurement data on a plant-specific basis essentially removes biases present in the analytical approach and mitigates the uncertainties that would result from the use of analysis alone.

That is, at the measurement points the uncertainty in the best estimate exposure is dominated by the uncertainties in the measurement process. At locations within the reactor vessel wall, additional uncertainty is incurred due to the analytically determined relative ratios among the various measurement points and locations within the reactor vessel wall.

The use of the bias factors derived from the measurement data base acts to remove plant-specific biases associated with the definition of the core source, actual versus assumed reactor dimensions, and operational variations in water density within the reactor. As a result, the overall uncertainty in the best estimate exposure projections within the vessel wall depends on the individual uncertainties in the measurement process, the uncertainty in the dosimetry location, and in the uncertainty in the calculated ratio of the neutron exposure at the point of interest to that at the measurement location.

The uncertainty in the derived neutron flux for an individual measurement is obtained directly from the results of a least squares evaluation of dosimetry data. The least squares approach combines individual uncertainty in the calculated neutron energy spectrum, the uncertainties in dosimetry cross-sections, and the uncertainties in measured foil specific activities to produce a net uncertainty in the derived neutron flux at the measurement point. The associated uncertainty in the plant specific bias factor, K, derived from the BE/C data base, in turn, depends on the total number of available measurements as well as on the uncertainty of each measurement.

In developing the overall uncertainty associated with the reactor vessel exposure, the positioning uncertainties for dosimetry are taken from parametric studies of sensor position performed as part a series of analytical sensitivity studies included in the qualification of the methodology. The uncertainties in the exposure ratios relating dosimetry results to positions within the vessel wall are again based on the analytical sensitivity studies of the vessel thickness tolerance, downcomer water density variations, and vessel inner radius tolerance. Thus, this portion of the overall uncertainty is controlled entirely by dimensional tolerances associated with the reactor design and by the operational characteristics of the reactor.

For St. Lucie Unit 1, the bias factor for $\Phi(E > 1.0 \text{ MeV})$ was developed as follows:

Capsule	Best Estimate	% Std Dev	Calculated	BE/C
	$\Phi(E > 1.0 \text{ MeV})$ [n/cm ²]		$\Phi(E > 1.0 \text{ MeV})$ [n/cm ²]	
284°	1.53E+19	6	1.45E+19	1.05
104°	8.29E+18	6	9.18E+18	0.90
97°	5.52E+18	6	5.91E+18	0.93
[BE]/[C] Bias Factor K				0.96
% standard deviation				8

In regard to the irradiation of these three surveillance capsules, it is noted that the 97° capsule was irradiated with the thermal shield in place for 5 fuel cycles. The 104° and 284° capsules were irradiated for 5 fuel cycles with the thermal shield in place and for 3 fuel cycles and 10 fuel cycles, respectively, with the thermal shield removed. A comparison of the BE/C ratios for the 104° and 284° capsules relative to the 97° capsule shows a lower BE/C ratio for the 104° data set and a higher BE/C for the 284° data set. There is no systematic trend in BE/C that could be attributable to either the removal of the thermal shield or to the earlier power uprate of the St. Lucie reactor. Therefore, the three capsule data set has been treated as a single population for the purpose of determining an overall BE/C. The variability of the BE/C ratios observed at St. Lucie are within the variability observed at other operating PWR's and are consistent within the standard deviation of the best estimate results.

Based on this set of [Best Estimate]/[Calculation] comparisons, the bias factor to be applied to the plant specific calculated neutron flux distributions is 0.96 with an associated standard deviation of 8%. Thus, the Best Estimate fluence at locations within the pressure vessel wall is given by:

$$\Phi_{\text{BestEst.}} = 0.96\Phi_{\text{Calc}}$$

In a similar manner, bias factors of $0.99 \pm 6\%$, and $0.97 \pm 7\%$ were developed for $\Phi(E > 0.1 \text{ MeV})$, and dpa, respectively. The overall uncertainty in the Best Estimate exposure projections for the pressure vessel wall stem primarily from two sources.

- 1 - The uncertainty in the average [BE]/[C] normalization factor that is applied to the plant specific transport calculations, and
- 2 - The additional analytical uncertainty associated with relating the [BE]/[C] results based on data from the measurement locations to the desired results within the pressure vessel wall.

Uncertainty in the [BE]/[C] bias factor derives directly from the individual uncertainties in the measurement process, in the least squares adjustment procedure, and from the number of data points comprising the overall [BE]/[C] data base for the reactor being evaluated. The additional positioning uncertainties are taken from analytical sensitivity studies of sensor positioning and pressure vessel wall tolerances performed as a part of the overall benchmarking of the fluence methodology.

Having the uncertainty in the [BE]/[C] bias factor (σ_K) and the uncertainty in the relative position of the reactor vessel wall relative to the measurement points (σ_P), the total uncertainty in the Best Estimate neutron exposure at locations within the pressure vessel wall (σ_T) is determined from the following relationship:

$$(\sigma_T)^2 = (\sigma_K)^2 + (\sigma_P)^2$$

For the St. Lucie application, the uncertainty in the BE/C bias factor was determined to be $\sigma_K = 8\%$ and the uncertainty associated with the tolerances in dosimetry positioning, vessel inner radius, and downcomer water temperature were determined to be $\sigma_P = 6\%$. Thus, the total uncertainty in the Best Estimate projection of neutron fluence at the pressure vessel wall is $\sigma_T = 10.2\%$. This level of uncertainty is well within the 20% 1σ uncertainty required by 10CFR50.61.

Tables 6-13 and 6-14 provide best estimate neutron exposure projections (which includes the bias factor, K) and calculated neutron exposure projections (which do not include K) for the 0° , 15° , 30° , and 45° azimuths at the vessel inner radius and within the vessel wall, respectively. It should be recognized that the Upper Shelf Energy (USE) projections are based on the peak fluence values at 0° . In addition, the data that is provided in Table 6-14 is based on both a $\Phi(E > 1.0 \text{ MeV})$ slope and a plant-specific dpa slope through the vessel wall.

Exposure projections for future operation are presented in Tables 6-13 and 6-14 for exposure periods of 25, 32, 35, 48, and 54 EFPY. The basis for all future exposure projections, beyond the current operating exposure of 17.23 EFPY, is that the Cycle 15 fuel management (In-out loading pattern and no Hafnium rods in the peripheral fuel assemblies, is representative of the fuel management to be used in all future fuel cycles.

In order to assess RT_{NDT} versus fluence curves, dpa equivalent fast neutron fluence levels for the $1/4T$ and $3/4T$ positions were defined by the relations:

$$\phi(1/4T) = \phi(0T) \frac{dpa(1/4T)}{dpa(0T)} \quad \text{and} \quad \phi(3/4T) = \phi(0T) \frac{dpa(3/4T)}{dpa(0T)}$$

Using this approach results in the dpa equivalent fluence values listed in Table 6-14.

In Table 6-15, updated lead factors are listed for each of the St. Lucie Unit 1 surveillance capsules.

Table 6-1

Calculated Fast Neutron Exposure Rates and Iron Atom
Displacement Rates at the Surveillance Capsule Center

$\phi(E > 1.0 \text{ MeV}) \text{ (n/cm}^2\text{-sec)}$		
<u>Capsule Positions</u>		
<u>Cycle(s)</u>	<u>7°</u>	<u>14°</u>
1-4	4.19E+10	2.96E+10
5	3.64E+10	2.40E+10
6-9	4.69E+10	3.29E+10
10	2.69E+10	2.33E+10
11	2.09E+10	1.93E+10
12	2.44E+10	2.15E+10
13	2.23E+10	2.00E+10
14	2.53E+10	2.25E+10
15	3.22E+10	2.48E+10

$\phi(E > 0.1 \text{ MeV}) \text{ (n/cm}^2\text{-sec)}$		
<u>Capsule Positions</u>		
<u>Cycle(s)</u>	<u>7°</u>	<u>14°</u>
1-4	9.51E+10	6.70E+10
5	8.32E+10	5.40E+10
6-9	8.49E+10	5.91E+10
10	4.85E+10	4.16E+10
11	3.75E+10	3.42E+10
12	4.38E+10	3.81E+10
13	3.99E+10	3.54E+10
14	4.54E+10	3.98E+10
15	5.81E+10	4.43E+10

Iron Atom Displacement Rate (dpa/sec)		
<u>Capsule Positions</u>		
<u>Cycle(s)</u>	<u>7°</u>	<u>14°</u>
1-4	6.36E-11	4.50E-11
5	5.55E-11	3.65E-11
6-9	6.81E-11	4.80E-11
10	3.91E-11	3.40E-11
11	3.05E-11	2.83E-11
12	3.55E-11	3.15E-11
13	3.25E-11	2.93E-11
14	3.68E-11	3.29E-11
15	4.68E-11	3.61E-11

Table 6-2

Calculated Azimuthal Variation of Fast Neutron Exposure Rates
and Iron Atom Displacement Rates at the Reactor Vessel
Clad/Base Metal Interface

<u>Cycle(s)</u>	$\phi(E > 1.0 \text{ MeV}) \text{ (n/cm}^2\text{-sec)}$			
	<u>0°</u>	<u>15°</u>	<u>30°</u>	<u>45°</u>
1-4	2.76E+10	1.70E+10	1.65E+10	1.22E+10
5	2.69E+10	1.41E+10	1.21E+10	8.51E+09
6-9	3.70E+10	2.12E+10	1.81E+10	1.33E+10
10	1.95E+10	1.56E+10	1.83E+10	1.40E+10
11	1.65E+10	1.37E+10	1.94E+10	1.45E+10
12	1.92E+10	1.49E+10	1.99E+10	1.42E+10
13	1.75E+10	1.40E+10	1.85E+10	1.41E+10
14	1.94E+10	1.53E+10	1.86E+10	1.46E+10
15	2.36E+10	1.59E+10	1.35E+10	1.09E+10

<u>Cycle(s)</u>	$\phi(E > 0.1 \text{ MeV}) \text{ (n/cm}^2\text{-sec)}$			
	<u>0°</u>	<u>15°</u>	<u>30°</u>	<u>45°</u>
1-4	7.03E+10	4.56E+10	4.19E+10	3.04E+10
5	6.85E+10	3.78E+10	3.06E+10	2.13E+10
6-9	8.03E+10	4.79E+10	3.96E+10	2.88E+10
10	4.25E+10	3.48E+10	3.98E+10	3.02E+10
11	3.57E+10	3.03E+10	4.22E+10	3.11E+10
12	4.15E+10	3.31E+10	4.33E+10	3.06E+10
13	3.80E+10	3.10E+10	4.02E+10	3.04E+10
14	4.21E+10	3.41E+10	4.04E+10	3.14E+10
15	5.13E+10	3.56E+10	2.94E+10	2.35E+10

<u>Cycle(s)</u>	Iron Atom Displacement Rate (dpa/sec)			
	<u>0°</u>	<u>15°</u>	<u>30°</u>	<u>45°</u>
1-4	4.38E-11	2.75E-11	2.62E-11	1.94E-11
5	4.26E-11	2.29E-11	1.92E-11	1.36E-11
6-9	5.64E-11	3.29E-11	2.79E-11	2.06E-11
10	3.00E-11	2.42E-11	2.80E-11	2.17E-11
11	2.53E-11	2.12E-11	2.98E-11	2.24E-11
12	2.93E-11	2.32E-11	3.05E-11	2.20E-11
13	2.68E-11	2.17E-11	2.84E-11	2.18E-11
14	2.97E-11	2.38E-11	2.86E-11	2.25E-11
15	3.62E-11	2.46E-11	2.07E-11	1.69E-11

Table 6-3

Relative Radial Distribution of $\phi(E > 1.0 \text{ MeV})$
Within the Reactor Vessel Wall

Radius (cm)	Azimuthal Angle			
	0°	15°	30°	45°
221.55	1.000	1.000	1.000	1.000
222.08	0.966	0.966	0.966	0.965
223.12	0.879	0.872	0.879	0.876
224.16	0.785	0.779	0.785	0.785
225.20	0.695	0.693	0.696	0.695
226.25	0.612	0.611	0.614	0.613
227.29	0.536	0.537	0.539	0.539
228.33	0.469	0.470	0.472	0.472
229.38	0.409	0.412	0.412	0.412
230.42	0.356	0.359	0.359	0.360
231.46	0.310	0.314	0.313	0.313
232.51	0.269	0.273	0.272	0.273
233.55	0.233	0.238	0.236	0.237
234.59	0.202	0.205	0.204	0.205
235.64	0.174	0.179	0.177	0.178
236.68	0.150	0.153	0.153	0.154
237.72	0.129	0.133	0.132	0.133
238.77	0.111	0.114	0.114	0.115
239.81	0.094	0.098	0.097	0.098
240.85	0.080	0.084	0.083	0.085
241.89	0.067	0.071	0.070	0.072
242.94	0.054	0.059	0.058	0.060
244.73	0.047	0.051	0.052	0.054

Note:	Base Metal Inner Radius	=	221.55 cm
	Base Metal $\frac{1}{4}T$	=	227.03 cm
	Base Metal $\frac{1}{2}T$	=	232.51 cm
	Base Metal $\frac{3}{4}T$	=	237.98 cm
	Base Metal Outer Radius	=	243.46 cm

Table 6-4

Relative Radial Distribution of $\phi(E > 0.1 \text{ MeV})$
Within the Reactor Vessel Wall

Radius (cm)	Azimuthal Angle			
	0°	15°	30°	45°
221.55	1.000	1.000	1.000	1.000
222.08	1.007	1.008	1.008	1.008
223.12	0.991	0.990	0.993	0.995
224.16	0.958	0.960	0.962	0.967
225.20	0.919	0.925	0.925	0.931
226.25	0.876	0.884	0.884	0.890
227.29	0.831	0.842	0.841	0.850
228.33	0.787	0.799	0.798	0.807
229.38	0.741	0.757	0.754	0.765
230.42	0.697	0.714	0.711	0.723
231.46	0.654	0.673	0.669	0.681
232.51	0.611	0.631	0.628	0.641
233.55	0.569	0.591	0.587	0.602
234.59	0.528	0.550	0.547	0.562
235.64	0.488	0.511	0.509	0.525
236.68	0.449	0.472	0.471	0.487
237.72	0.410	0.434	0.434	0.451
238.77	0.372	0.397	0.397	0.415
239.81	0.335	0.360	0.361	0.380
240.85	0.297	0.324	0.326	0.346
241.89	0.259	0.286	0.290	0.311
242.94	0.219	0.247	0.254	0.276
244.73	0.195	0.223	0.232	0.255

Note: Base Metal Inner Radius = 221.55 cm
Base Metal $\frac{1}{4}$ T = 227.03 cm
Base Metal $\frac{1}{2}$ T = 232.51 cm
Base Metal $\frac{3}{4}$ T = 237.98 cm
Base Metal Outer Radius = 243.46 cm

Table 6-5

Relative Radial Distribution of dpa/sec
Within the Reactor Vessel Wall

Radius (cm)	Azimuthal Angle			
	0°	15°	30°	45°
221.55	1.000	1.000	1.000	1.000
222.08	0.971	0.972	0.971	0.970
223.12	0.899	0.895	0.899	0.896
224.16	0.821	0.820	0.822	0.822
225.20	0.747	0.750	0.750	0.748
226.25	0.678	0.683	0.682	0.680
227.29	0.614	0.621	0.619	0.618
228.33	0.556	0.564	0.562	0.561
229.38	0.503	0.514	0.510	0.509
230.42	0.455	0.467	0.463	0.464
231.46	0.412	0.425	0.420	0.420
232.51	0.373	0.386	0.381	0.383
233.55	0.337	0.351	0.346	0.348
234.59	0.304	0.318	0.313	0.315
235.64	0.274	0.289	0.283	0.287
236.68	0.246	0.260	0.257	0.260
237.72	0.221	0.235	0.231	0.236
238.77	0.197	0.211	0.208	0.213
239.81	0.174	0.188	0.186	0.191
240.85	0.153	0.167	0.165	0.171
241.89	0.132	0.146	0.146	0.152
242.94	0.110	0.126	0.126	0.134
244.73	0.098	0.113	0.115	0.124

Note:	Base Metal Inner Radius	=	221.55 cm
	Base Metal $\frac{1}{4}$ T	=	227.03 cm
	Base Metal $\frac{1}{2}$ T	=	232.51 cm
	Base Metal $\frac{3}{4}$ T	=	237.98 cm
	Base Metal Outer Radius	=	243.46 cm

Table 6-6

Nuclear Parameters Used in the Evaluation of Neutron Sensors

Monitor Material	Reaction of Interest	Target Atom Fraction	Response Range	Product Half-life	Fission Yield (%)
Copper	$^{63}\text{Cu} (n, \alpha)$	0.6917	$E > 4.7 \text{ MeV}$	5.271 y	
Titanium	$^{46}\text{Ti} (n, p)$	0.0825	$E > 4.4 \text{ MeV}$	83.79 d	
Iron	$^{54}\text{Fe} (n, p)$	0.0585	$E > 1.0 \text{ MeV}$	312.3 d	
Nickel	$^{58}\text{Ni} (n, p)$	0.6808	$E > 1.0 \text{ MeV}$	70.82 d	
Cobalt-Al	$^{59}\text{Co} (n, \gamma)$	0.0015	non-threshold	5.271 y	
Uranium-238	$^{238}\text{U} (n, f)$	0.9996	$E > 0.4 \text{ MeV}$	30.07 y	6.02

Notes:

1. Various monitors are cadmium shielded.
2. Target atom fraction for ^{238}U assumed 350 ppm ^{235}U .

Table 6-7

Monthly Thermal Generation During the First Fifteen Fuel Cycles
of the St. Lucie Unit 1 Reactor
(Reactor Power of 2700 MWt)

Year	Month	Thermal Generat. (MW-hr)	Year	Month	Thermal Generat. (MW-hr)	Year	Month	Thermal Generat. (MW-hr)
1976	5	440372	1979	7	1836859	1982	9	1872813
1976	6	97690	1979	8	1897496	1982	10	1897947
1976	7	308019	1979	9	1082095	1982	11	1816532
1976	8	0	1979	10	1439455	1982	12	1956855
1976	9	0	1979	11	1820321	1983	1	1872765
1976	10	0	1979	12	1901210	1983	2	1659657
1976	11	0	1980	1	1818926	1983	3	0
1976	12	347603	1980	2	1775685	1983	4	0
1977	1	1317560	1980	3	892672	1983	5	0
1977	2	1389034	1980	4	0	1983	6	0
1977	3	1592703	1980	5	890501	1983	7	0
1977	4	407185	1980	6	625543	1983	8	0
1977	5	1519476	1980	7	1874604	1983	9	0
1977	6	1377938	1980	8	1697623	1983	10	0
1977	7	1705677	1980	9	1810963	1983	11	0
1977	8	1865335	1980	10	1885676	1983	12	0
1977	9	1450241	1980	11	1814059	1984	1	0
1977	10	1270278	1980	12	1902530	1984	2	0
1977	11	1764776	1981	1	1873725	1984	3	0
1977	12	1841408	1981	2	1717790	1984	4	0
1978	1	1569897	1981	3	1901230	1984	5	798009
1978	2	1678630	1981	4	1517646	1984	6	1884155
1978	3	1642702	1981	5	1881121	1984	7	1732947
1978	4	0	1981	6	1838626	1984	8	1882130
1978	5	0	1981	7	1885109	1984	9	1415580
1978	6	1488742	1981	8	1893652	1984	10	1990103
1978	7	1877051	1981	9	438971	1984	11	1930083
1978	8	1781953	1981	10	0	1984	12	1834566
1978	9	1742015	1981	11	0	1985	1	1950365
1978	10	1598034	1981	12	1127901	1985	2	1801216
1978	11	1284581	1982	1	1946002	1985	3	1964733
1978	12	1705329	1982	2	1791664	1985	4	1927520
1979	1	1505641	1982	3	1984448	1985	5	1990987
1979	2	1641249	1982	4	1922445	1985	6	1930233
1979	3	1891957	1982	5	768617	1985	7	1971995
1979	4	0	1982	6	1897597	1985	8	1975243
1979	5	0	1982	7	1990892	1985	9	1929908
1979	6	1025125	1982	8	1965785	1985	10	1214386

Table 6-7 Cont'd

Monthly Thermal Generation During the First Fifteen Fuel Cycles
of the St. Lucie Unit 1 Reactor
(Reactor Power of 2700 MWt)

<u>Year</u>	<u>Month</u>	<u>Thermal Generat. (MW-hr)</u>	<u>Year</u>	<u>Month</u>	<u>Thermal Generat. (MW-hr)</u>	<u>Year</u>	<u>Month</u>	<u>Thermal Generat. (MW-hr)</u>
1985	11	0	1989	1	1977328	1992	3	2008800
1985	12	98138	1989	2	1800643	1992	4	1903500
1986	1	1963711	1989	3	1987159	1992	5	2008800
1986	2	1773239	1989	4	1934223	1992	6	1865700
1986	3	2004406	1989	5	1994532	1992	7	2008800
1986	4	1862951	1989	6	1783978	1992	8	1919700
1986	5	2009078	1989	7	849129	1992	9	1085400
1986	6	1081761	1989	8	1989644	1992	10	2003400
1986	7	2008970	1989	9	1834971	1992	11	1930500
1986	8	1975834	1989	10	1982298	1992	12	1979100
1986	9	1722036	1989	11	1907837	1993	1	1962900
1986	10	1998087	1989	12	1894712	1993	2	1787400
1986	11	1933003	1990	1	1248855	1993	3	1806300
1986	12	1993847	1990	2	0	1993	4	0
1987	1	2002084	1990	3	0	1993	5	0
1987	2	386909	1990	4	229500	1993	6	734400
1987	3	0	1990	5	1560600	1993	7	2003400
1987	4	832420	1990	6	1852200	1993	8	1965600
1987	5	1891173	1990	7	99900	1993	9	1350000
1987	6	1877939	1990	8	1476900	1993	10	1971000
1987	7	2003731	1990	9	1944000	1993	11	1898100
1987	8	2004433	1990	10	1876500	1993	12	1944000
1987	9	1933003	1990	11	1941300	1994	1	1906200
1987	10	1286517	1990	12	1952100	1994	2	1814400
1987	11	1937190	1991	1	1914300	1994	3	1765800
1987	12	1973080	1991	2	1800900	1994	4	1741500
1988	1	2007107	1991	3	2008800	1994	5	1962900
1988	2	1877156	1991	4	1898100	1994	6	1536300
1988	3	1903649	1991	5	1825200	1994	7	1941300
1988	4	1941214	1991	6	1809000	1994	8	1871100
1988	5	2000153	1991	7	1806300	1994	9	1903500
1988	6	1878506	1991	8	1952100	1994	10	1657800
1988	7	612621	1991	9	1838700	1994	11	0
1988	8	2511	1991	10	1144800	1994	12	1863000
1988	9	1556411	1991	11	0	1995	1	2008800
1988	10	2011022	1991	12	480600	1995	2	1679400
1988	11	1944291	1992	1	2008800	1995	3	1482300
1988	12	1938835	1992	2	1879200	1995	4	1944000

Table 6-7 Cont'd

Monthly Thermal Generation During the First Fifteen Fuel Cycles
of the St. Lucie Unit 1 Reactor
(Reactor Power of 2700 MWt)

<u>Year</u>	<u>Month</u>	<u>Thermal Generat. (MW-hr)</u>	<u>Year</u>	<u>Month</u>	<u>Thermal Generat. (MW-hr)</u>
1995	5	2008800	1997	8	2008800
1995	6	1930500	1997	9	1941300
1995	7	1760400	1997	10	1225800
1995	8	37800	1997	11	0
1995	9	0	1997	12	0
1995	10	1109700	1998	1	1228500
1995	11	1768500	1998	2	1336500
1995	12	2008800	1998	3	2008800
1996	1	1998000	1998	4	1938600
1996	2	1655100	1998	5	2008800
1996	3	1925100	1998	6	1868400
1996	4	1822500	1998	7	2008800
1996	5	0	1998	8	2008800
1996	6	0	1998	9	1930500
1996	7	288900	1998	10	2008800
1996	8	1952100	1998	11	1919700
1996	9	1331100	1998	12	2008800
1996	10	1981800	1999	1	2006100
1996	11	1917000	1999	2	1795500
1996	12	1976400	1999	3	2003400
1997	1	1995300	1999	4	1938600
1997	2	1806300	1999	5	2008800
1997	3	1806300	1999	6	1941300
1997	4	1649700	1999	7	2006100
1997	5	2006100	1999	8	1676700
1997	6	1944000	1999	9	764100
1997	7	1984500			

Table 6-8

Measured Sensor Activities and Reaction Rates

284° Surveillance Capsule

<u>Reaction</u>	<u>Location</u>	<u>Measured Activity (dps/gm)</u>	<u>Saturated Activity (dps/gm)</u>	<u>Reaction Rate (rps/atom)</u>
$^{63}\text{Cu} (n,\alpha) ^{60}\text{Co} (\text{Cd})$	CAP37614	1.96E+05	2.74E+05	4.18E-17
	CAP67641	1.82E+05	2.55E+05	3.88E-17
	CAP67673	1.94E+05	2.71E+05	4.14E-17
$^{46}\text{Ti} (n, p) ^{46}\text{Sc}$	CAP37614	1.46E+05	8.98E+05	8.30E-16
	CAP67641	1.26E+05	7.75E+05	7.17E-16
	CAP67673	1.38E+05	8.49E+05	7.85E-16
$^{54}\text{Fe} (n,p) ^{54}\text{Mn}$	CAP37614	1.20E+06	2.19E+06	3.48E-15
	CAP67641	1.07E+06	1.96E+06	3.10E-15
	CAP67673	1.14E+06	2.08E+06	3.30E-15
$^{58}\text{Ni} (n,p) ^{58}\text{Co} (\text{Cd})$	CAP37614	5.10E+06	4.47E+07	6.39E-15
	CAP67641	4.35E+06	3.81E+07	5.45E-15
	CAP67673	4.76E+06	4.17E+07	5.97E-15
$^{59}\text{Co} (n,\gamma) ^{60}\text{Co}$	CAP37614	1.41E+07	2.86E+07	1.87E-12
	CAP67641	1.50E+07	3.04E+07	1.99E-12
	CAP67673	1.14E+07	2.31E+07	1.51E-12
$^{59}\text{Co} (n,\gamma) ^{60}\text{Co} (\text{Cd})$	CAP37614	1.89E+06	3.84E+06	2.50E-13
	CAP67641	1.97E+06	4.00E+06	2.61E-13
	CAP67673	1.93E+06	3.92E+06	2.56E-13
$^{238}\text{U} (n,f) ^{137}\text{Cs}$	CAP37614	1.04E+06	3.41E+06	2.24E-14
	CAP67641	1.02E+06	3.35E+06	2.20E-14
	CAP67673	8.62E+05	2.83E+06	1.86E-14
Average Including ^{235}U , ^{239}Pu , and γ , fission corrections				1.48E-14

Table 6-8 cont'd

Measured Sensor Activities and Reaction Rates

104° Surveillance Capsule

<u>Reaction</u>	<u>Location</u>	<u>Measured Activity (dps/gm)</u>	<u>Saturated Activity (dps/gm)</u>	<u>Reaction Rate (rps/atom)</u>
$^{63}\text{Cu} (n,\alpha) ^{60}\text{Co} (\text{Cd})$	1-7314	1.78E+05	2.66E+05	4.06E-17
	1-7341	1.66E+05	2.48E+05	3.79E-17
	1-7373	1.79E+05	2.68E+05	4.09E-17
$^{46}\text{Ti} (n, p) ^{46}\text{Sc}$	2-7314	1.84E+05	6.13E+05	5.67E-16
	2-7341	1.55E+05	5.16E+05	4.77E-16
	2-7373	1.61E+05	5.36E+05	4.96E-16
$^{54}\text{Fe} (n,p) ^{54}\text{Mn}$	2-7314	1.40E+06	1.87E+06	2.97E-15
	2-7341	1.28E+06	1.71E+06	2.71E-15
	2-7373	1.31E+06	1.75E+06	2.78E-15
$^{58}\text{Ni} (n,p) ^{58}\text{Co} (\text{Cd})$	1-7314	6.18E+06	2.75E+07	3.93E-15
	1-7341	5.34E+06	2.37E+07	3.40E-15
	1-7373	5.19E+06	2.31E+07	3.30E-15
$^{59}\text{Co} (n,\gamma) ^{60}\text{Co}$	2-7314	1.92E+07	3.93E+07	2.56E-12
	2-7341	1.96E+07	4.01E+07	2.61E-12
	2-7373	1.24E+07	2.54E+07	1.65E-12
$^{59}\text{Co} (n,\gamma) ^{60}\text{Co} (\text{Cd})$	1-7314	2.43E+06	4.97E+06	3.24E-13
	1-7341	2.48E+06	5.07E+06	3.31E-13
	1-7373	2.43E+06	4.97E+06	3.24E-13
$^{238}\text{U} (n,f) ^{137}\text{Cs}$	2-7314	8.55E+05	4.44E+06	2.91E-14
	2-7341	8.96E+05	4.65E+06	3.05E-14
	2-7373	6.78E+05	3.52E+06	2.31E-14
Average Including ^{235}U , ^{239}Pu , and γ ,fission corrections				1.92E-14
$^{238}\text{U} (n,f) ^{137}\text{Cs} (\text{Cd})$	1-7314	3.18E+05	1.65E+06	1.08E-14
	1-7341	3.03E+05	1.57E+06	1.03E-14
	1-7373	3.49E+05	1.81E+06	1.19E-14
Average Including ^{235}U , ^{239}Pu , and γ ,fission corrections				7.67E-15

Table 6-8 cont'd

Measured Sensor Activities and Reaction Rates

97° Surveillance Capsule

<u>Reaction</u>	<u>Location</u>	<u>Measured Activity (dps/gm)</u>	<u>Saturated Activity (dps/gm)</u>	<u>Reaction Rate (rps/atom)</u>
$^{63}\text{Cu} (n,\alpha) ^{60}\text{Co} (\text{Cd})$	A	1.43E+05	3.42E+05	5.22E-17
	B	1.38E+05	3.30E+05	5.03E-17
	C	1.52E+05	3.63E+05	5.54E-17
$^{46}\text{Ti} (n, p) ^{46}\text{Sc}$	A	5.87E+05	6.98E+05	6.46E-16
	B	6.30E+05	7.49E+05	6.93E-16
	C	6.60E+05	7.85E+05	7.26E-16
$^{54}\text{Fe} (n,p) ^{54}\text{Mn}$	A	1.82E+06	2.36E+06	3.73E-15
	B	1.97E+06	2.55E+06	4.04E-15
	C	1.93E+06	2.50E+06	3.96E-15
$^{58}\text{Ni} (n,p) ^{58}\text{Co} (\text{Cd})$	A	3.25E+07	3.83E+07	5.49E-15
	B	3.45E+07	4.07E+07	5.82E-15
	C	2.90E+07	3.42E+07	4.90E-15
$^{59}\text{Co} (n,\gamma) ^{60}\text{Co}$	A	3.05E+07	7.29E+07	4.76E-12
	B	2.20E+07	5.26E+07	3.43E-12
	C	3.00E+07	7.17E+07	4.68E-12
$^{59}\text{Co} (n,\gamma) ^{60}\text{Co} (\text{Cd})$	A	4.58E+06	1.10E+07	7.15E-13
	B	4.63E+06	1.11E+07	7.22E-13
	C	4.60E+06	1.10E+07	7.18E-13
$^{238}\text{U} (n,f) ^{137}\text{Cs}$	A	6.10E+05	6.13E+06	4.03E-14
	B	8.27E+05	8.32E+06	5.46E-14
	C	7.17E+05	7.21E+06	4.74E-14
Average Including ^{235}U , ^{239}Pu , and γ ,fission corrections				
$^{238}\text{U} (n,f) ^{137}\text{Cs} (\text{Cd})$	A	2.48E+05	2.49E+06	1.64E-14
	B	3.35E+05	3.37E+06	2.21E-14
	C	3.83E+05	3.85E+06	2.53E-14
Average Including ^{235}U , ^{239}Pu , and γ ,fission corrections				
				1.67E-14

Table 6-9

Summary of Neutron Dosimetry Results
97°, 104°, and 284° Surveillance Capsules

Best Estimate Flux and Fluence for 284° Capsule

<u>Quantity</u>	<u>Flux</u> <u>[n/cm²-sec]</u>	<u>Quantity</u>	<u>Fluence</u> <u>[n/cm²]</u>	<u>Uncertainty</u>
ϕ (E > 1.0 MeV)	2.82E+10	Φ (E > 1.0 MeV)	1.53E+19	6%
ϕ (E > 0.1 MeV)	5.40E+10	Φ (E > 0.1 MeV)	2.93E+19	9%
ϕ (E < 0.414 eV)	6.30E+10	Φ (E < 0.414 eV)	3.43E+19	8%
dpa/sec	4.11E-11	dpa	2.23E-02	6%

Best Estimate Flux and Fluence for 104° Capsule

<u>Quantity</u>	<u>Flux</u> <u>[n/cm²-sec]</u>	<u>Quantity</u>	<u>Fluence</u> <u>[n/cm²]</u>	<u>Uncertainty</u>
ϕ (E > 1.0 MeV)	2.76E+10	Φ (E > 1.0 MeV)	8.29E+18	6%
ϕ (E > 0.1 MeV)	5.95E+10	Φ (E > 0.1 MeV)	1.78E+19	9%
ϕ (E < 0.414 eV)	8.01E+10	Φ (E < 0.414 eV)	2.40E+19	8%
dpa/sec	4.10E-11	dpa	1.23E-02	6%

Best Estimate Flux and Fluence for 97° Capsule

<u>Quantity</u>	<u>Flux</u> <u>[n/cm²-sec]</u>	<u>Quantity</u>	<u>Fluence</u> <u>[n/cm²]</u>	<u>Uncertainty</u>
ϕ (E > 1.0 MeV)	3.78E+10	Φ (E > 1.0 MeV)	5.52E+18	6%
ϕ (E > 0.1 MeV)	8.71E+10	Φ (E > 0.1 MeV)	1.27E+19	10%
ϕ (E < 0.414 eV)	1.48E+11	Φ (E < 0.414 eV)	2.16E+19	9%
dpa/sec	5.77E-11	dpa	8.43E-03	6%

Table 6-10

Comparison of Measured, Calculated, and Best Estimate
Reaction Rates at the Surveillance Capsule Center

Surveillance 284° Capsule

<u>Reaction</u>	<u>Measured</u>	<u>Calculated</u>	<u>Best Estimate</u>	<u>BE / Meas</u>	<u>BE/ Calc</u>	<u>Meas/Calc</u>
$^{63}\text{Cu} (n,\alpha)$	4.07E-17	4.20E-17	4.25E-17	1.05	1.01	0.97
$^{46}\text{Ti} (n, p)$	7.77E-16	6.45E-16	7.04E-16	0.91	1.09	1.20
$^{54}\text{Fe} (n,p)$	3.29E-15	3.57E-15	3.64E-15	1.11	1.02	0.92
$^{59}\text{Co} (n,\gamma)$	1.79E-12	1.51E-12	1.78E-12	1.00	1.18	1.18
$^{59}\text{Co} (n,\gamma) (\text{Cd})$	2.55E-13	3.07E-13	2.58E-13	1.01	0.84	0.83
$^{238}\text{U} (n,f) (\text{Cd})$	1.48E-14	1.20E-14	1.26E-14	0.86	1.05	1.23

Surveillance 104° Capsule

<u>Reaction</u>	<u>Measured</u>	<u>Calculated</u>	<u>Best Estimate</u>	<u>BE / Meas</u>	<u>BE/ Calc</u>	<u>Meas/Calc</u>
$^{63}\text{Cu} (n,\alpha)$	3.98E-17	4.43E-17	3.69E-17	0.93	0.83	0.90
$^{46}\text{Ti} (n, p)$	5.13E-16	6.85E-16	5.36E-16	1.04	0.78	0.75
$^{54}\text{Fe} (n,p)$	2.82E-15	3.87E-15	3.09E-15	1.10	0.80	0.73
$^{58}\text{Ni} (n,p)$	3.54E-15	5.07E-15	3.99E-15	1.13	0.79	0.70
$^{59}\text{Co} (n,\gamma)$	2.28E-12	1.99E-12	2.27E-12	1.00	1.14	1.14
$^{59}\text{Co} (n,\gamma) (\text{Cd})$	3.26E-13	4.01E-13	3.29E-13	1.01	0.82	0.81
$^{238}\text{U} (n,f)$	1.92E-14	1.35E-14	1.18E-14	0.61	0.87	1.43

Surveillance 97° Capsule

<u>Reaction</u>	<u>Measured</u>	<u>Calculated</u>	<u>Best Estimate</u>	<u>BE / Meas</u>	<u>BE/ Calc</u>	<u>Meas/Calc</u>
$^{63}\text{Cu} (n,\alpha)$	5.26E-17	4.41E-17	4.86E-17	0.92	1.10	1.19
$^{46}\text{Ti} (n, p)$	6.88E-16	7.00E-16	7.07E-16	1.03	1.01	0.98
$^{54}\text{Fe} (n,p)$	3.91E-15	4.27E-15	4.12E-15	1.05	0.97	0.92
$^{58}\text{Ni} (n,p)$	5.40E-15	5.66E-15	5.49E-15	1.02	0.97	0.95
$^{59}\text{Co} (n,\gamma)$	4.29E-12	3.81E-12	4.28E-12	1.00	1.12	1.13
$^{59}\text{Co} (n,\gamma) (\text{Cd})$	7.18E-13	7.56E-13	7.20E-13	1.00	0.95	0.95
$^{238}\text{U} (n,f) (\text{Cd})$	1.67E-14	1.67E-14	1.59E-14	0.95	0.95	1.00

Table 6-11

Best Estimate Neutron Energy Spectrum at the
Center of Surveillance Capsules

284° Capsule					
<u>Group #</u>	<u>Energy (MeV)</u>	<u>Flux (n/cm²-sec)</u>	<u>Group #</u>	<u>Energy (MeV)</u>	<u>Flux (n/cm²-sec)</u>
1	1.73E+01	6.59E+06	28	9.12E-03	2.06E+09
2	1.49E+01	1.40E+07	29	5.53E-03	2.08E+09
3	1.35E+01	4.89E+07	30	3.36E-03	6.63E+08
4	1.16E+01	1.27E+08	31	2.84E-03	6.44E+08
5	1.00E+01	2.82E+08	32	2.40E-03	6.38E+08
6	8.61E+00	4.80E+08	33	2.04E-03	1.91E+09
7	7.41E+00	1.24E+09	34	1.23E-03	1.90E+09
8	6.07E+00	1.77E+09	35	7.49E-04	1.82E+09
9	4.97E+00	3.07E+09	36	4.54E-04	1.72E+09
10	3.68E+00	2.84E+09	37	2.75E-04	1.80E+09
11	2.87E+00	4.54E+09	38	1.67E-04	1.68E+09
12	2.23E+00	4.38E+09	39	1.01E-04	1.83E+09
13	1.74E+00	4.46E+09	40	6.14E-05	1.85E+09
14	1.35E+00	3.35E+09	41	3.73E-05	1.89E+09
15	1.11E+00	4.66E+09	42	2.26E-05	1.92E+09
16	8.21E-01	4.30E+09	43	1.37E-05	1.93E+09
17	6.39E-01	3.83E+09	44	8.32E-06	1.96E+09
18	4.98E-01	2.67E+09	45	5.04E-06	2.03E+09
19	3.88E-01	3.02E+09	46	3.06E-06	2.05E+09
20	3.02E-01	4.54E+09	47	1.86E-06	2.06E+09
21	1.83E-01	3.74E+09	48	1.13E-06	2.02E+09
22	1.11E-01	2.98E+09	49	6.83E-07	1.86E+09
23	6.74E-02	2.59E+09	50	4.14E-07	2.42E+09
24	4.09E-02	1.91E+09	51	2.51E-07	8.59E+09
25	2.55E-02	1.37E+09	52	1.52E-07	1.53E+10
26	1.99E-02	1.17E+09	53	9.24E-08	3.67E+10
27	1.50E-02	2.01E+09			

Note: Tabulated energy levels represent the upper energy in each group.

Table 6-11 cont'd

Best Estimate Neutron Energy Spectrum at the
Center of Surveillance Capsules

104° Capsule					
<u>Group #</u>	<u>Energy (MeV)</u>	<u>Flux (n/cm²-sec)</u>	<u>Group #</u>	<u>Energy (MeV)</u>	<u>Flux (n/cm²-sec)</u>
1	1.73E+01	5.74E+06	28	9.12E-03	2.48E+09
2	1.49E+01	1.19E+07	29	5.53E-03	2.52E+09
3	1.35E+01	4.10E+07	30	3.36E-03	8.05E+08
4	1.16E+01	1.05E+08	31	2.84E-03	7.82E+08
5	1.00E+01	2.31E+08	32	2.40E-03	7.72E+08
6	8.61E+00	3.89E+08	33	2.04E-03	2.33E+09
7	7.41E+00	9.87E+08	34	1.23E-03	2.33E+09
8	6.07E+00	1.42E+09	35	7.49E-04	2.26E+09
9	4.97E+00	2.57E+09	36	4.54E-04	2.15E+09
10	3.68E+00	2.55E+09	37	2.75E-04	2.24E+09
11	2.87E+00	4.36E+09	38	1.67E-04	2.16E+09
12	2.23E+00	4.49E+09	39	1.01E-04	2.30E+09
13	1.74E+00	4.84E+09	40	6.14E-05	2.33E+09
14	1.35E+00	3.77E+09	41	3.73E-05	2.38E+09
15	1.11E+00	5.46E+09	42	2.26E-05	2.41E+09
16	8.21E-01	5.21E+09	43	1.37E-05	2.41E+09
17	6.39E-01	4.77E+09	44	8.32E-06	2.45E+09
18	4.98E-01	3.33E+09	45	5.04E-06	2.54E+09
19	3.88E-01	3.78E+09	46	3.06E-06	2.56E+09
20	3.02E-01	5.69E+09	47	1.86E-06	2.58E+09
21	1.83E-01	4.67E+09	48	1.13E-06	2.53E+09
22	1.11E-01	3.71E+09	49	6.83E-07	2.33E+09
23	6.74E-02	3.20E+09	50	4.14E-07	3.04E+09
24	4.09E-02	2.34E+09	51	2.51E-07	1.08E+10
25	2.55E-02	1.66E+09	52	1.52E-07	1.94E+10
26	1.99E-02	1.42E+09	53	9.24E-08	4.68E+10
27	1.50E-02	2.43E+09			

Note: Tabulated energy levels represent the upper energy in each group.

Table 6-11 cont'd

Best Estimate Neutron Energy Spectrum at the
Center of Surveillance Capsules

97° Capsule					
<u>Group #</u>	<u>Energy (MeV)</u>	<u>Flux (n/cm²-sec)</u>	<u>Group #</u>	<u>Energy (MeV)</u>	<u>Flux (n/cm²-sec)</u>
1	1.73E+01	6.83E+06	28	9.12E-03	4.75E+09
2	1.49E+01	1.46E+07	29	5.53E-03	4.88E+09
3	1.35E+01	5.26E+07	30	3.36E-03	1.58E+09
4	1.16E+01	1.40E+08	31	2.84E-03	1.55E+09
5	1.00E+01	3.11E+08	32	2.40E-03	1.54E+09
6	8.61E+00	5.26E+08	33	2.04E-03	4.67E+09
7	7.41E+00	1.28E+09	34	1.23E-03	4.76E+09
8	6.07E+00	1.84E+09	35	7.49E-04	4.69E+09
9	4.97E+00	3.42E+09	36	4.54E-04	4.52E+09
10	3.68E+00	3.46E+09	37	2.75E-04	4.73E+09
11	2.87E+00	5.86E+09	38	1.67E-04	4.79E+09
12	2.23E+00	6.14E+09	39	1.01E-04	4.94E+09
13	1.74E+00	6.77E+09	40	6.14E-05	5.00E+09
14	1.35E+00	5.34E+09	41	3.73E-05	5.08E+09
15	1.11E+00	7.85E+09	42	2.26E-05	5.12E+09
16	8.21E-01	7.67E+09	43	1.37E-05	5.13E+09
17	6.39E-01	7.21E+09	44	8.32E-06	5.14E+09
18	4.98E-01	5.08E+09	45	5.04E-06	5.35E+09
19	3.88E-01	5.86E+09	46	3.06E-06	5.41E+09
20	3.02E-01	9.18E+09	47	1.86E-06	5.44E+09
21	1.83E-01	7.77E+09	48	1.13E-06	5.29E+09
22	1.11E-01	6.42E+09	49	6.83E-07	4.88E+09
23	6.74E-02	5.67E+09	50	4.14E-07	6.07E+09
24	4.09E-02	4.26E+09	51	2.51E-07	2.08E+10
25	2.55E-02	3.05E+09	52	1.52E-07	3.66E+10
26	1.99E-02	2.65E+09	53	9.24E-08	8.46E+10
27	1.50E-02	4.60E+09			

Note: Tabulated energy levels represent the upper energy in each group.

Table 6-12

Comparison of Calculated and Best Estimate Integrated Neutron
Exposure of the 97°, 104°, and 284° Surveillance Capsules

284° CAPSULE

	<u>Calculated</u>	<u>Best Estimate</u>	<u>BE/C</u>
$\Phi(E > 1.0 \text{ MeV}) \text{ [n/cm}^2\text{]}$	1.45E+19	1.53E+19	1.05
$\Phi(E > 0.1 \text{ MeV}) \text{ [n/cm}^2\text{]}$	2.80E+19	2.93E+19	1.05
dpa	2.12E-02	2.23E-02	1.05

104° CAPSULE

	<u>Calculated</u>	<u>Best Estimate</u>	<u>BE/C</u>
$\Phi(E > 1.0 \text{ MeV}) \text{ [n/cm}^2\text{]}$	9.18E+18	8.29E+18	0.90
$\Phi(E > 0.1 \text{ MeV}) \text{ [n/cm}^2\text{]}$	1.84E+19	1.78E+19	0.97
dpa	1.35E-02	1.23E-02	0.91

97° CAPSULE

	<u>Calculated</u>	<u>Best Estimate</u>	<u>BE/C</u>
$\Phi(E > 1.0 \text{ MeV}) \text{ [n/cm}^2\text{]}$	5.91E+18	5.52E+18	0.93
$\Phi(E > 0.1 \text{ MeV}) \text{ [n/cm}^2\text{]}$	1.35E+19	1.27E+19	0.94
dpa	8.86E-03	8.43E-03	0.95

AVERAGE BE/C RATIOS

	<u>BE/C</u>
$\Phi(E > 1.0 \text{ MeV}) \text{ [n/cm}^2\text{]}$	0.96
$\Phi(E > 0.1 \text{ MeV}) \text{ [n/cm}^2\text{]}$	0.99
dpa	0.97

Table 6-13

Azimuthal Variations of The Neutron Exposure Projections
On The Reactor Vessel Clad/Base Metal Interface At Core Midplane

	Best Estimate			
	<u>0°[a]</u>	<u>15°</u>	<u>30°</u>	<u>45°</u>
17.23 EFPY				
E>1.0 MeV	1.39E+19	8.96E+18	9.05E+18	6.76E+18
E>0.1 MeV	3.25E+19	2.16E+19	2.10E+19	1.55E+19
dpa	2.17E-02	1.42E-02	1.41E-02	1.06E-02
Projection Data:				
E>1.0 MeV Fluence/EFPY	7.19E+17	4.82E+17	4.11E+17	3.32E+17
E>0.1 MeV Fluence/EFPY	1.60E+18	1.11E+18	9.18E+17	7.32E+17
dpa/EFPY	1.11E-03	7.53E-04	6.37E-04	5.18E-04
25 EFPY				
E>1.0 MeV	1.95E+19	1.27E+19	1.22E+19	9.34E+18
E>0.1 MeV	4.49E+19	3.02E+19	2.81E+19	2.12E+19
dpa	3.03E-02	2.00E-02	1.91E-02	1.46E-02
32 EFPY				
E>1.0 MeV	2.46E+19	1.61E+19	1.51E+19	1.17E+19
E>0.1 MeV	5.61E+19	3.80E+19	3.45E+19	2.63E+19
dpa	3.81E-02	2.53E-02	2.35E-02	1.83E-02
35 EFPY				
E>1.0 MeV	2.67E+19	1.75E+19	1.64E+19	1.27E+19
E>0.1 MeV	6.09E+19	4.13E+19	3.73E+19	2.85E+19
dpa	4.14E-02	2.75E-02	2.54E-02	1.98E-02
48 EFPY				
E>1.0 MeV	3.61E+19	2.38E+19	2.17E+19	1.70E+19
E>0.1 MeV	8.17E+19	5.57E+19	4.92E+19	3.80E+19
dpa	5.58E-02	3.73E-02	3.37E-02	2.65E-02
54 EFPY				
E>1.0 MeV	4.04E+19	2.67E+19	2.42E+19	1.90E+19
E>0.1 MeV	9.13E+19	6.23E+19	5.48E+19	4.24E+19
dpa	6.25E-02	4.18E-02	3.76E-02	2.97E-02

Note:

a) Maximum neutron exposure projection.

Table 6-13, cont'd

Azimuthal Variations of The Neutron Exposure Projections
On The Reactor Vessel Clad/Base Metal Interface At Core Midplane

	Calculated			
	<u>0°[a]</u>	<u>15°</u>	<u>30°</u>	<u>45°</u>
17.23 EFPY				
E>1.0 MeV	1.45E+19	9.29E+18	9.39E+18	7.01E+18
E>0.1 MeV	3.29E+19	2.19E+19	2.13E+19	1.57E+19
dpa	2.23E-02	1.46E-02	1.45E-02	1.09E-02
Projection Data:				
E>1.0 MeV Fluence/EFPY	7.46E+17	5.00E+17	4.26E+17	3.45E+17
E>0.1 MeV Fluence/EFPY	1.62E+18	1.12E+18	9.30E+17	7.42E+17
dpa/EFPY	1.14E-03	7.75E-04	6.56E-04	5.33E-04
25 EFPY				
E>1.0 MeV	2.03E+19	1.32E+19	1.27E+19	9.69E+18
E>0.1 MeV	4.55E+19	3.06E+19	2.85E+19	2.14E+19
dpa	3.12E-02	2.06E-02	1.96E-02	1.51E-02
32 EFPY				
E>1.0 MeV	2.55E+19	1.67E+19	1.57E+19	1.21E+19
E>0.1 MeV	5.68E+19	3.85E+19	3.50E+19	2.66E+19
dpa	3.92E-02	2.60E-02	2.42E-02	1.88E-02
35 EFPY				
E>1.0 MeV	2.77E+19	1.82E+19	1.70E+19	1.31E+19
E>0.1 MeV	6.17E+19	4.18E+19	3.78E+19	2.88E+19
dpa	4.26E-02	2.83E-02	2.62E-02	2.04E-02
48 EFPY				
E>1.0 MeV	3.74E+19	2.47E+19	2.25E+19	1.76E+19
E>0.1 MeV	8.27E+19	5.64E+19	4.99E+19	3.85E+19
dpa	5.75E-02	3.84E-02	3.47E-02	2.73E-02
54 EFPY				
E>1.0 MeV	4.19E+19	2.77E+19	2.51E+19	1.97E+19
E>0.1 MeV	9.24E+19	6.31E+19	5.55E+19	4.29E+19
dpa	6.43E-02	4.31E-02	3.86E-02	3.05E-02

Note:

a) Maximum neutron exposure projection.

Table 6-14

Neutron Exposure Values Within The
St. Lucie Unit 1 Reactor Vessel

Best Estimate Fluence (n/cm²) Based on E > 1.0 MeV Slope

	<u>0°[a]</u>	<u>15°</u>	<u>30°</u>	<u>45°</u>
17.23 EFPY, E>1.0 MeV	1.39E+19	8.96E+18	9.05E+18	6.76E+18
Projection Data Beyond Current 17.23 EFPY: E>1.0 MeV Fluence/EFPY	7.19E+17	4.82E+17	4.11E+17	3.32E+17
Attenuation Functions From Table 6-3:				
¼ T	0.536	0.537	0.539	0.539
¾ T	0.129	0.133	0.132	0.133
25 EFPY				
Surface	1.95E+19	1.27E+19	1.22E+19	9.34E+18
¼ T	1.05E+19	6.82E+18	6.60E+18	5.03E+18
¾ T	2.52E+18	1.69E+18	1.61E+18	1.25E+18
32 EFPY				
Surface	2.46E+19	1.61E+19	1.51E+19	1.17E+19
¼ T	1.32E+19	8.63E+18	8.15E+18	6.28E+18
¾ T	3.17E+18	2.14E+18	1.99E+18	1.56E+18
35 EFPY				
Surface	2.67E+19	1.75E+19	1.64E+19	1.27E+19
¼ T	1.43E+19	9.41E+18	8.81E+18	6.82E+18
¾ T	3.45E+18	2.33E+18	2.15E+18	1.69E+18
48 EFPY				
Surface	3.61E+19	2.38E+19	2.17E+19	1.70E+19
¼ T	1.94E+19	1.28E+19	1.17E+19	9.15E+18
¾ T	4.66E+18	3.16E+18	2.86E+18	2.26E+18
54 EFPY				
Surface	4.04E+19	2.67E+19	2.42E+19	1.90E+19
¼ T	2.17E+19	1.43E+19	1.30E+19	1.02E+19
¾ T	5.21E+18	3.55E+18	3.18E+18	2.53E+18

Note:

a) Maximum neutron exposure projection.

Table 6-14, cont'd

Neutron Exposure Values Within The
St. Lucie Unit 1 Reactor Vessel

Best Estimate Fluence (n/cm ²) Based on dpa Slope				
	0°[a]	15°	30°	45°
17.23 EFPY, E>1.0 MeV	1.39E+19	8.96E+18	9.05E+18	6.76E+18
Projection Data Beyond Current 17.23 EFPY:				
E>1.0 MeV Fluence/EFPY	7.19E+17	4.82E+17	4.11E+17	3.32E+17
Attenuation Functions From Table 6-5:				
¼ T	0.614	0.621	0.619	0.618
¾ T	0.221	0.235	0.231	0.236
25 EFPY				
Surface	1.95E+19	1.27E+19	1.22E+19	9.34E+18
¼ T	1.20E+19	7.89E+18	7.58E+18	5.77E+18
¾ T	4.31E+18	2.98E+18	2.83E+18	2.20E+18
32 EFPY				
Surface	2.46E+19	1.61E+19	1.51E+19	1.17E+19
¼ T	1.51E+19	9.99E+18	9.36E+18	7.21E+18
¾ T	5.42E+18	3.78E+18	3.49E+18	2.75E+18
35 EFPY				
Surface	2.67E+19	1.75E+19	1.64E+19	1.27E+19
¼ T	1.64E+19	1.09E+19	1.01E+19	7.83E+18
¾ T	5.90E+18	4.11E+18	3.78E+18	2.98E+18
48 EFPY				
Surface	3.61E+19	2.38E+19	2.17E+19	1.70E+19
¼ T	2.22E+19	1.48E+19	1.34E+19	1.05E+19
¾ T	7.96E+18	5.59E+18	5.01E+18	4.00E+18
54 EFPY				
Surface	4.04E+19	2.67E+19	2.42E+19	1.90E+19
¼ T	2.48E+19	1.66E+19	1.49E+19	1.17E+19
¾ T	8.91E+18	6.27E+18	5.58E+18	4.47E+18

Note:

- Maximum neutron exposure projection.
- The ¼T and ¾T values were determined using the calculational methods described in Section 6.2 and not by the empirical relation described in Regulatory Guide 1.99, Rev. 2.

Table 6-14, cont'd

Neutron Exposure Values Within The
St. Lucie Unit 1 Reactor Vessel

	Calculated Fluence (n/cm ²) Based on E > 1.0 MeV Slope			
	0°[a]	15°	30°	45°
17.23 EFPY, E>1.0 MeV	1.45E+19	9.29E+18	9.39E+18	7.01E+18
Projection Data Beyond Current 17.23 EFPY: E>1.0 MeV Fluence/EFPY	7.46E+17	5.00E+17	4.26E+17	3.45E+17
Attenuation Functions From Table 6-3:				
¼ T	0.536	0.537	0.539	0.539
¾ T	0.129	0.133	0.132	0.133
25 EFPY				
Surface	2.03E+19	1.32E+19	1.27E+19	9.69E+18
¼ T	1.09E+19	7.08E+18	6.84E+18	5.22E+18
¾ T	2.61E+18	1.75E+18	1.67E+18	1.29E+18
32 EFPY				
Surface	2.55E+19	1.67E+19	1.57E+19	1.21E+19
¼ T	1.37E+19	8.95E+18	8.45E+18	6.52E+18
¾ T	3.29E+18	2.22E+18	2.06E+18	1.61E+18
35 EFPY				
Surface	2.77E+19	1.82E+19	1.70E+19	1.31E+19
¼ T	1.49E+19	9.76E+18	9.14E+18	7.07E+18
¾ T	3.58E+18	2.42E+18	2.23E+18	1.75E+18
48 EFPY				
Surface	3.74E+19	2.47E+19	2.25E+19	1.76E+19
¼ T	2.01E+19	1.33E+19	1.21E+19	9.49E+18
¾ T	4.83E+18	3.28E+18	2.96E+18	2.35E+18
54 EFPY				
Surface	4.19E+19	2.77E+19	2.51E+19	1.97E+19
¼ T	2.25E+19	1.49E+19	1.35E+19	1.06E+19
¾ T	5.41E+18	3.68E+18	3.30E+18	2.62E+18

Note:

- Maximum neutron exposure projection.
- The ¼T and ¾T values were determined using the calculational methods described in Section 6.2 and not by the empirical relation described in Regulatory Guide 1.99, Rev. 2.

Table 6-14, cont'd

Neutron Exposure Values Within The
St. Lucie Unit 1 Reactor Vessel

	Calculated Fluence (n/cm ²) Based on dpa Slope			
	0°[a]	15°	30°	45°
17.23 EFPY, E>1.0 MeV	1.45E+19	9.29E+18	9.39E+18	7.01E+18
Projection Data Beyond Current 17.23 EFPY: E>1.0 MeV Fluence/EFPY	7.46E+17	5.00E+17	4.26E+17	3.45E+17
Attenuation Functions From Table 6-5:				
¼ T	0.614	0.621	0.619	0.618
¾ T	0.221	0.235	0.231	0.236
25 EFPY				
Surface	2.03E+19	1.32E+19	1.27E+19	9.69E+18
¼ T	1.24E+19	8.19E+18	7.86E+18	5.99E+18
¾ T	4.47E+18	3.09E+18	2.94E+18	2.28E+18
32 EFPY				
Surface	2.55E+19	1.67E+19	1.57E+19	1.21E+19
¼ T	1.56E+19	1.04E+19	9.70E+18	7.48E+18
¾ T	5.62E+18	3.92E+18	3.62E+18	2.85E+18
35 EFPY				
Surface	2.77E+19	1.82E+19	1.70E+19	1.31E+19
¼ T	1.70E+19	1.13E+19	1.05E+19	8.12E+18
¾ T	6.12E+18	4.27E+18	3.92E+18	3.10E+18
48 EFPY				
Surface	3.74E+19	2.47E+19	2.25E+19	1.76E+19
¼ T	2.30E+19	1.53E+19	1.39E+19	1.09E+19
¾ T	8.25E+18	5.79E+18	5.20E+18	4.15E+18
54 EFPY				
Surface	4.19E+19	2.77E+19	2.51E+19	1.97E+19
¼ T	2.57E+19	1.72E+19	1.55E+19	1.22E+19
¾ T	9.24E+18	6.50E+18	5.79E+18	4.64E+18

Note:

- a) Maximum neutron exposure projection.
- b) The ¼T and ¾T values were determined using the calculational methods described in Section 6.2 and not by the empirical relation described in Regulatory Guide 1.99, Rev. 2.

Table 6-15

Updated Lead Factors for St. Lucie Unit 1
Surveillance Capsules

<u>Capsule</u>	<u>Lead Factor</u>
97 ^{o[a]}	1.53
104 ^{o[b]}	0.98
284 ^{o[c]}	1.00
263 ^{o[d]}	1.36
277 ^{o[d]}	1.36
83 ^{o[d]}	1.36

[a] - Withdrawn at the end of Cycle 5.

[b] - Withdrawn at the end of Cycle 9.

[c] - Withdrawn at the end of Cycle 15.

[d] - Not withdrawn; standby.

The surveillance capsule lead factor is defined by:

$$\frac{\Phi_{\text{Surveillance Capsule Calculated}}}{\Phi_{\text{Clad / Base Metal Interface Axial Peak Calculated}}}$$

where Φ is the neutron fluence ($E > 1.0$ MeV) at the time of the capsule withdrawal. In the case of the standby capsules, the neutron fluence is at the time of the latest withdrawn capsule.

Table 6-16

C_j Values for the St. Lucie Unit 1
Sensor Reaction Rate Evaluation

		CU-63	TI-46	FE-54	NI-58	CO-59	U-238
97° Capsule EOC 5	Cycles 1-4	ALL MATERIALS = 1.032					
	Cycle 5	ALL MATERIALS = 0.899					
104° Capsule EOC 9	Cycles 1-4	0.803	0.810	0.846	0.856	1.304	0.926
	Cycle 5	0.672	0.673	0.695	0.702	1.038	0.752
	Cycles 6-9	1.279	1.272	1.230	1.219	0.687	1.136
284° Capsule EOC 15	Cycles 1-4	0.834	0.847	0.903	0.917	1.682	1.023
	Cycle 5	0.698	0.703	0.741	0.752	1.339	0.831
	Cycles 6-9	1.328	1.330	1.313	1.306	0.885	1.255
	Cycle 10	0.973	0.967	0.943	0.937	0.614	0.893
	Cycle 11	0.859	0.843	0.806	0.799	0.487	0.748
	Cycle 12	0.941	0.926	0.890	0.883	0.548	0.830
	Cycle 13	0.886	0.870	0.832	0.826	0.506	0.773
	Cycle 14	0.984	0.969	0.930	0.923	0.575	0.868
	Cycle 15	1.015	1.013	0.994	0.989	0.663	0.947

7 SURVEILLANCE CAPSULE REMOVAL SCHEDULE

The following surveillance capsule removal schedule meets the intent of ASTM E185-82 and is recommended for future capsules to be removed from the St. Lucie Unit 1 reactor vessel. This recommended removal schedule is applicable to 32 EFPY of operation.

TABLE 7-1				
St. Lucie Unit 1 Reactor Vessel Surveillance Capsule Withdrawal Schedule				
Capsule	Location	Lead Factor ^(a)	Removal Time (EFPY) ^(b)	Fluence (n/cm ² , E > 1.0 MeV) ^(a)
97°	97°	1.53	4.67	5.91×10^{18} (c)
104°	104°	0.98	9.515	9.18×10^{18} (c)
284°	284°	1.00	17.23	1.45×10^{19} (c)
263°	263°	1.36	23	2.55×10^{19} (d)
83°	83°	1.36	35	3.74×10^{19} (e)
277°	277°	1.36	Standby	(e)

Notes:

- (a) Updated in Capsule 284° dosimetry analysis.
- (b) Effective Full Power Years (EFPY) from plant startup.
- (c) Plant specific evaluation.
- (d) Capsule 263° will reach a EOL (32 EFPY) fluence of 2.55×10^{19} n/cm² (E > 1.0 MeV) at approximately 23 EFPY.
- (e) Capsules 277° and 83° will reach an EOL license renewal (48 EFPY) fluence of 3.74×10^{19} n/cm² (E > 1.0 MeV) at 35 EFPY. Thus, at this time Capsule 83° should be removed/tested, while Capsule 277° should be removed and placed in storage.

8 REFERENCES

1. Regulatory Guide 1.99, Revision 2, *Radiation Embrittlement of Reactor Vessel Materials*, U.S. Nuclear Regulatory Commission, May, 1988.
2. Code of Federal Regulations, 10CFR50, Appendix G, *Fracture Toughness Requirements*, and Appendix H, *Reactor Vessel Material Surveillance Program Requirements*, U.S. Nuclear Regulatory Commission, Washington, D.C.
3. TR-F-MCM-005, "Florida Power and Light Company St. Lucie Unit 1 – Evaluation of Baseline Specimens Reactor Vessel Materials Irradiation Surveillance Program", S.D. Crossman, August 9, 1984.
4. Section XI of the ASME Boiler and Pressure Vessel Code, Appendix G, *Fracture Toughness Criteria for Protection Against Failure*
5. ASTM E208, *Standard Test Method for Conducting Drop-Weight Test to Determine Nil-Ductility Transition Temperature of Ferritic Steels*, in ASTM Standards, Section 3, American Society for Testing and Materials, Philadelphia, PA
6. CENPD-39, "Summary Report on Manufacture of Test Specimens and Assembly of Capsules For Irradiation Surveillance of Hutchinson Island Plant – Unit 1 Reactor Vessel Materials", A.D. Emery, April 1972.
7. ASTM E185-82, *Standard Practice for Conducting Surveillance Tests for Light-Water Cooled Nuclear Power Reactor Vessels, E706 (IF)*, in ASTM Standards, Section 3, American Society for Testing and Materials, Philadelphia, PA, 1993.
8. ASTM E23-98, *Standard Test Methods for Notched Bar Impact Testing of Metallic Materials*, in ASTM Standards, Section 3, American Society for Testing and Materials, Philadelphia, PA, 1998.
9. ASTM A370-97, *Standard Test Methods and Definitions for Mechanical Testing of Steel Products*, in ASTM Standards, Section 3, American Society for Testing and Materials, Philadelphia, PA, 1997.
10. ASTM E8-99, *Standard Test Methods for Tension Testing of Metallic Materials*, in ASTM Standards, Section 3, American Society for Testing and Materials, Philadelphia, PA, 1999.
11. ASTM E21-92 (1998), *Standard Test Methods for Elevated Temperature Tension Tests of Metallic Materials*, in ASTM Standards, Section 3, American Society for Testing and Materials, Philadelphia, PA, 1998.
12. ASTM E83-93, *Standard Practice for Verification and Classification of Extensometers*, in ASTM Standards, Section 3, American Society for Testing and Materials, Philadelphia, PA, 1993.
13. RSIC Computer Code Collection CCC-650, "DOORS 3.1 One, Two- and Three-Dimensional Discrete Ordinates Neutron/Photon Transport Code System, ", August 1996.
14. RSIC DLC-185, "BUGLE-96 Coupled 47 Neutron, 20 Gamma-Ray Group Cross-Section Library Derived from ENDF/B-VI for LWR Shielding and Pressure Vessel Dosimetry Applications", March 1996

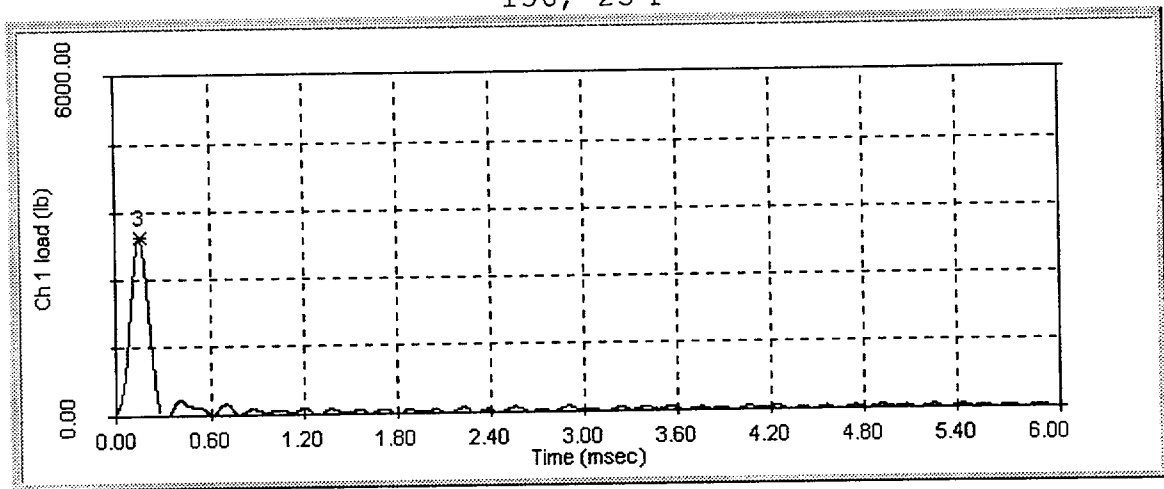
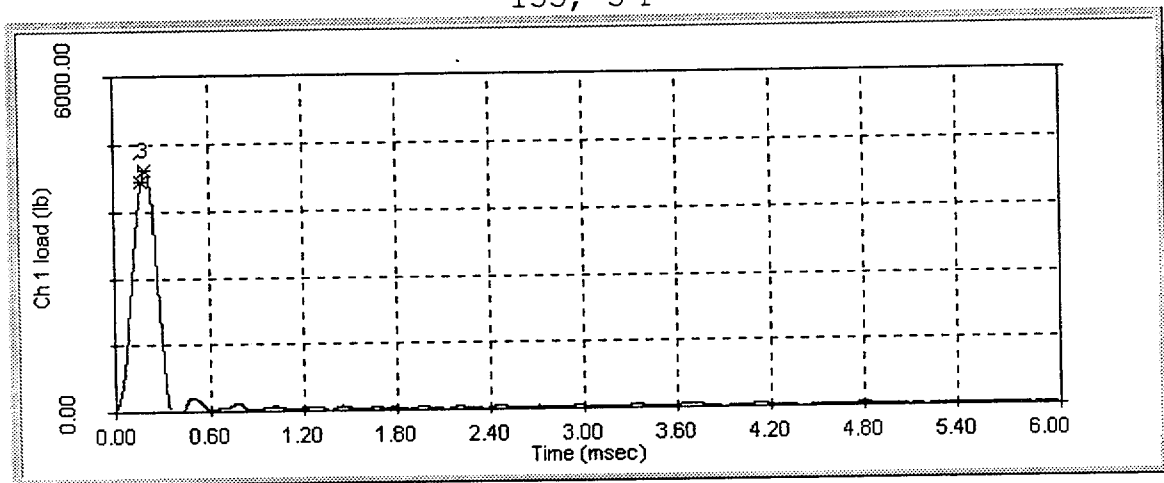
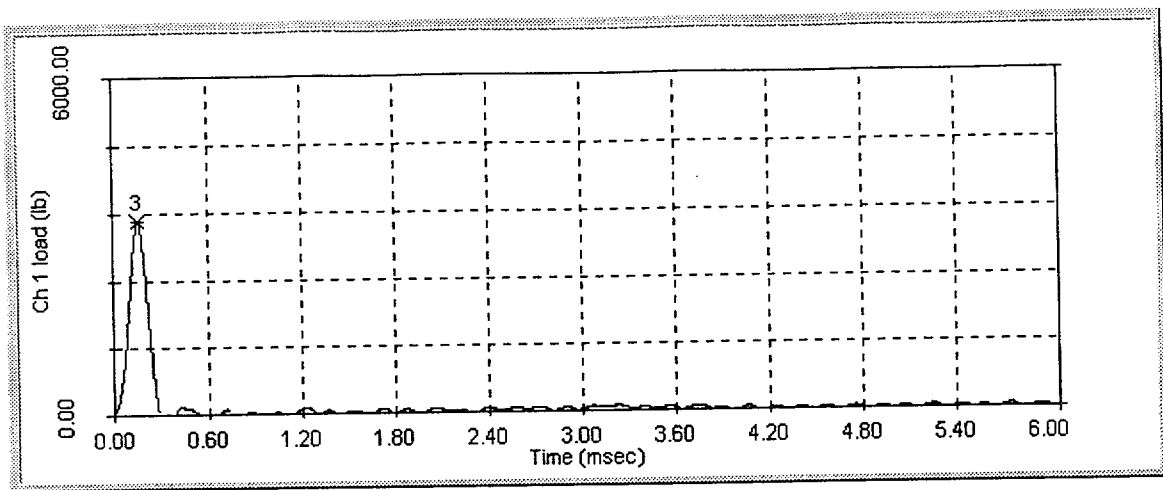
15. R. E. Maerker, et al., *Accounting for Changing Source Distributions in Light Water Reactor Surveillance Dosimetry Analysis*, Nuclear Science and Engineering, Volume 94, Pages 291-308, 1986.
16. ASTM Designation E482-89 (Re-approved 1996), *Standard Guide for Application of Neutron Transport Methods for Reactor Vessel Surveillance*, in ASTM Standards, Section 12, American Society for Testing and Materials, Philadelphia, PA, 1999.
17. ASTM Designation E560-84 (Re-approved 1996), *Standard Recommended Practice for Extrapolating Reactor Vessel Surveillance Dosimetry Results*, in ASTM Standards, Section 12, American Society for Testing and Materials, Philadelphia, PA, 1999.
18. ASTM Designation E693-94, *Standard Practice for Characterizing Neutron Exposures in Iron and Low Alloy Steels in Terms of Displacements per Atom (dpa)*, in ASTM Standards, Section 12, American Society for Testing and Materials, Philadelphia, PA, 1999.
19. ASTM Designation E706-87 (Re-approved 1994), *Standard Master Matrix for Light-Water Reactor Pressure Vessel Surveillance Standard*, in ASTM Standards, Section 12, American Society for Testing and Materials, Philadelphia, PA, 1999.
20. ASTM Designation E853-87 (Re-approved 1995), *Standard Practice for Analysis and Interpretation of Light-Water Reactor Surveillance Results*, in ASTM Standards, Section 12, American Society for Testing and Materials, Philadelphia, PA, 1999.
21. ASTM Designation E261-96, *Standard Practice for Determining Neutron Fluence Rate, Fluence, and Spectra by Radioactivation Techniques*, in ASTM Standards, Section 12, American Society for Testing and Materials, Philadelphia, PA, 1999.
22. ASTM Designation E262-97, *Standard Method for Determining Thermal Neutron Reaction and Fluence Rates by Radioactivation Techniques*, in ASTM Standards, Section 12, American Society for Testing and Materials, Philadelphia, PA, 1999.
23. ASTM Designation E263-93, *Standard Method for Measuring Fast-Neutron Reaction Rates by Radioactivation of Iron*, in ASTM Standards, Section 12, American Society for Testing and Materials, Philadelphia, PA, 1999.
24. ASTM Designation E264-92 (Re-approved 1996), *Standard Method for Measuring Fast-Neutron Reaction Rates by Radioactivation of Nickel*, in ASTM Standards, Section 12, American Society for Testing and Materials, Philadelphia, PA, 1999.
25. ASTM Designation E481-97, *Standard Method for Measuring Neutron-Fluence Rate by Radioactivation of Cobalt and Silver*, in ASTM Standards, Section 12, American Society for Testing and Materials, Philadelphia, PA, 1999.

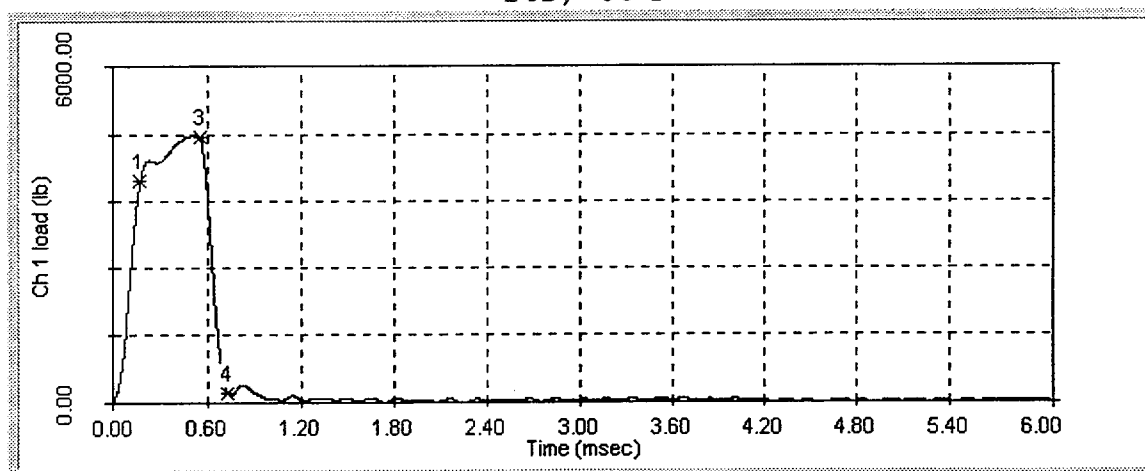
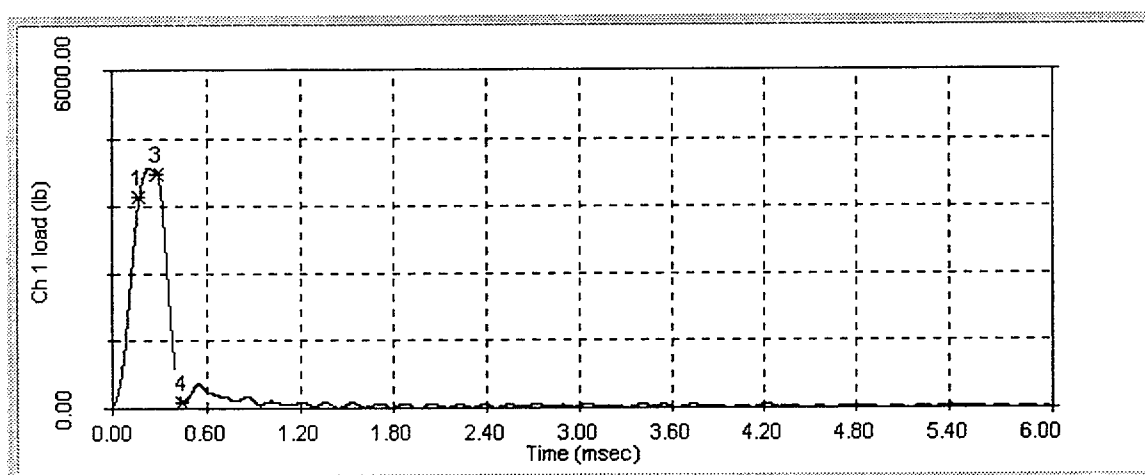
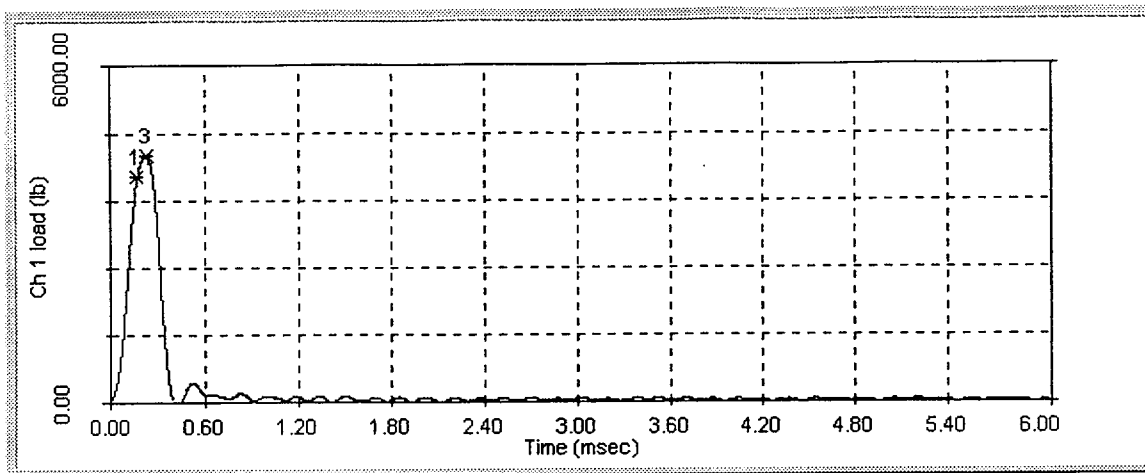
26. ASTM Designation E523-92 (Re-approved 1996), *Standard Test Method for Measuring Fast-Neutron Reaction Rates by Radioactivation of Copper*, in ASTM Standards, Section 12, American Society for Testing and Materials, Philadelphia, PA, 1999.
27. ASTM Designation E704-96, *Standard Test Method for Measuring Reaction Rates by Radioactivation of Uranium-238*, in ASTM Standards, Section 12, American Society for Testing and Materials, Philadelphia, PA, 1999.
28. ASTM Designation E1005-97, *Standard Test Method for Application and Analysis of Radiometric Monitors for Reactor Vessel Surveillance*, in ASTM Standards, Section 12, American Society for Testing and Materials, Philadelphia, PA, 1999.
29. Letter from R.S. Boggs to Ed Terek supplying Tcold data and monthly operating history reports from 01/90 through 12/00 for St. Lucie Unit 1, March 15, 2000.
30. Letter from R.S. Boggs to Ed Terek supplying axial power distributions and relative assembly powers for St. Lucie Unit No. 1 Cycles 110, 11 and 12, April 4, 2000.
31. F. A. Schmittroth, *FERRET Data Analysis Core*, HEDL-TME 79-40, Hanford Engineering Development Laboratory, Richland, WA, September 1979.
32. W. N. McElroy, S. Berg and T. Crocket, *A Computer-Automated Iterative Method of Neutron Flux Spectra Determined by Foil Activation*, AFWL-TR-7-41, Vol. I-IV, Air Force Weapons Laboratory, Kirkland AFB, NM, July 1967
33. RSIC Data Library Collection DLC-178, "SNLRML Recommended Dosimetry Cross-Section Compendium", July 1994.
34. EPRI-NP-2188, *Development and Demonstration of an Advanced Methodology for LWR Dosimetry Applications*, R. E. Maerker, et al., 1981.
35. Letters FPL-01-145, from D.H. Warren to R.A. Symes, "Model Errors in Fluence Calculations for Surveillance Capsules", Dated 10/31/01.
[Sub-Reference: Letter FPL-01-146, Surveillance Capsule Analysis Applicability Time of PT Curves Given Corrected Fluence Values]

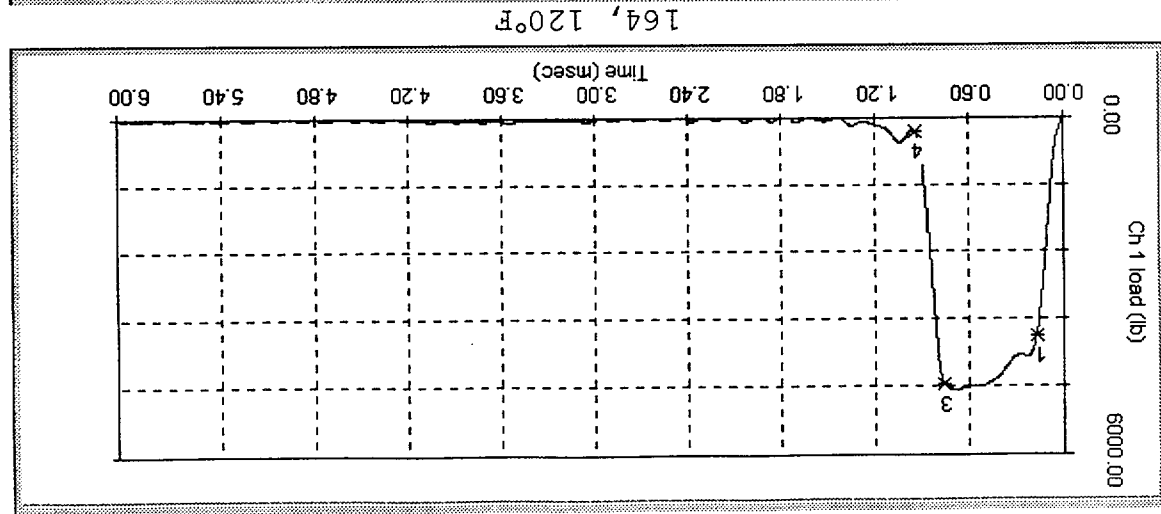
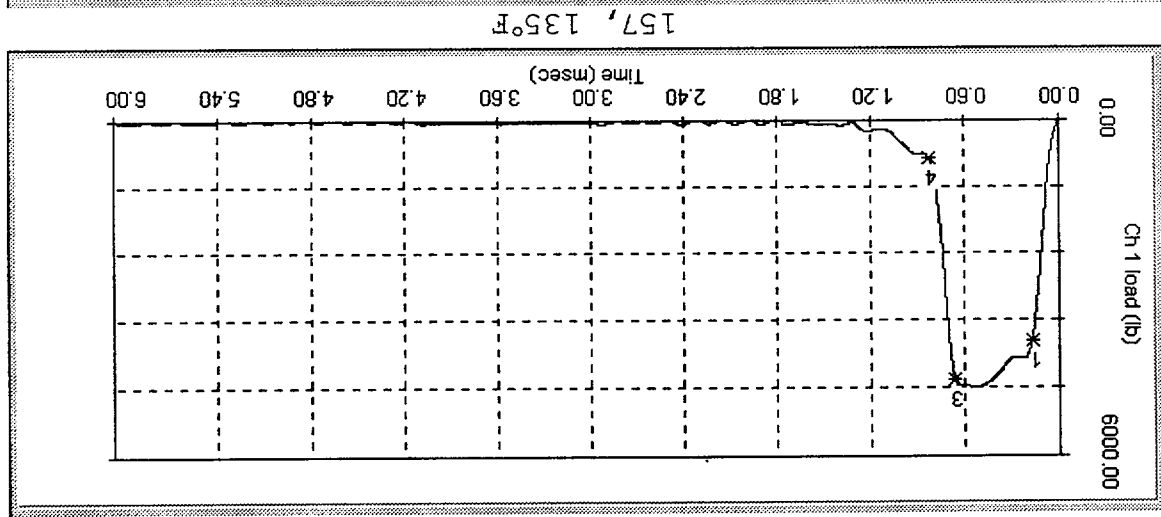
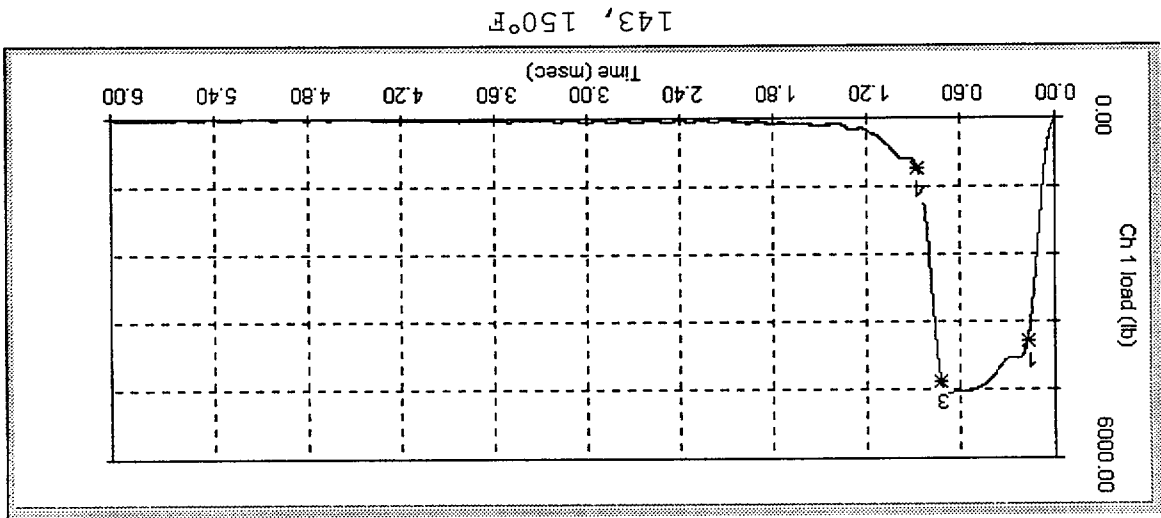
APPENDIX A

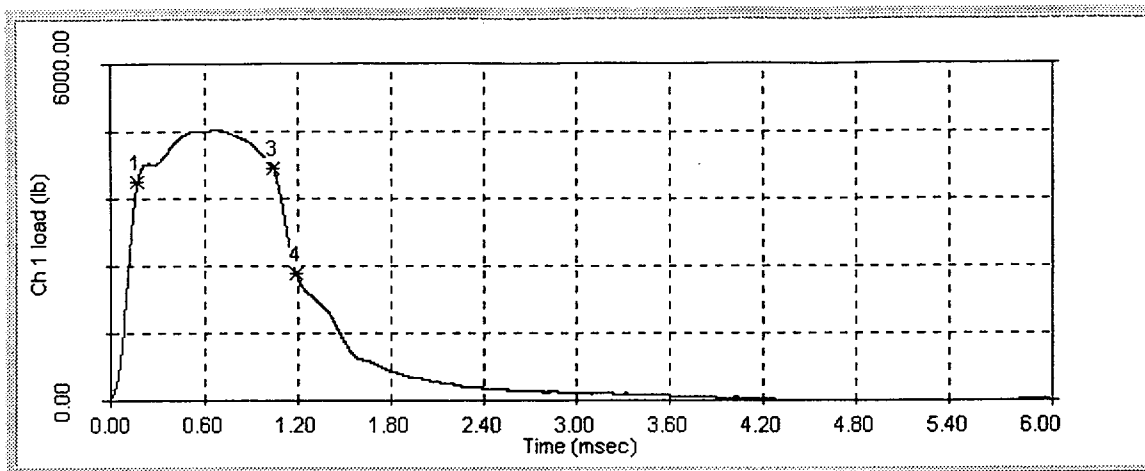
INSTRUMENTED CHARPY IMPACT TEST CURVES

- Specimen prefix “1” denotes Lower Plate, Longitudinal Orientation
- Specimen prefix “2” denotes Lower Plate, Transverse Orientation
- Specimen prefix “3” denotes weld material
- Specimen prefix “4” denotes Heat-Affected Zone material

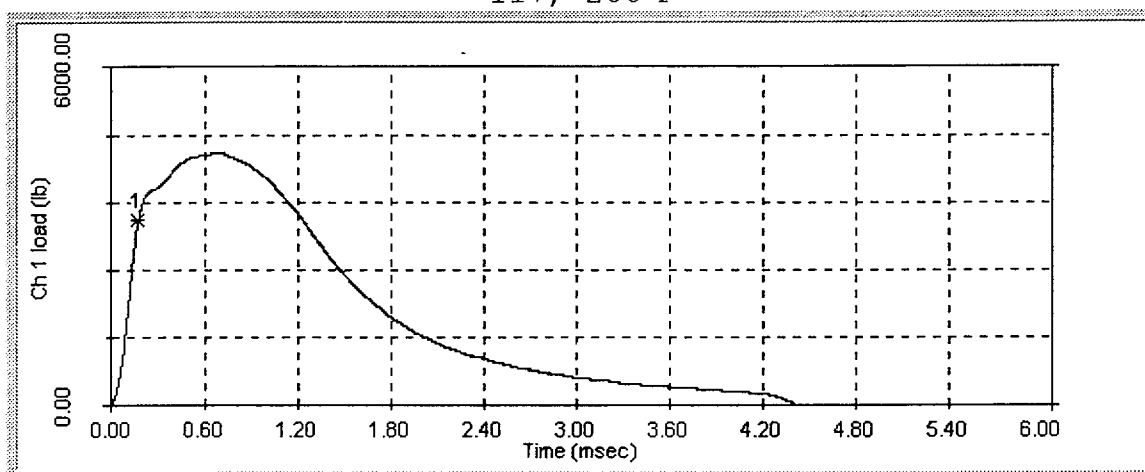




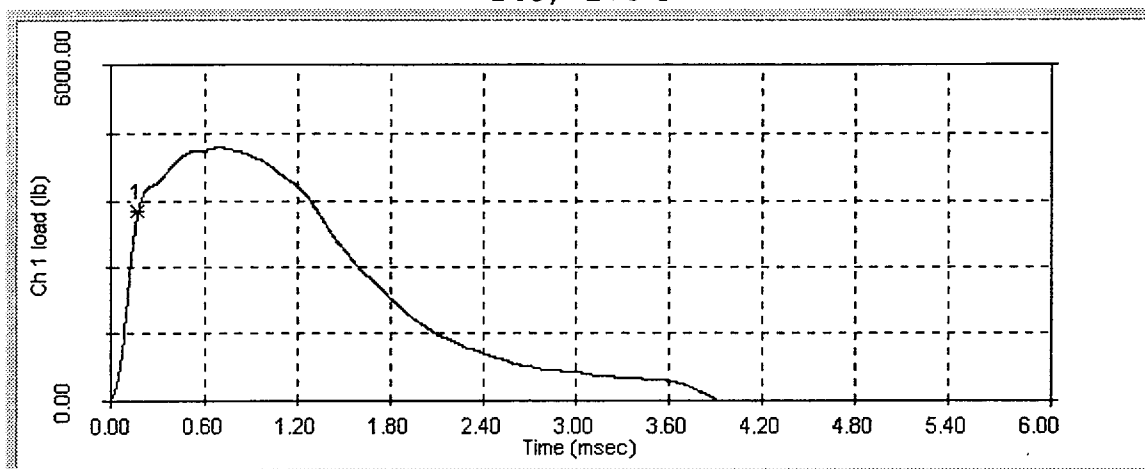




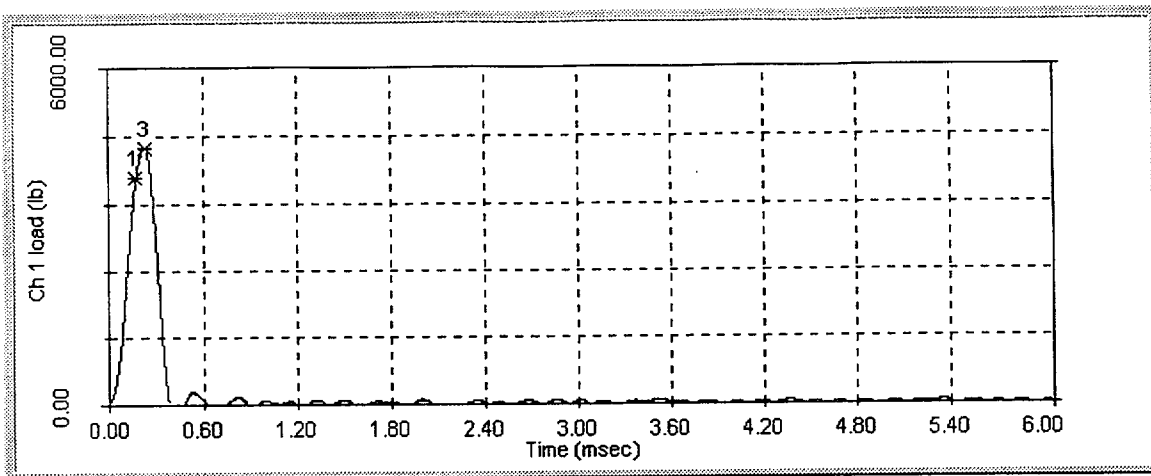
117, 200°F



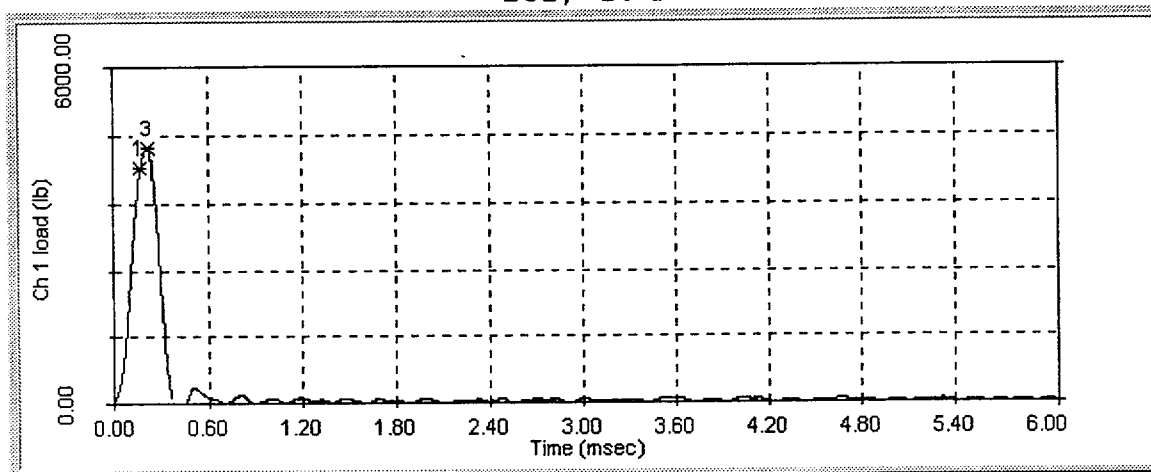
14U, 275°F



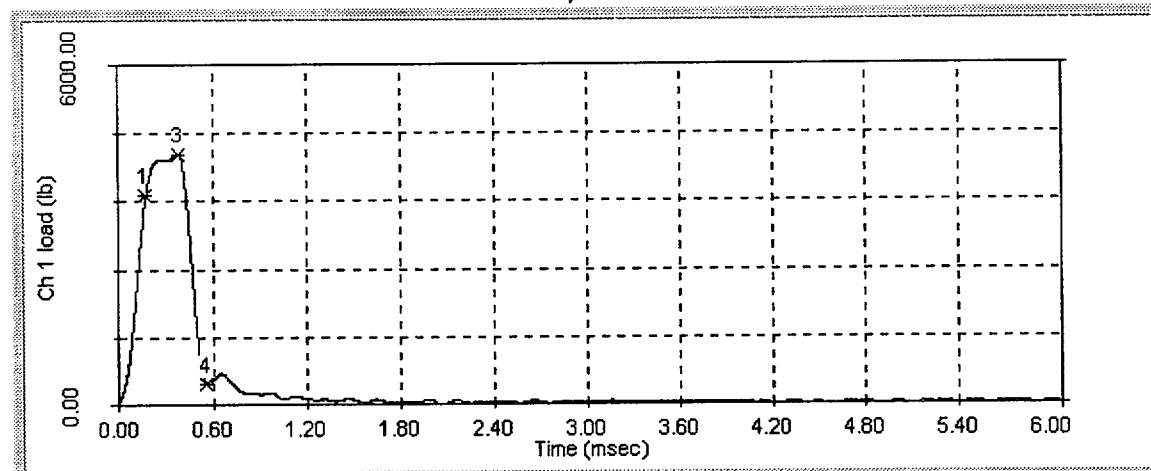
14E, 325°F



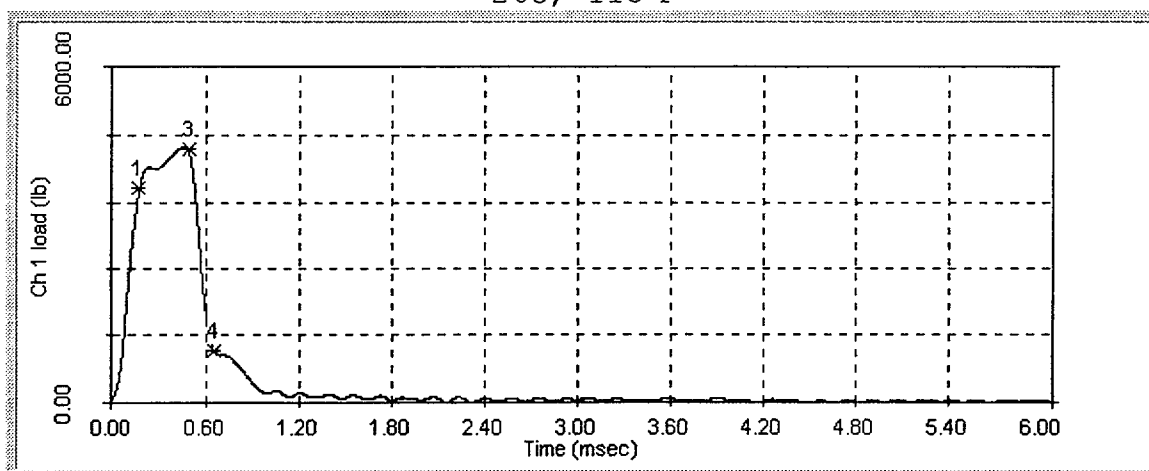
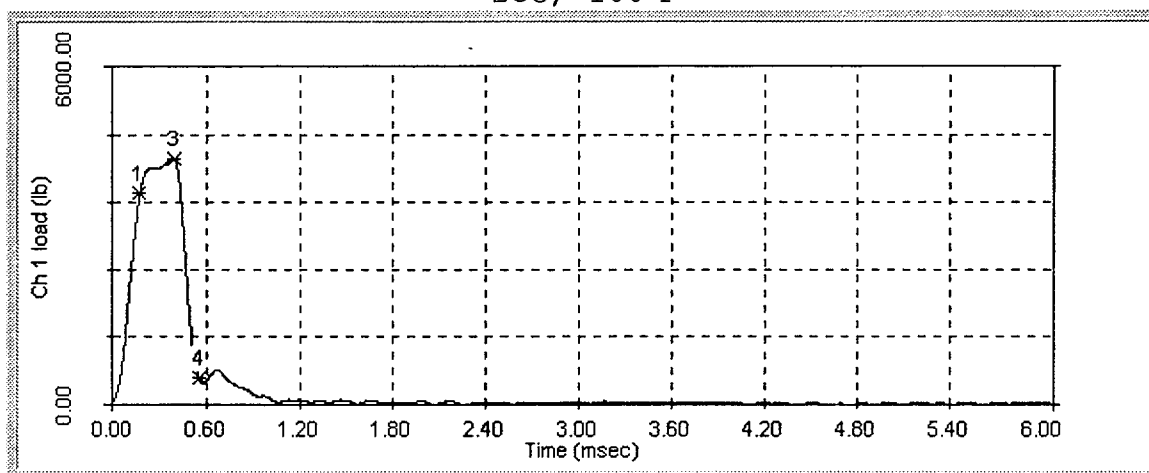
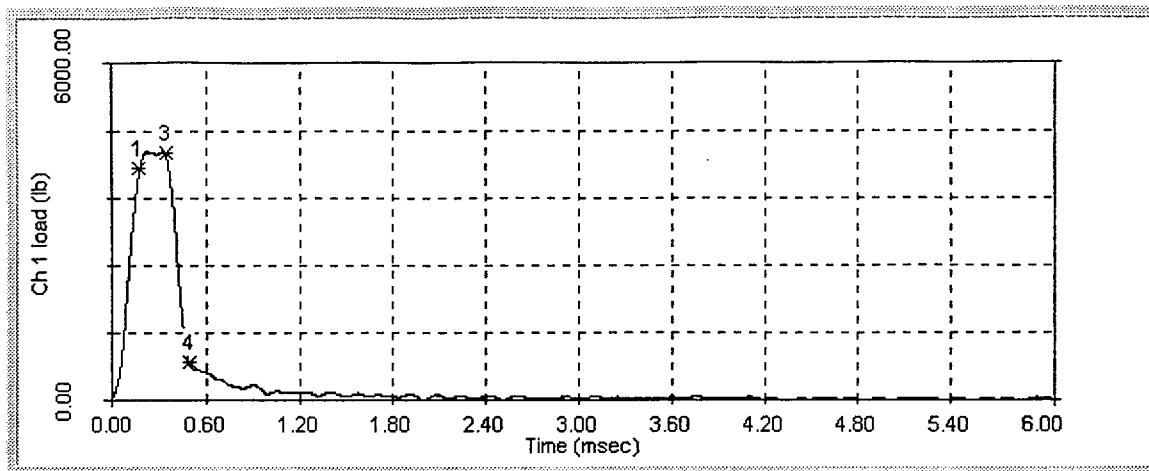
252, 10°F

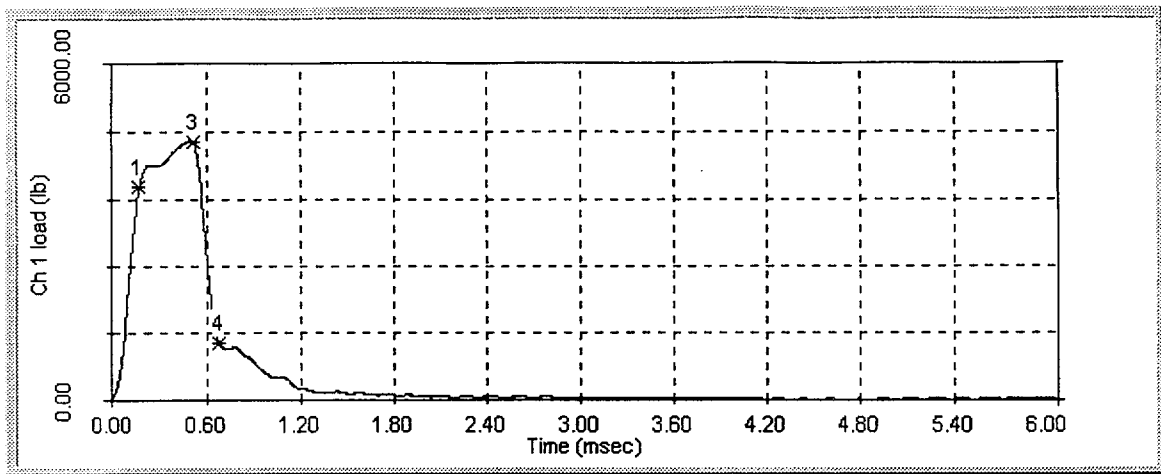


25M, 50°F

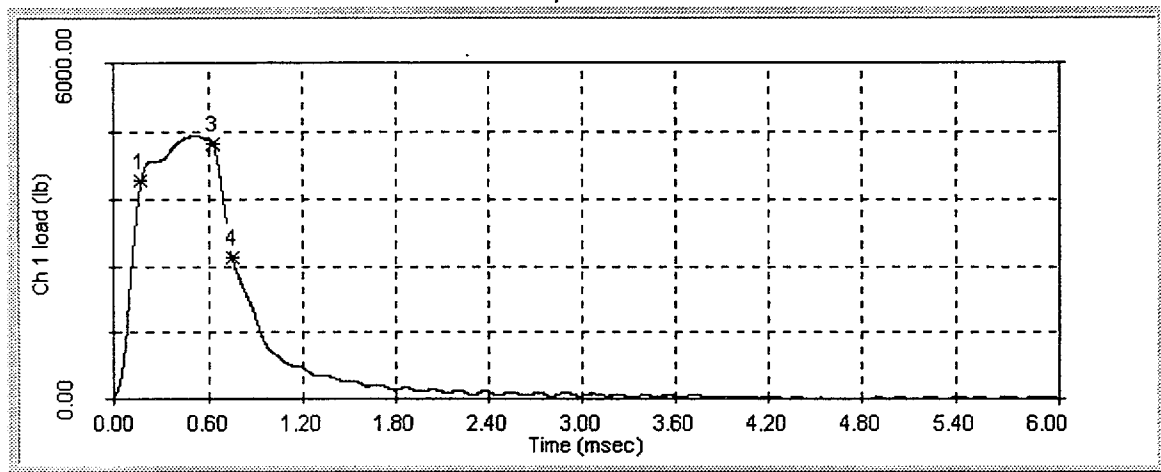


25L, 90°F

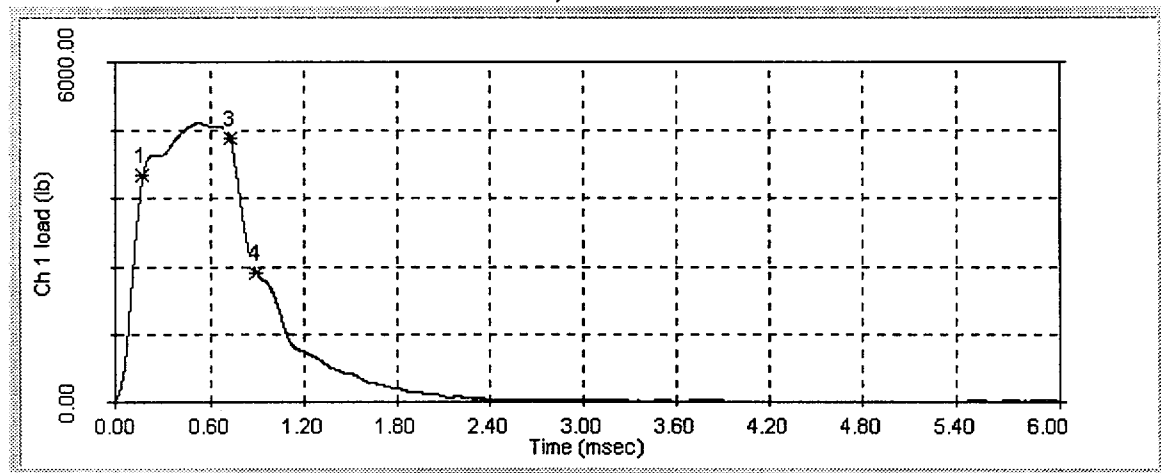




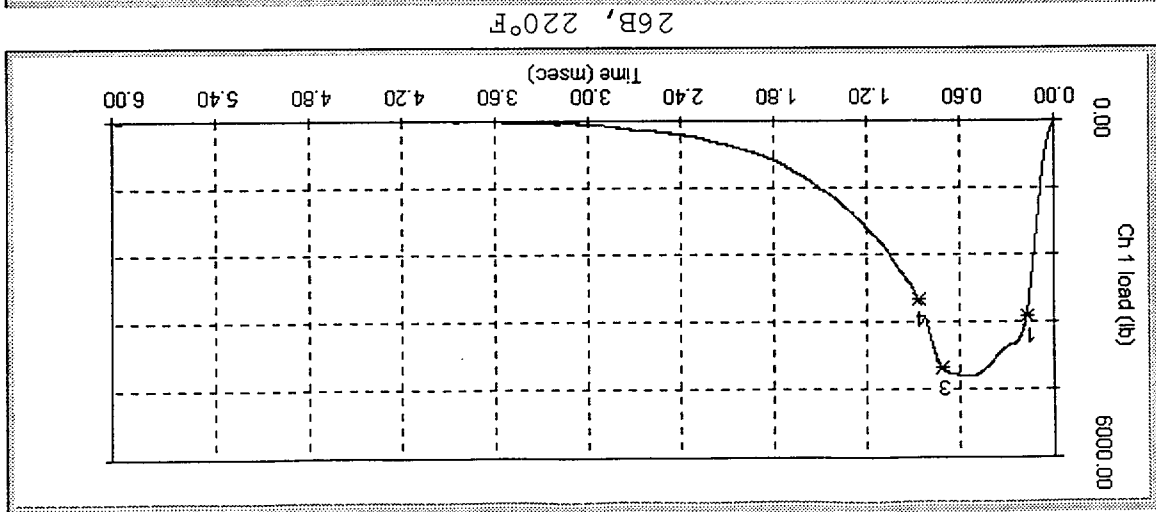
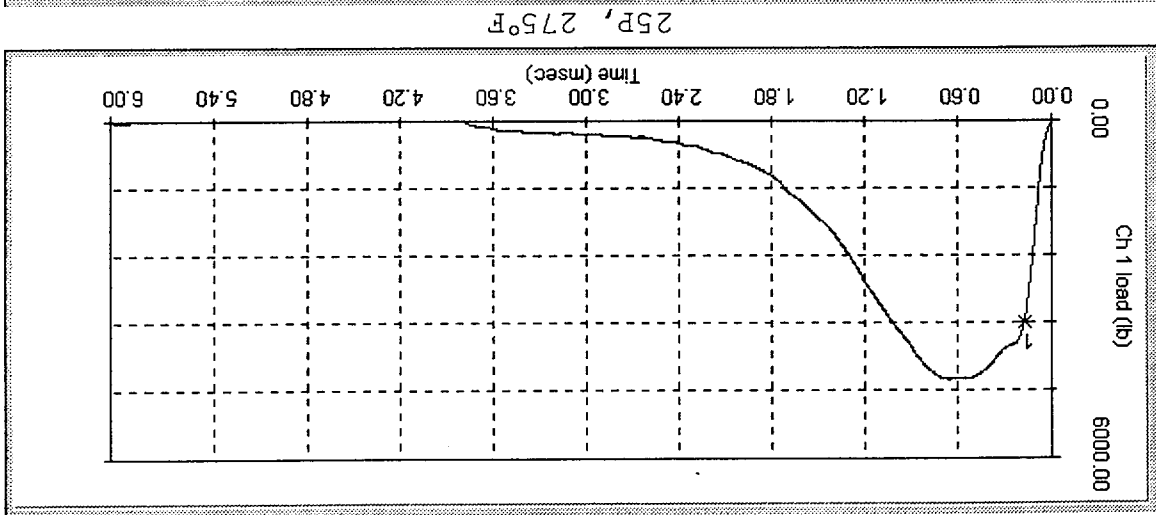
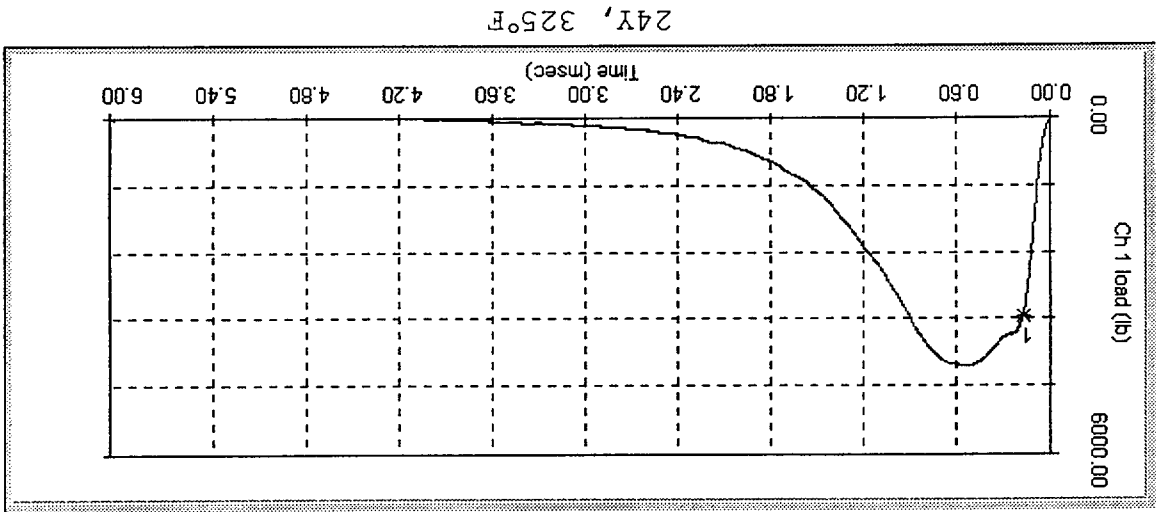
25J, 135°F

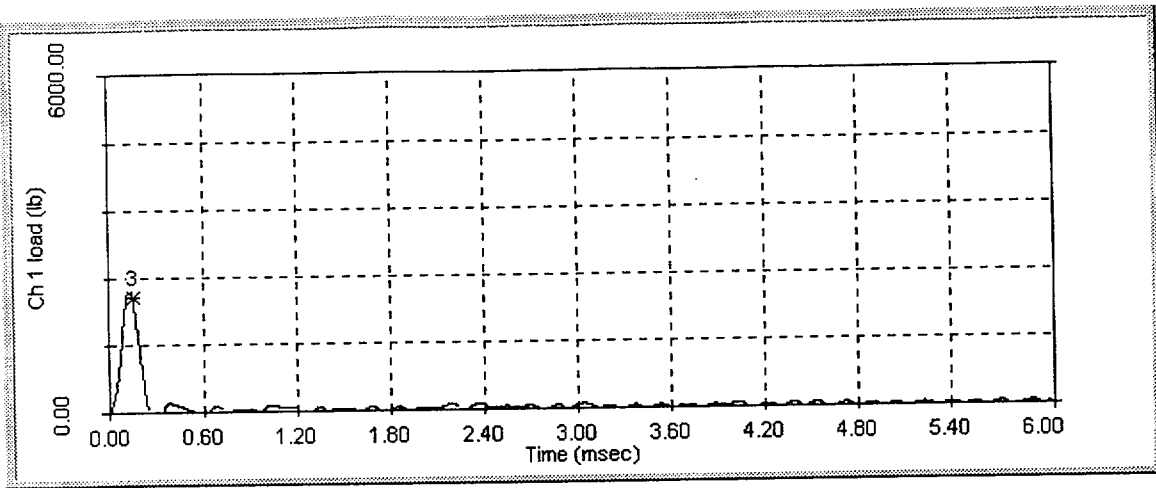


251, 150°F

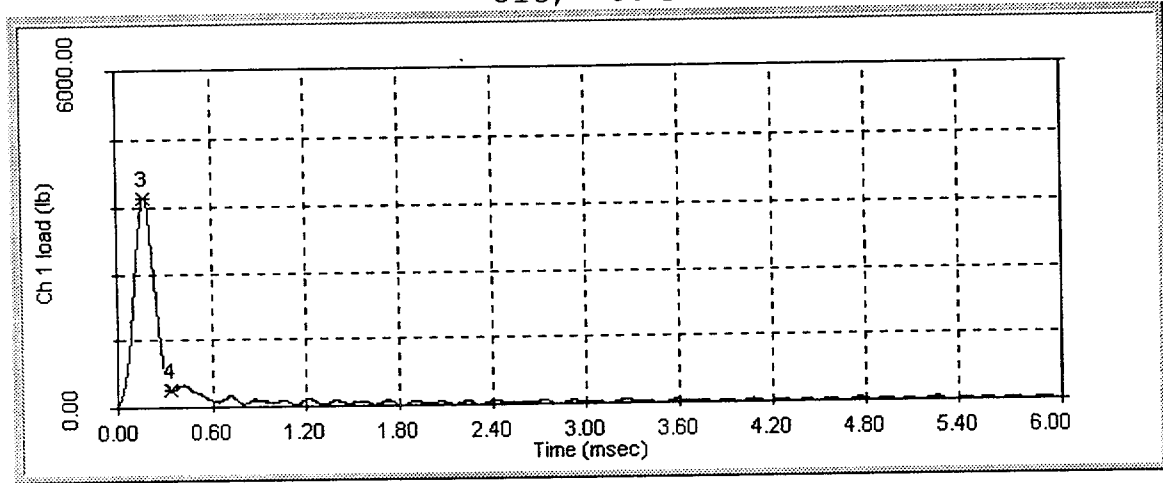


253, 175°F

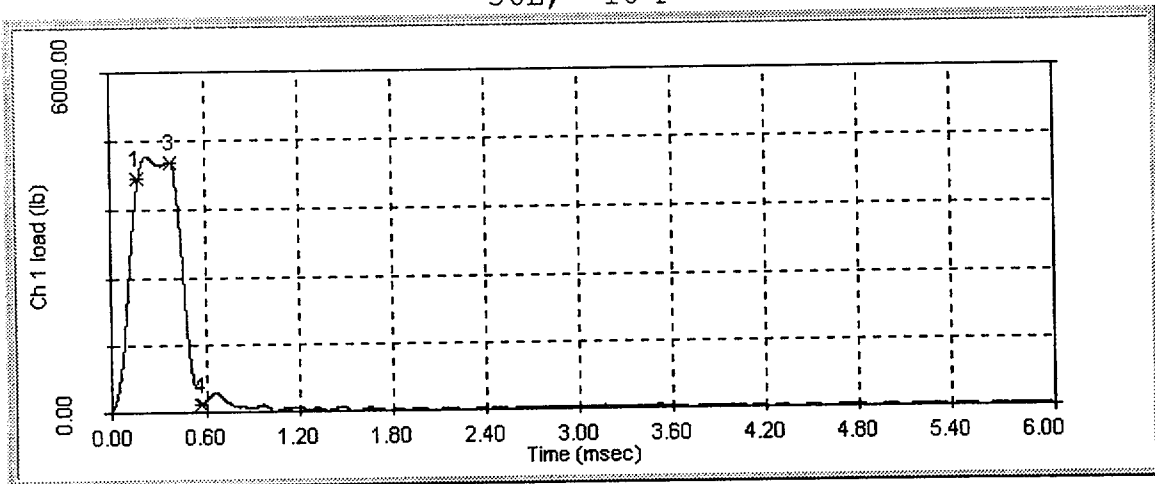




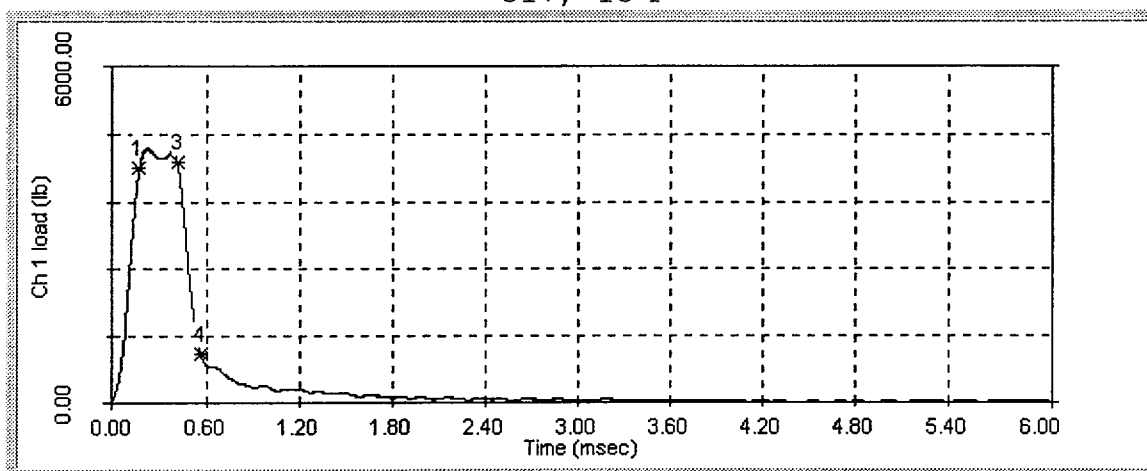
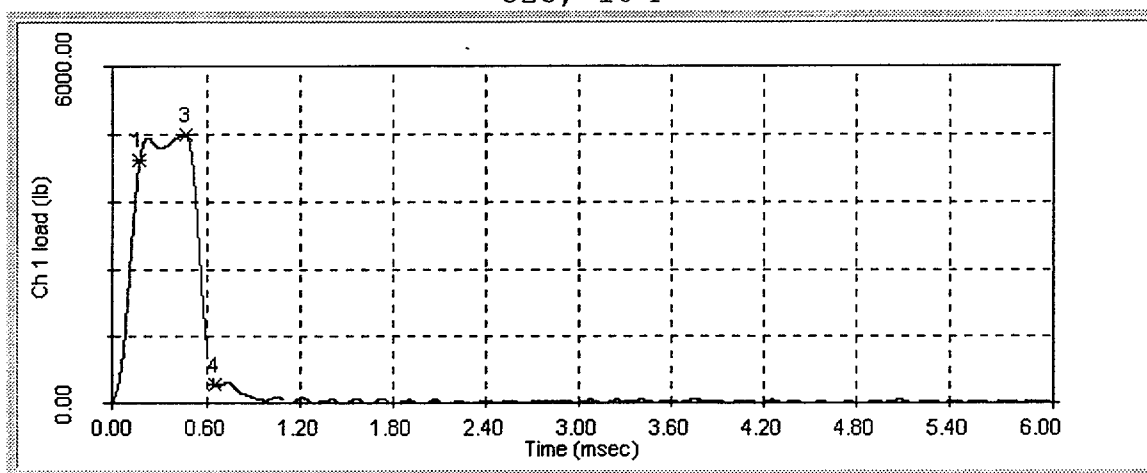
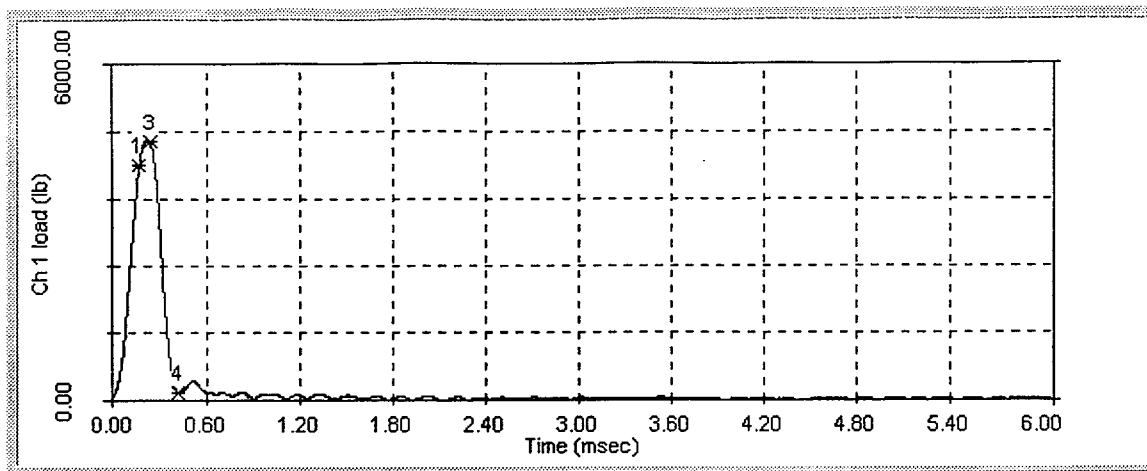
31C, -50°F

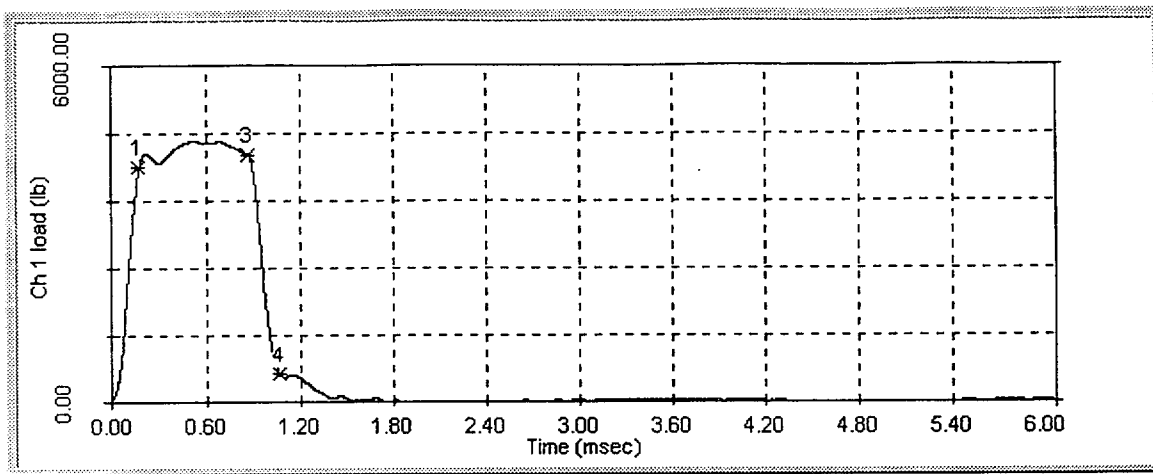


36L, -10°F

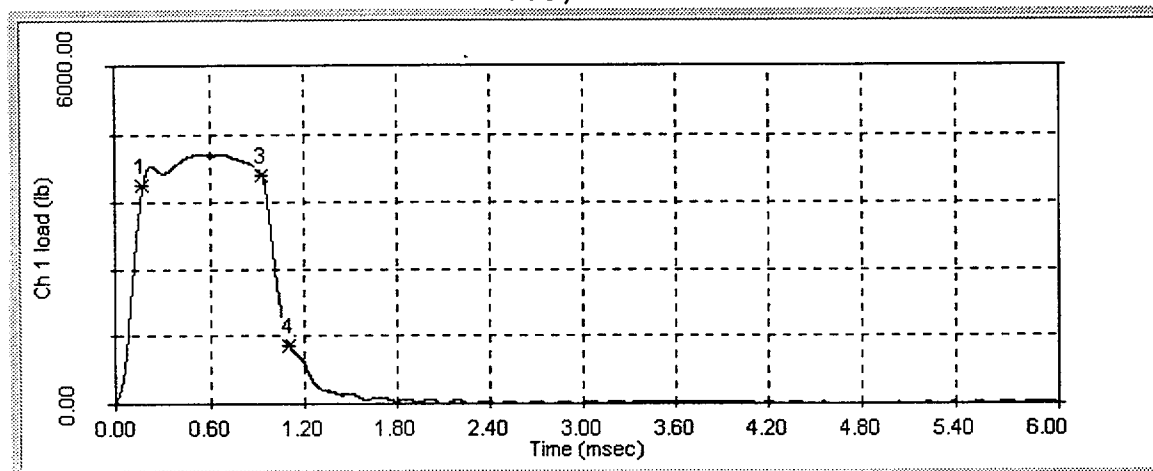


343, 0°F

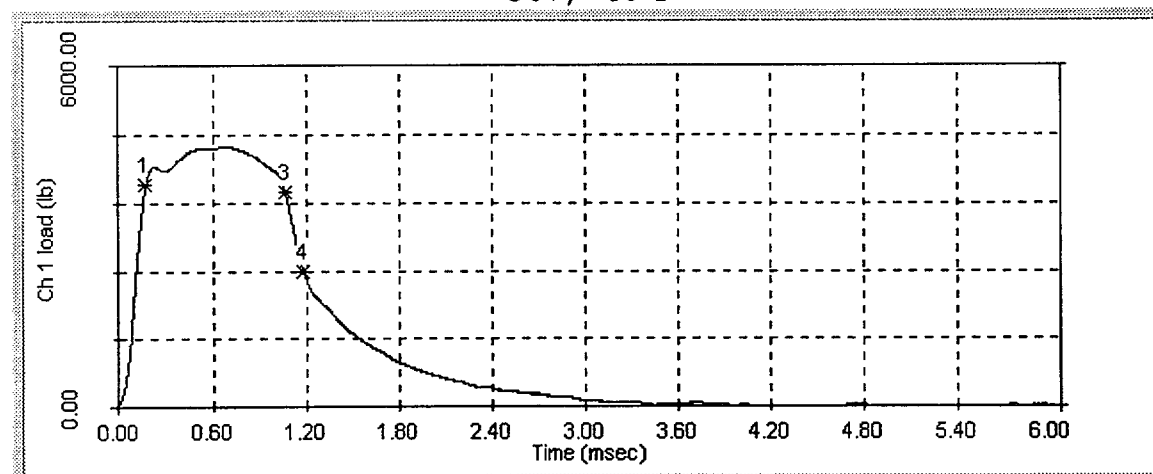




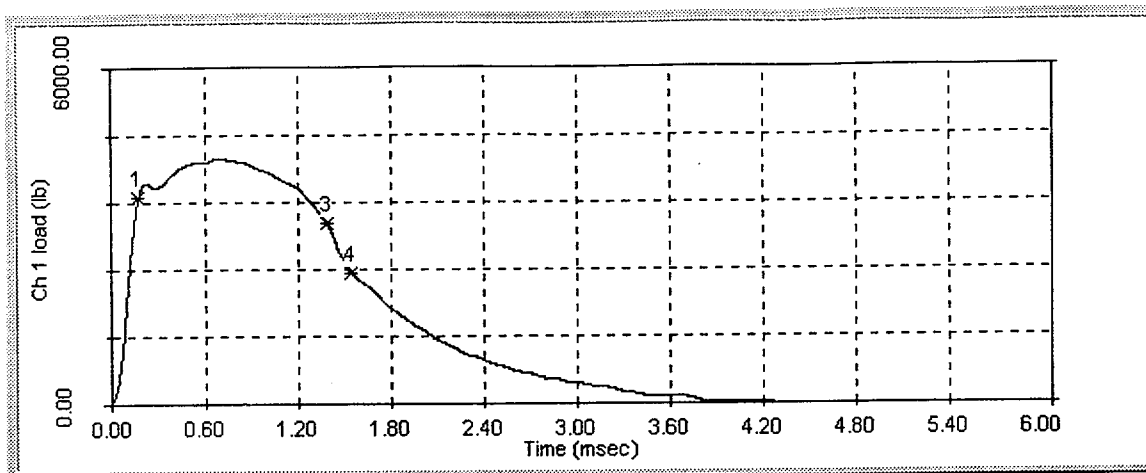
35J, 30°F



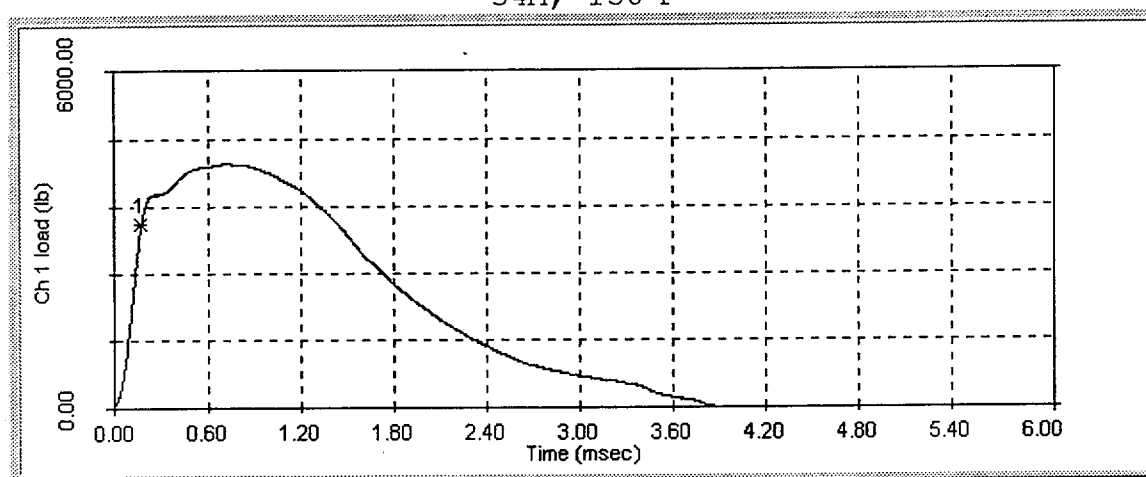
367, 40°F



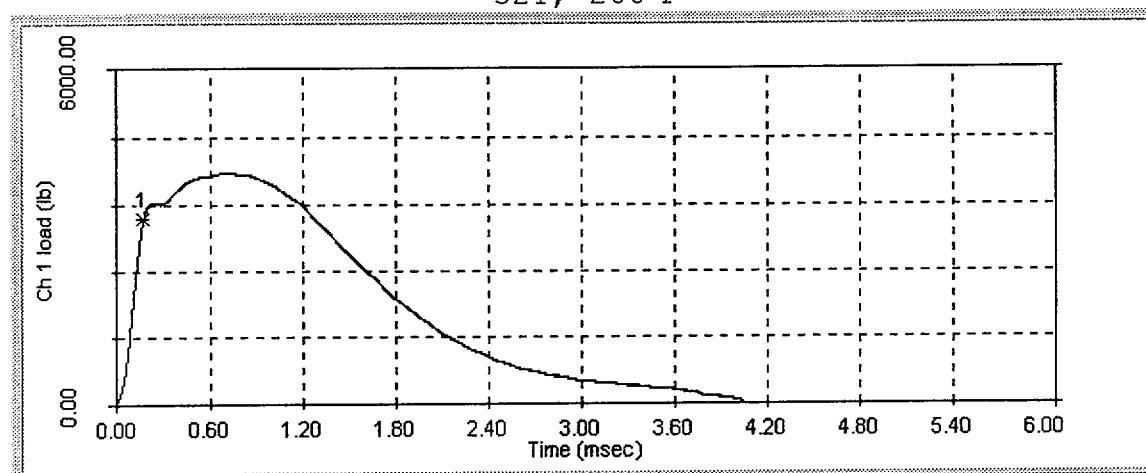
31D, 100°F



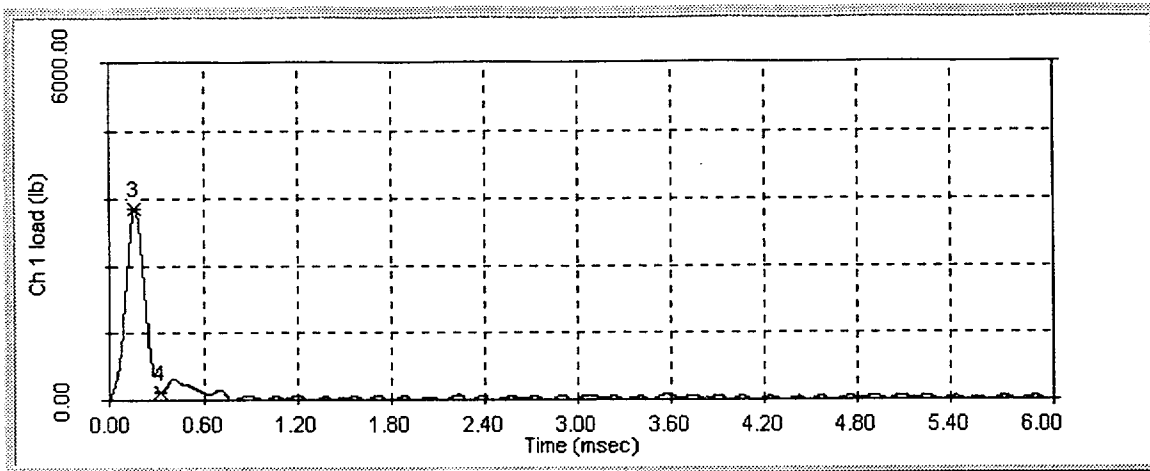
34M, 150°F



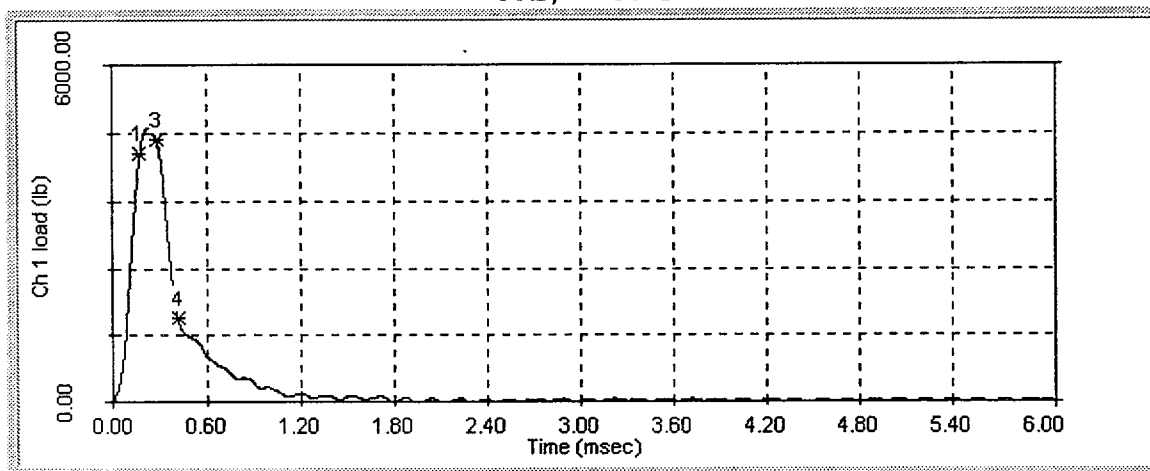
32T, 200°F



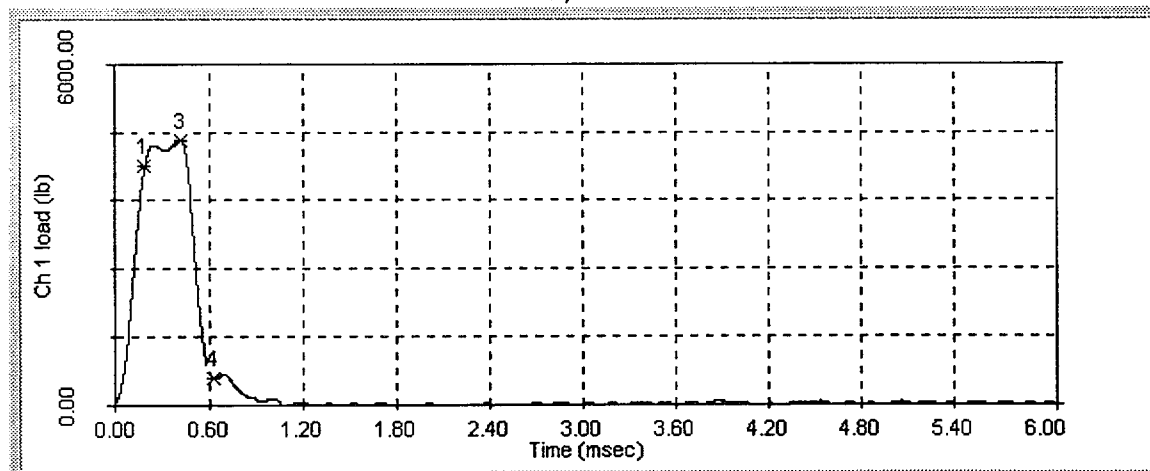
353, 250°F



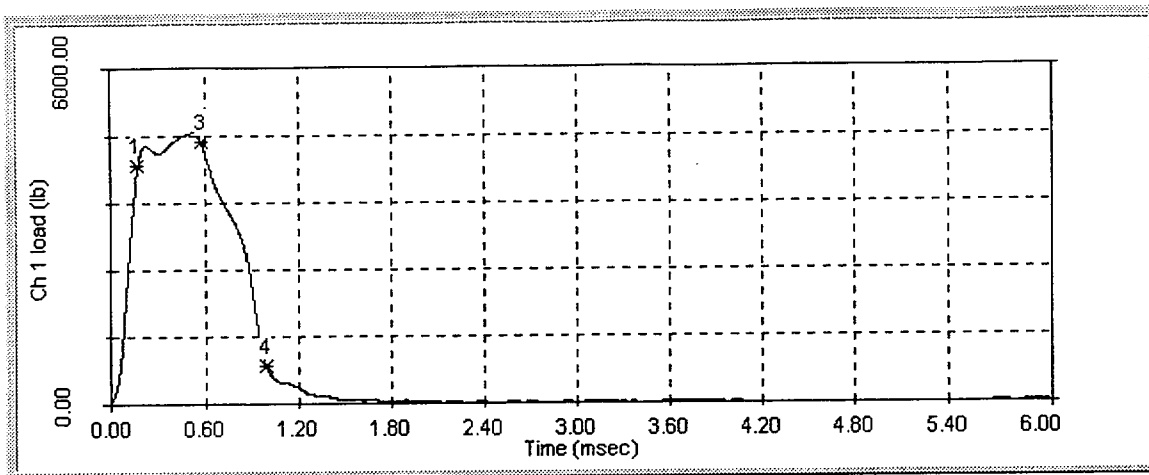
45L, -40°F



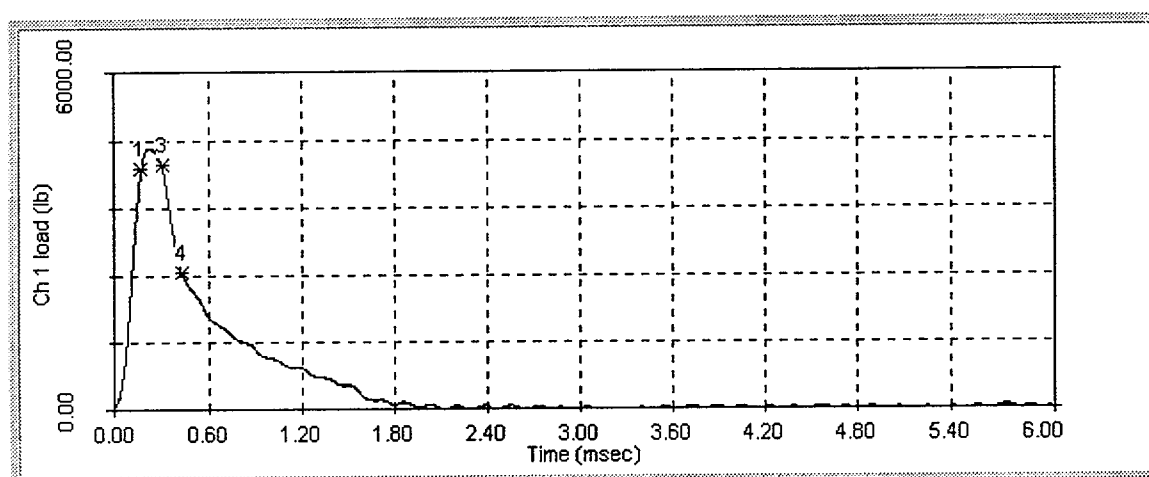
46C, -5°F



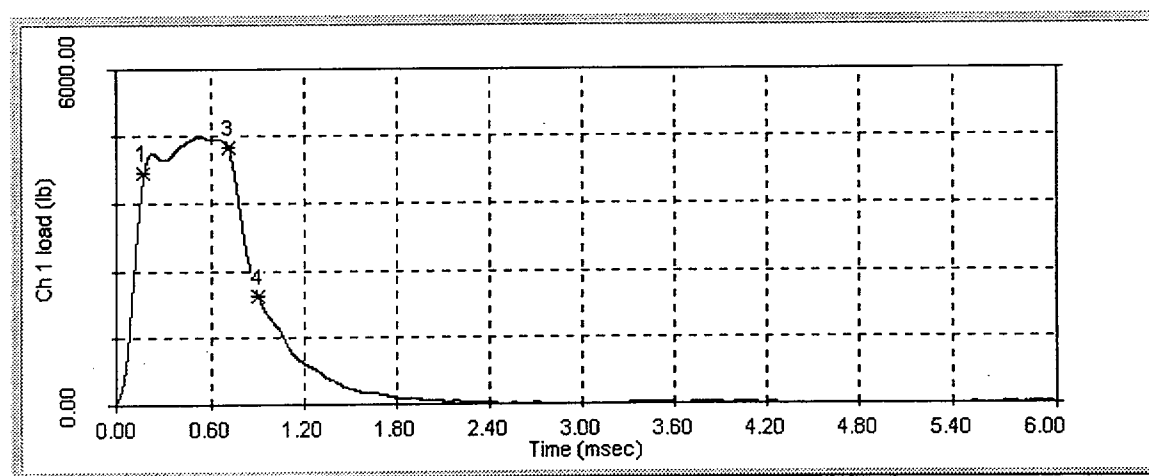
46B, 10°F



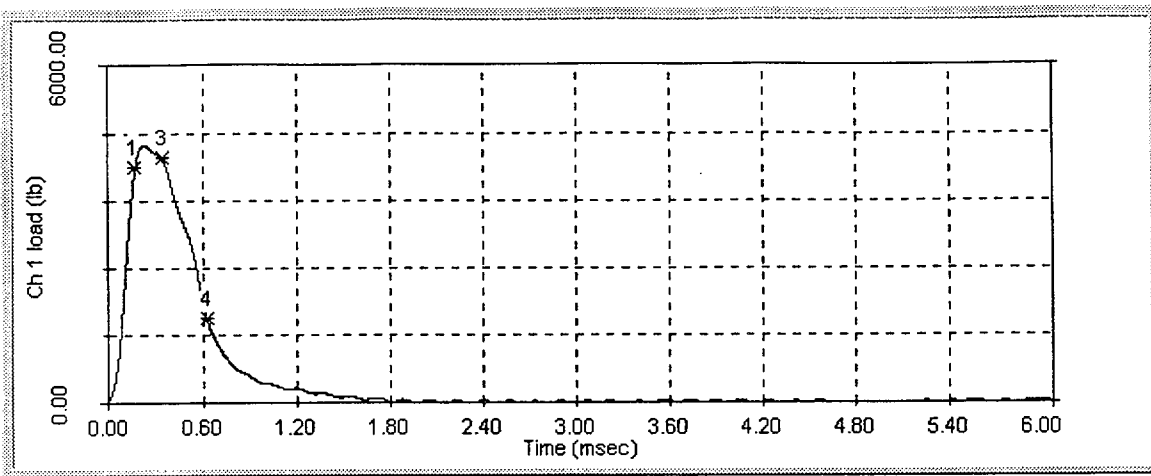
421, 20°F



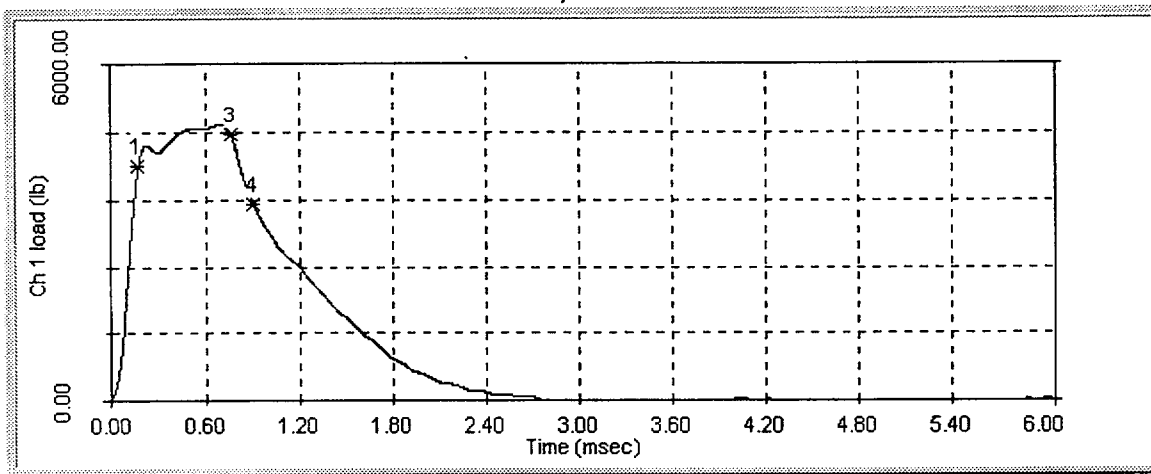
45M, 30°F



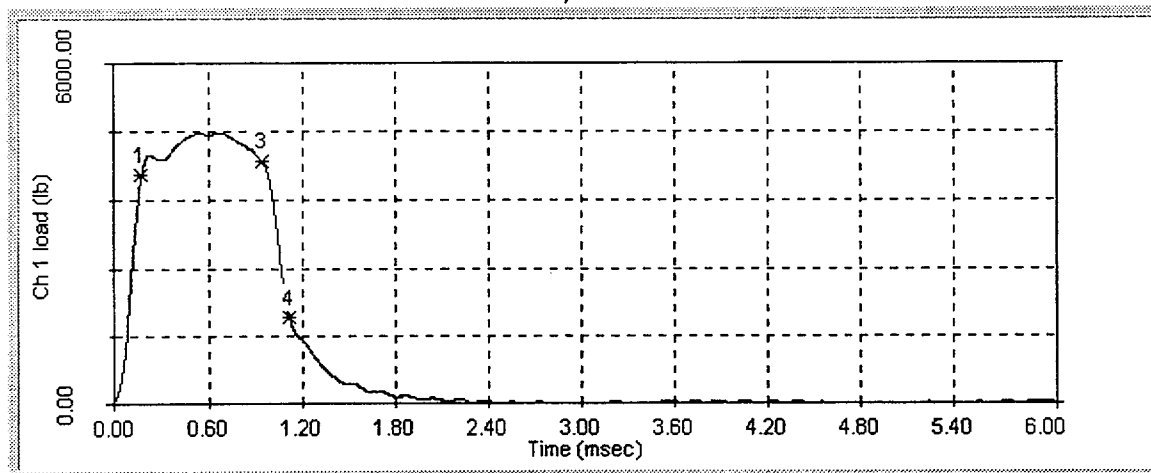
461, 40°F



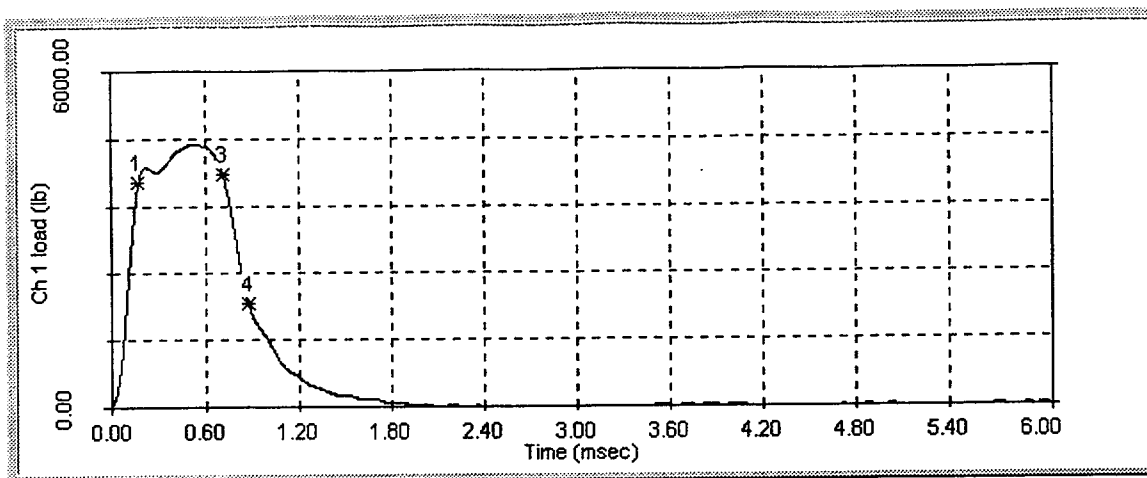
463, 60°F



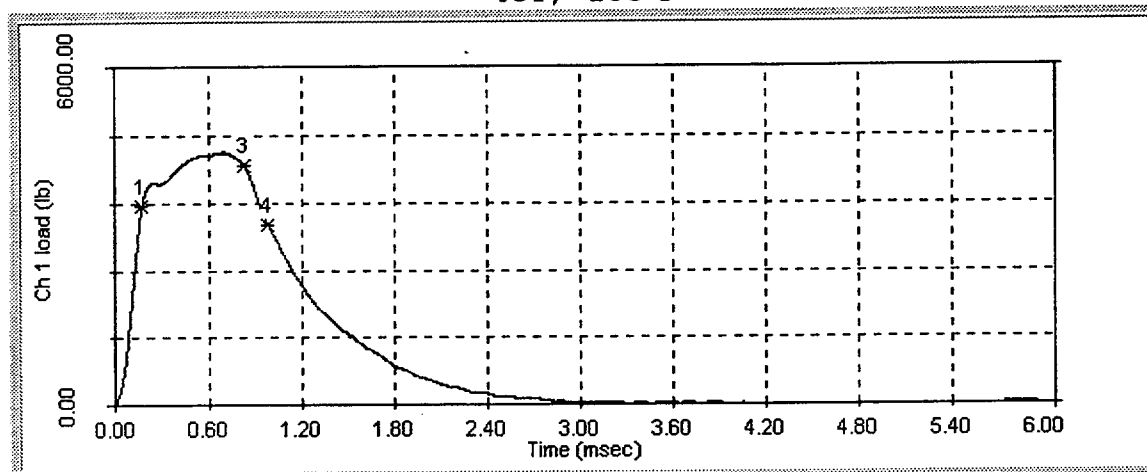
46D, 72°F



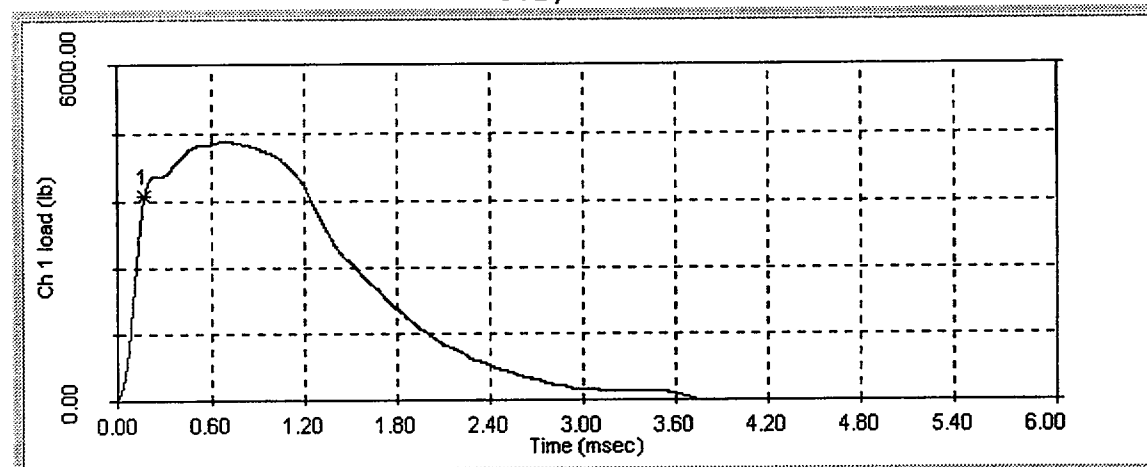
45U, 100°F



45T, 135°F



462, 200°F



464, 250°F